Investigation of the Trade-off Between Lightweight and Battery Cost for an Aluminium-intensive Electric Vehicle

Report 106330

Forschungsgesellschaft Kraftfahrwesen mbH Aachen
Body Department

Final Report

Investigation of the Trade-off between Lightweight and Battery Cost for an Aluminium-intensive Electric Vehicle

Project Number
106330

Contractor:
European Aluminium Association AISBL

International Aluminium Institute

Project Leader:

Dipl.-Ing. Sven Faßbender

Project Engineer:

Dipl.-Ing. Ernö Dux

Dipl.-Ing. Bastian Hartmann

Dr.-Ing. Peter Urban
Senior Manager Body Department

Univ.-Prof. Dr.-Ing. Lutz Eckstein
Chairman of the Advisory Board

Dr.-Ing. Markus Bröckerhoff
Managing Director fka

Aachen, March 2012

Forschungsgesellschaft
Kraftfahrwesen mbH Aachen
Steinbachstr. 7
52074 Aachen, Germany

Registered in Aachen HRB 2435
Phone +49 241 8861 0
Fax +49 241 8861 110
www.fka.de

Managing Director:
Dr.-Ing. Markus Bröckerhoff
Chairman of the Advisory Board:
Univ.-Prof. Dr.-Ing. Lutz Eckstein

IBAN DE 31 3907 0020 0201 339 900
SWIFT-Code (BIC) DEUTDEDK 390
Deutsche Bank Aachen BLZ 390 700 20
Account no. 201 339 900

Executive Summary

Electric vehicles are today rather expensive, mainly because of the cost of batteries. It is therefore important to make electric cars as energy efficient as possible. Lightweighting is one of the most obvious ways of improving the energy efficiency of any vehicle, including electric vehicles. Lightweighting comes at a cost, however. The material used for lightweighting is often slightly more expensive than heavier classical materials. A study aimed at investigating whether the cost of lightweighting a C-segment car with the intensive use of aluminium could be offset, or even more than compensated for, by a reduction in the cost of the batteries needed to drive the car over the same range was initiated. The study was conducted and published by the Forschungsgesellschaft Kraftfahrwesen mbH Aachen (fka).

A C-segment crash reference vehicle with steel unibody and internal combustion engine was chosen as the basis for this study. The mass and crashworthiness properties of this vehicle were analysed in four Euro NCAP and FMVSS 301 high-speed load cases, designated as the benchmark for the various vehicle designs within the project. Both the Electric vehicles (steel-based or aluminium-based) should at least be as safe as the crash reference vehicle.

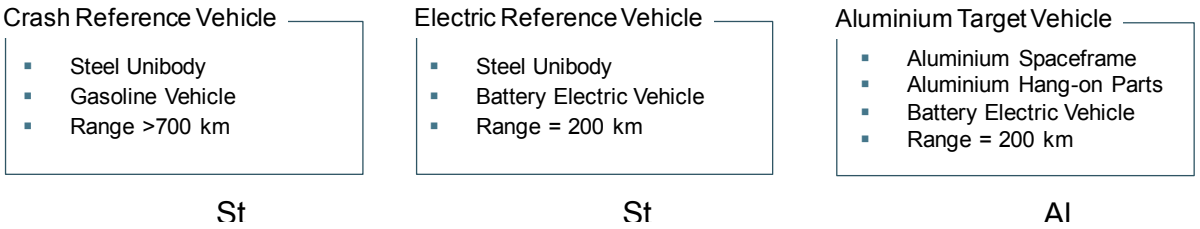

As a first step this car was then converted into an Electric version using a conversion design strategy. This means that the original steel unibody structure was conserved and only minor changes were made in order to adapt the structure around the battery pack for safety reasons. In a second step the car was converted to a full aluminium space frame electric vehicle. The shape of the outer skin of the vehicle was kept identical to that of steel vehicles. A combination of extrusion parts, complex casting nodes and sheet parts are used for the vehicle structure. The following picture shows the various manufacturing methods used in the aluminium design (**blue: sheet**, **green: extrusion**, **red: casting**)

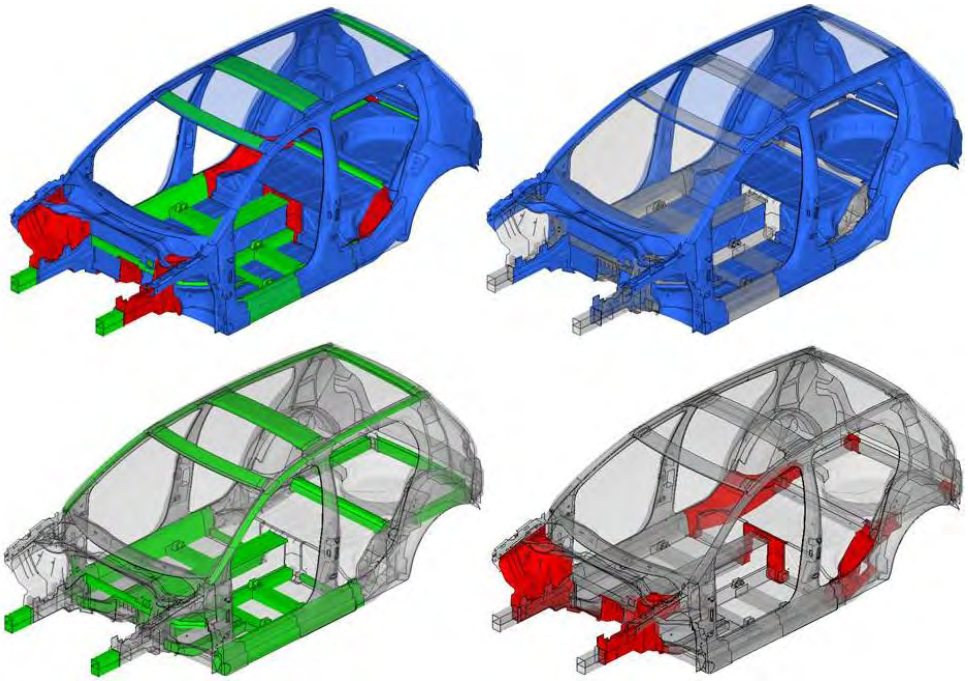

While reaching the defined crashworthiness targets, the weight of the total body structure could be reduced by 162 kg compared to the electric reference steel-unibody. As a secondary effect, the battery system capacity could be downsized by 3.3 kWh while still maintaining the intended driving range of 200 km. This also means an additional weight reduction of 25 kg[1], making **the aluminium electric vehicle in total 187 kg lighter than the steel electric vehicle.**

	Electric reference vehicle	Aluminium target vehicle	Difference	
Vehicle body	375 kg	213 kg	-162 kg	-43.2 %
Battery system	232 kg	207 kg	-25 kg	-10.8 %
Total vehicle weight	**1,327 kg**	**1,140 kg**	**-187 kg**	**-14.2 %**

The cost implications were then quantified using the fka in-house cost tool. Assuming a production volume of 100,000 vehicles per year, aluminium lightweighting measures can be carried out at **additional part and joining costs of 1,015 € per vehicle.** This additional cost should be compared to the cost reduction related to the battery capacity downsizing of 3.3 kWh. Assuming energy-specific battery system costs of 500 €/kWh (assumption for the year 2015), the **reduction in total battery system costs is 1,650 €.** If we compare the additional costs of the lightweight design with the reduction in battery system costs, it can be concluded that the benefits obtained from lower battery costs more than outweigh the additional costs for the lightweight aluminium vehicle. With the assumptions made in this

[1] Assuming battery technology features available in 2015

report, **the total cost of the aluminium electric vehicle is 635 € lower than for the steel electric vehicle.** To clear up some uncertainties about several powertrain cost-influencing factors, a cost tool was developed to enable the impact of a wide variation range of each factor to be evaluated. The cost tool can be found on the EAA website www.alueurope.eu/publications-automotive/

It should be noted that, in order to achieve a complete aluminium design, some parts represent a somewhat high specific lightweight cost (€/kg lightweighting). This increases the average specific lightweight cost. It is important to understand that, even with a lower battery price in the future, the lightweighting of a large number of parts will still be cost-efficient.

Finally, life cycle analyses of the full-steel and the full-aluminium electric vehicles were carried out, revealing that the **aluminium electric vehicle emits 1.5 tons of greenhouse gases less over its complete cradle to cradle life-cycle,** including production, a driving distance of 150,000 km, and recycling. As shown in the graph below, the carbon footprint of the production of the aluminium electric vehicle, including the end of life recycling benefits as recommended in ISO 14044 standards, is lower than that of the steel electric vehicle. As an additional benefit, the aluminium electric vehicle also consumes less energy during the use phase. Hence, whatever the mileage distance over the vehicle life time, the aluminium vehicles is always less intensive in term of GHG emission and energy use.

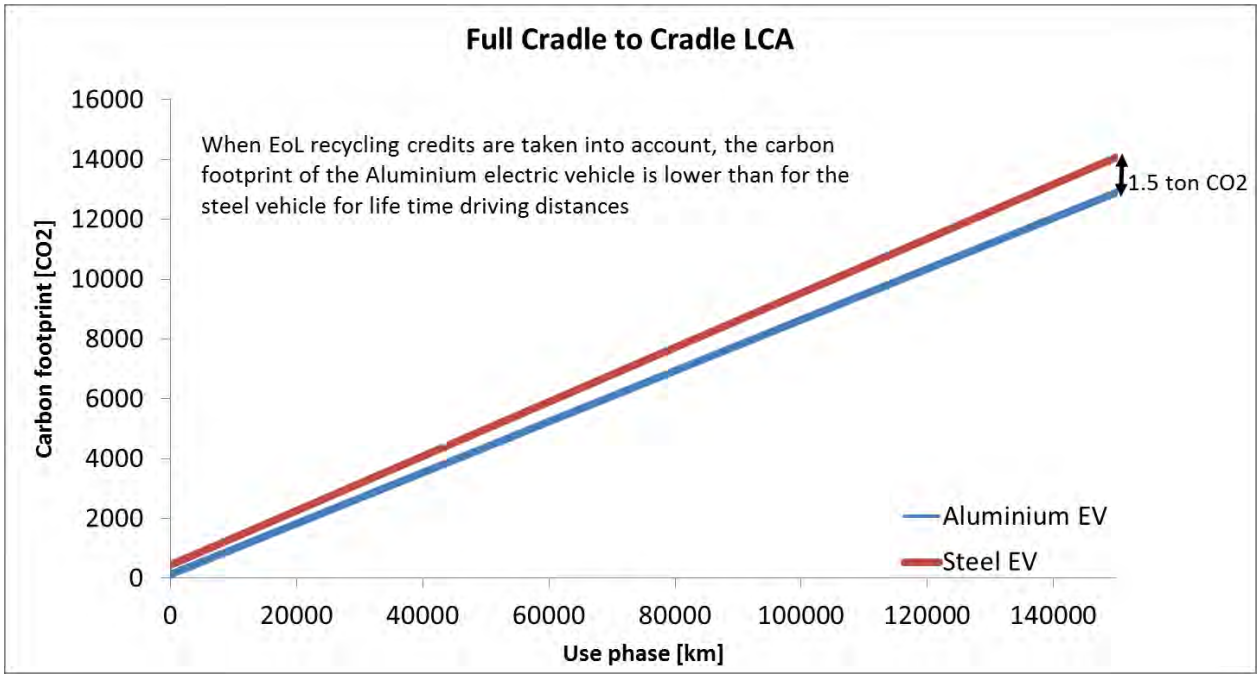

If only the production and use phases are considered (i.e. excluding End-of-Life (EoL) recycling), the break-even point at which the carbon footprint of the aluminium electric vehicle is lower than that of the steel vehicle occurs at a mileage of 47,000 km.

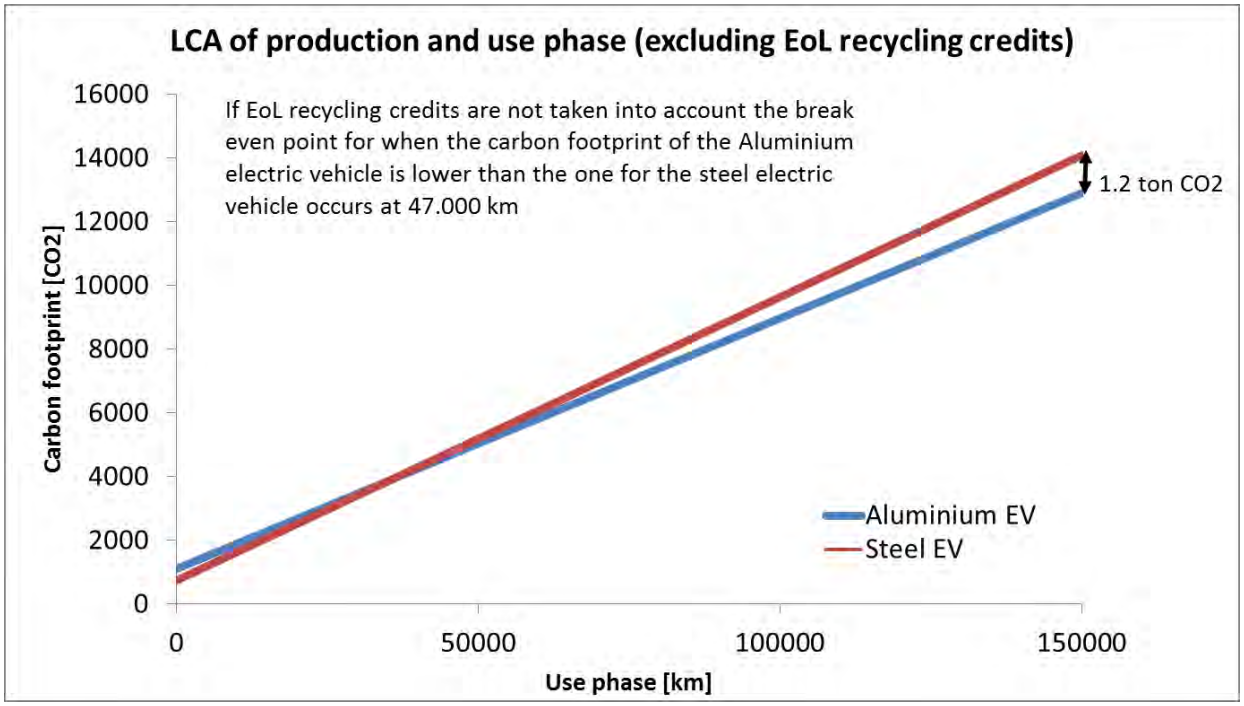

GHG intensity for the 2 vehicles (kg CO_2-Equiv)		Steel electric reference vehicle	Aluminium electric vehicle
Indicators for the vehicle body structure and difference for batteries			
	Production	735 kg	1,405 kg
	End of life (EoL) benefits	-300 kg	-980 kg
	Battery production (only difference)	0 kg	-300 kg
	Total emissions for the production	435 kg	125 kg
Indicators for the electricity consumption (use phase impact)		14,086 kg	12,901 kg

Contents

1 Study Introduction – Motivation and Task Description

The electrification of vehicles is of increasing interest both for policy makers and automotive OEMs. However, the development of electric cars suffers from the high cost of the battery systems compared to the power and autonomous range they can provide. One way to reduce the required battery capacity and hence the costs of the battery system of an electric vehicle is to reduce the kerb weight of the vehicle. A secondary effect of the weight saving is that it also reduces the energy consumption during the use phase of the vehicle, leading to additional positive effects both on the environment and the cost of ownership of the vehicle.

This study develops models to assess the two economic aspects of lightweight engineering, i.e. cost savings for the battery system and cost savings during the use phase. These cost reductions are compared to the additional costs related to lightweight solutions in cars.

The lightweight solutions in the focus of this study are aluminium lightweight designs for the vehicle body structure in comparison to a steel unibody structural design. The central aim is to determine the trade-off between additional lightweight costs for aluminium intensive car production and battery cost savings considering technologies available in the year 2015, modelling a mass market for full electric vehicles. To quantify the possible trade-off in detail, the study applies the described lightweight strategy to a representative C segment vehicle example. The study consists of two design steps (c.f. Fig. 1-1).

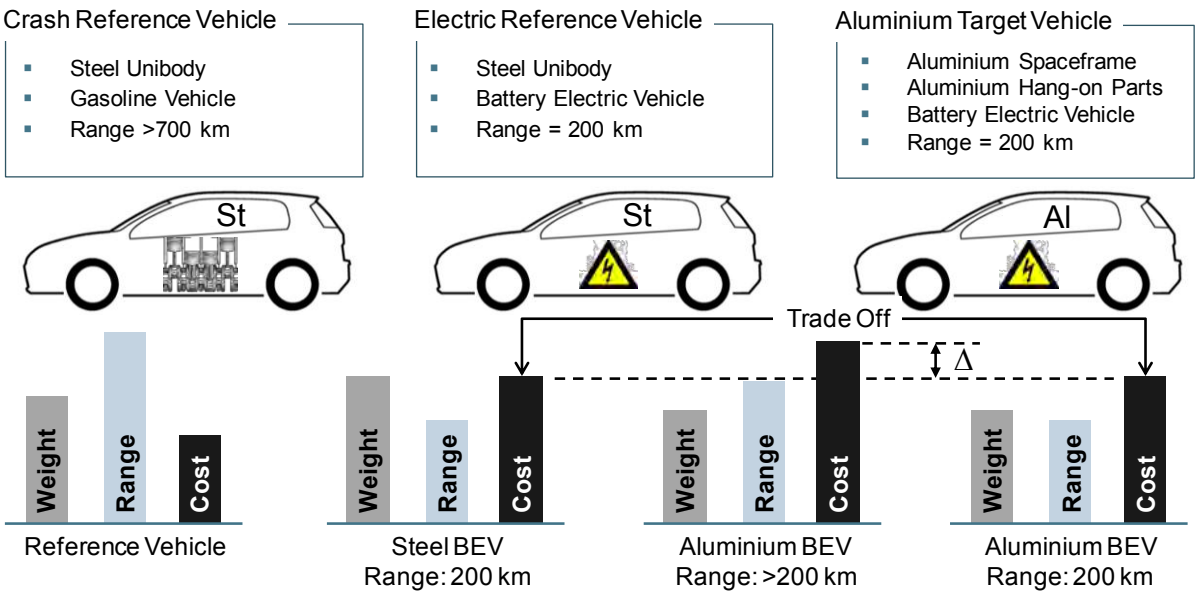

Fig. 1-1 The study task design steps

In a first step, an electric reference vehicle with 200 km autonomous range and a steel unibody structure will be defined by conversion design, based on a chosen steel unibody vehicle with gasoline engine. The structural behaviour of the gasoline vehicle (named “crash reference vehicle”), represented by its crash performance, is to be conserved throughout the different vehicle design stages within the study. The design of the electric powertrain to reach

a range of 200 km in the New European Driving Cycle (NEDC) and the necessary structural modifications to integrate the powertrain are to be specified as well for the electric reference vehicle.

In a second step lightweight measures will be applied to reduce the vehicle's structural weight. These measures have to consist of the application of different aluminium materials and manufacturing methods to fully replace the conventional steel body structure. The special requirements of aluminium as structural material in design and production of a vehicle will be taken into account, while the reference crash behaviour has to be conserved. Due to the reduced structural weight of the aluminium intensive vehicle, a downsizing of the initial electric drivetrain will be possible and executed conserving the defined NEDC driving range.

In addition to the described design tasks, the cost effects of the applied study measures have to be quantified. Therefore, detailed analysis has to focus on the additional lightweight costs of the structural material substitution on the one hand and the battery cost savings due to powertrain downsizing in production and throughout the vehicle's use phase on the other hand. For this task, estimated material and battery cell costs in the year 2015 will be assumed and a series production volume of 100,000 vehicles per year considered. As some cost influencing factors, such as battery cell costs, are supposed to undergo uncertain change in future, a cost tool is to be created to cover a larger range of cost influencing factors.

Finally, a life cycle analysis (LCA) will be carried out to determine the respective life cycle greenhouse gas intensity of the full-aluminium target vehicle model in comparison to the steel unibody electric reference vehicle model.

2 Analysis of the Reference Vehicle

A C segment vehicle for mass market production is chosen as crash reference vehicle model with gasoline engine. The chosen Volkswagen Golf 5 (c.f. Fig. 2-1) represents a vehicle size large enough to be considered as main car for its owner but small enough for an electrification assuring 200 km drive range in the NEDC with a near future battery system.

Fig. 2-1 Volkswagen Golf 5 [STE03]

For crashworthiness simulation needs, a simplified model of the Volkswagen Golf 5 was already defined for the “Super Light Car” (SLC) project (c.f. Fig. 2-2) [GOE09].

Fig. 2-2 Simplified Volkswagen Golf 5 in finite element modelling

This finite element (FE) model of the vehicle, chosen as simulation reference for the structural analysis within this study, has the following features:

- Total vehicle mass: 1,247 kg (with 90 % fuel tank fill, equivalent to 36.7 kg of fuel)
- Axle load distribution (front/rear): 62/38
- Weight of body-in-white structure (steel unibody): 258 kg

The vehicle structure is made from conventional steel materials with known grades (c.f. Fig. 2-3).

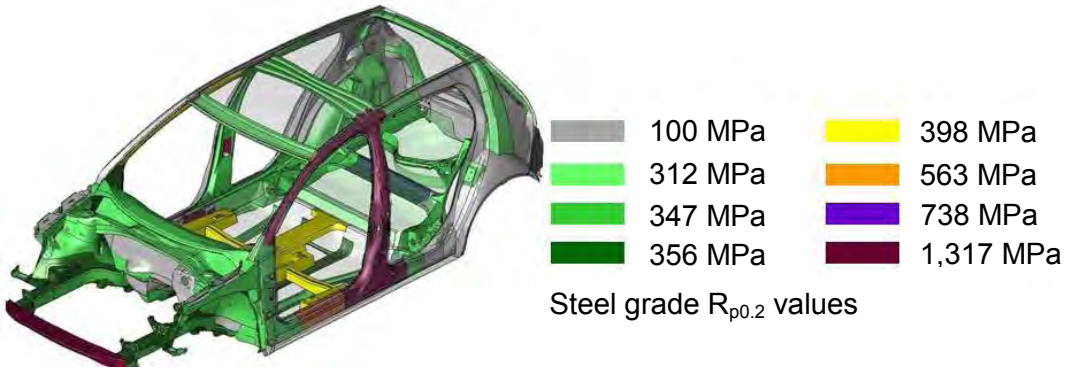

Fig. 2-3 Steel grades used in the SLC Golf 5 FE model's body-in-white structure

2.1 Analysis of the Crash Reference Vehicle's Crash Performance

One key aspect for the success of any new vehicle structure is the fulfilment of highspeed crash requirements imposed by legislation and consumer protection organisations. The crashworthiness simulations conducted in this study are based on consumer protection crash tests (European New Car Assessment Program – Euro NCAP) and legislation based crash tests (Federal Motor Vehicle Safety Standards – FMVSS) for high speed impacting onto the vehicle's front, side and rear end. The four crash loadcases in the focus of the conducted structural simulation are the Euro NCAP front crash, the Euro NCAP side and side pole crash and the FMVSS 301 rear crash. A detailed description of the different loadcase configurations is given in appendix (c.f. chapter 12.1).

The assessment of vehicle crash performance is usually based on passenger dummy response data. To simplify the evaluation and the structural comparison between the different vehicle designs within the study, only structural intrusions into the passenger survival space of the vehicle and the body-in-white accelerations are analysed. In this way complex dummy modelling is avoided, but qualified crashworthiness assessment is still possible. Especially an A to B comparison between the crash reference vehicle and all following vehicle designs is well possible. If comparable levels of intrusion and acceleration are achieved, a comparable passenger safety level can be assumed.

For front impacts, the general intrusion on the bulkhead level as front limit to the passenger compartment is analysed. For a better tracking of the deformation behaviour in critical front areas (near the driver's feet on the footwell, the steering column and passage and finally at the A pillar to evaluate the risk of door jam), discrete point evaluation over crash progression (Δ t = 140 ms) is performed at nine points. The acceleration is measured at a point near the vehicle's centre of gravity above the floor tunnel (c.f. Fig. 2-4).

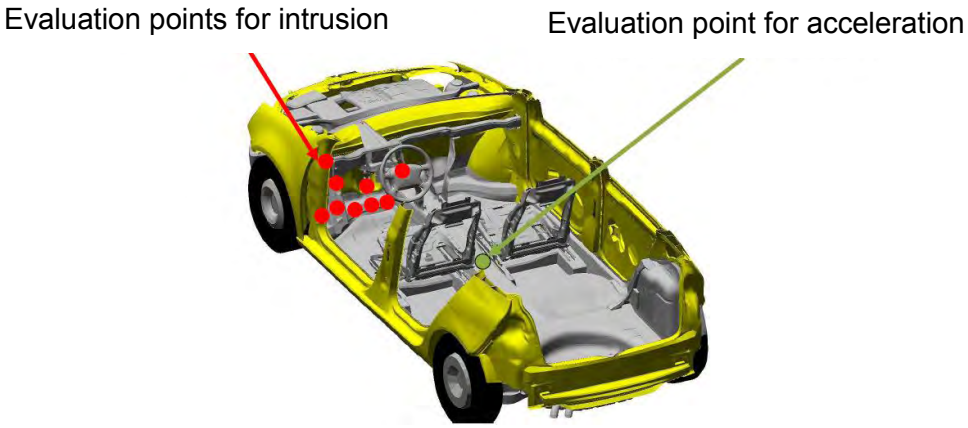

Fig. 2-4 Evaluation points for front crash assessment

In a comparable way, the intrusion behaviour of the whole side area from the A to the C pillar including the driver side doors is evaluated for the side crash loadcases. In addition 13 critical points were chosen for intrusion tracking over the whole crash progression (c.f. Fig. 2-5). The same evaluation point for vehicle acceleration is chosen as for the front crash loadcase.

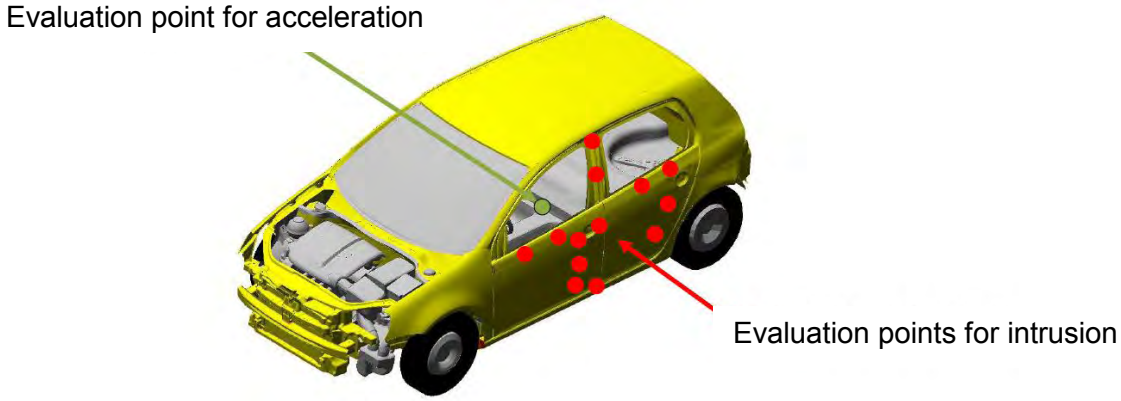

Fig. 2-5 Evaluation points for side crash assessment

As the FMVSS 301 rear crash standard is originally meant to monitor the fuel spillage behaviour of gasoline vehicles, a detailed intrusion monitoring into the passenger compartment is not performed. Instead, only the highest displacement of the rear end of the body-in-white in crash direction is determined and the deformation of the fuel tank (for gasoline vehicles) or battery system (for electric vehicles) is regarded. In addition, the acceleration behaviour is monitored as for all other described loadcases.

2.1.1 Euro NCAP Front Crash Behaviour of the Crash Reference Model

Fig. 2-6 shows the course of the Euro NCAP front crash as simulated for the crash reference model.

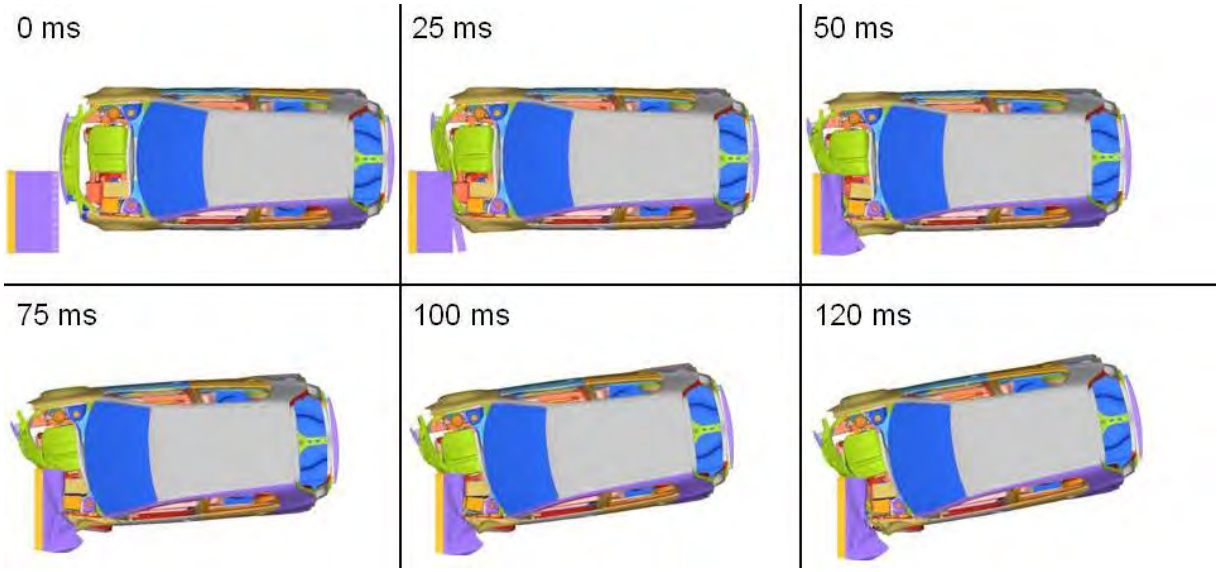

Fig. 2-6: Euro NCAP front crash progression for crash reference model

As shown, the offset impacting of the deformable barrier leads to a rotational movement of the vehicle around the barrier. The kinetic energy of the vehicle is reduced by the deformation of the front longitudinal beam elements. In the mean time, the package components of the vehicle front are pushed backwards hitting the vehicle's bulkhead. In this way, an intrusion of the bulkhead into the passenger compartment occurs. In the same way, the steering column is pushed into the passenger compartment.

Fig. 2-7 shows the intrusion over the crash duration at the monitored points, while Fig. 2-8 shows the general crash behaviour at the time of maximum intrusion. Fig. 2-9 presents the acceleration of the vehicle's centre of gravity in the x-y-plane.

As visible, the intrusion of the bulkhead area into the passenger compartment peaks at the inner edge of the driver side wheel house at a value of 85 mm. Generally, intrusion at the specially evaluated points remains below 50 mm. Acceleration in x-direction peaks at values below 550 m/s².

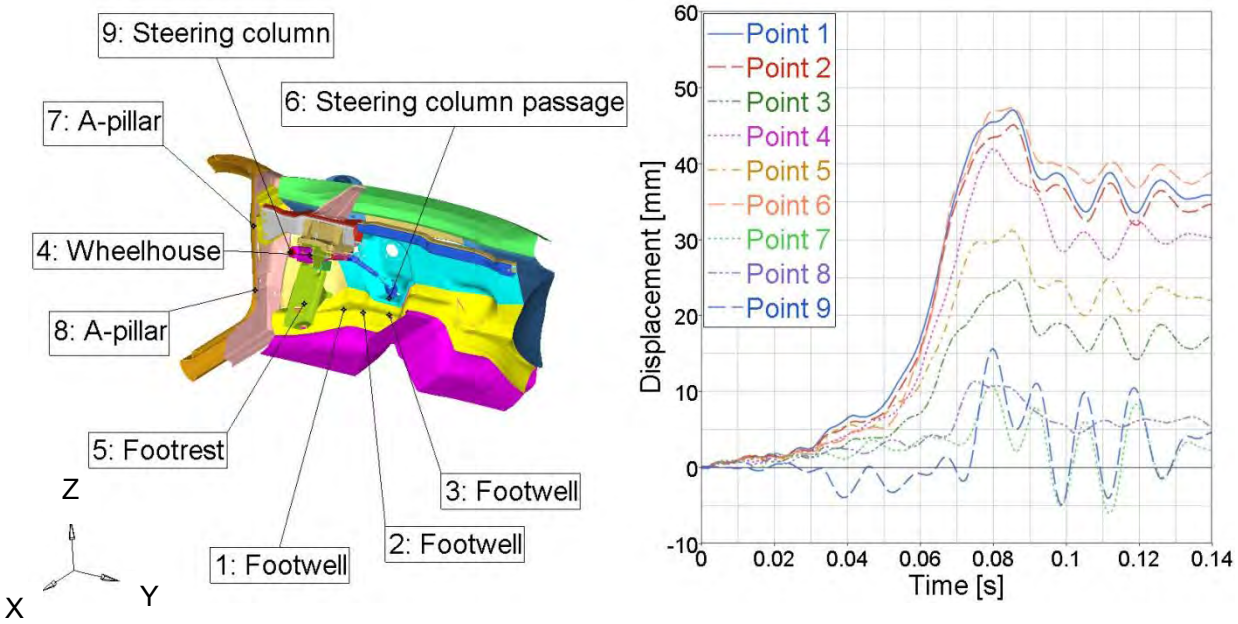

Fig. 2-7 Crash reference model – Intrusion at evaluation points during front crash

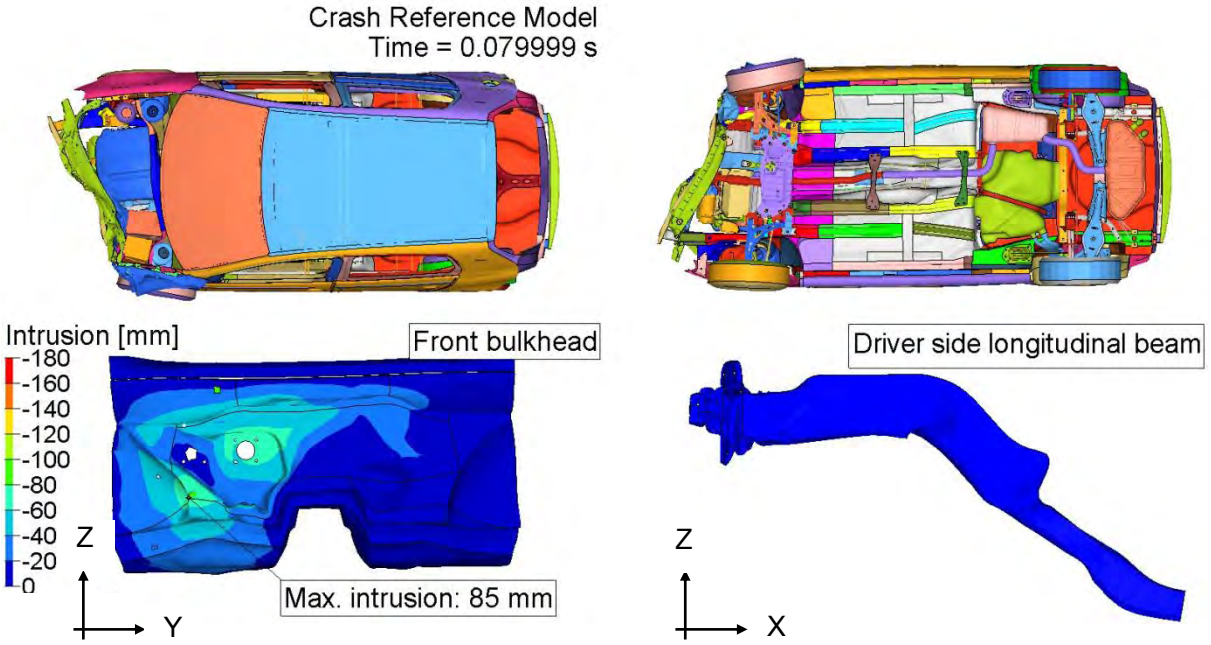

Fig. 2-8 Crash reference model – Front crash behaviour at time of maximum intrusion

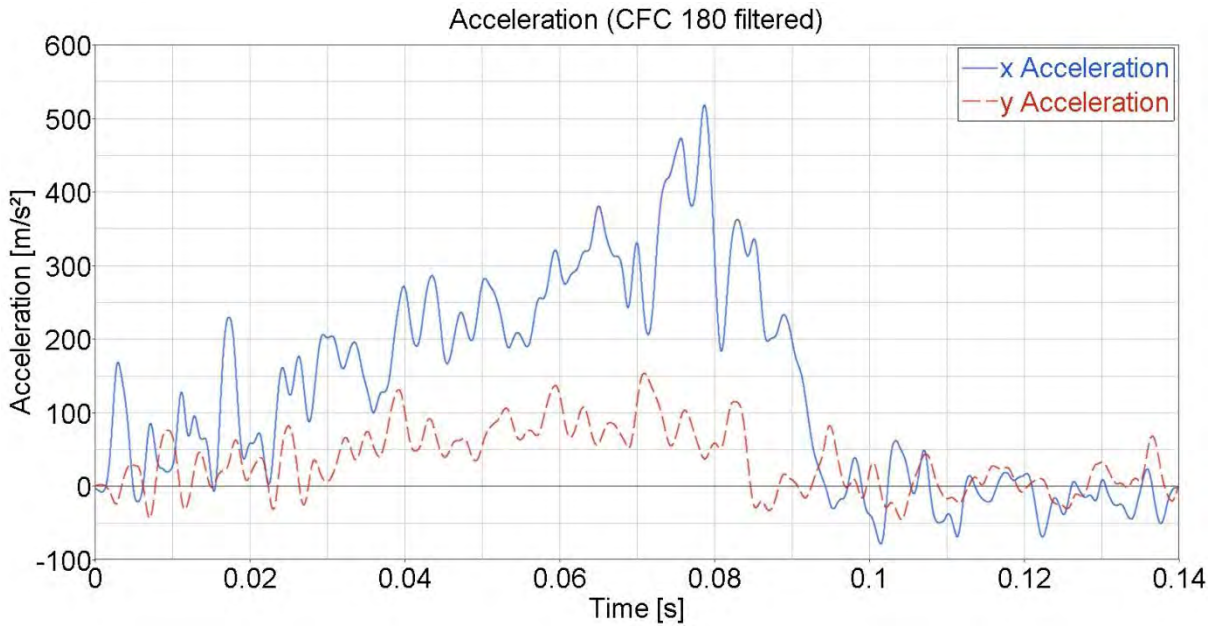

Fig. 2-9 Crash reference model – Deceleration of vehicle centre during front crash

2.1.2 Euro NCAP Side Crash Behaviour of the Crash Reference Model

Fig. 2-10 shows the course of the Euro NCAP side crash for the crash reference model.

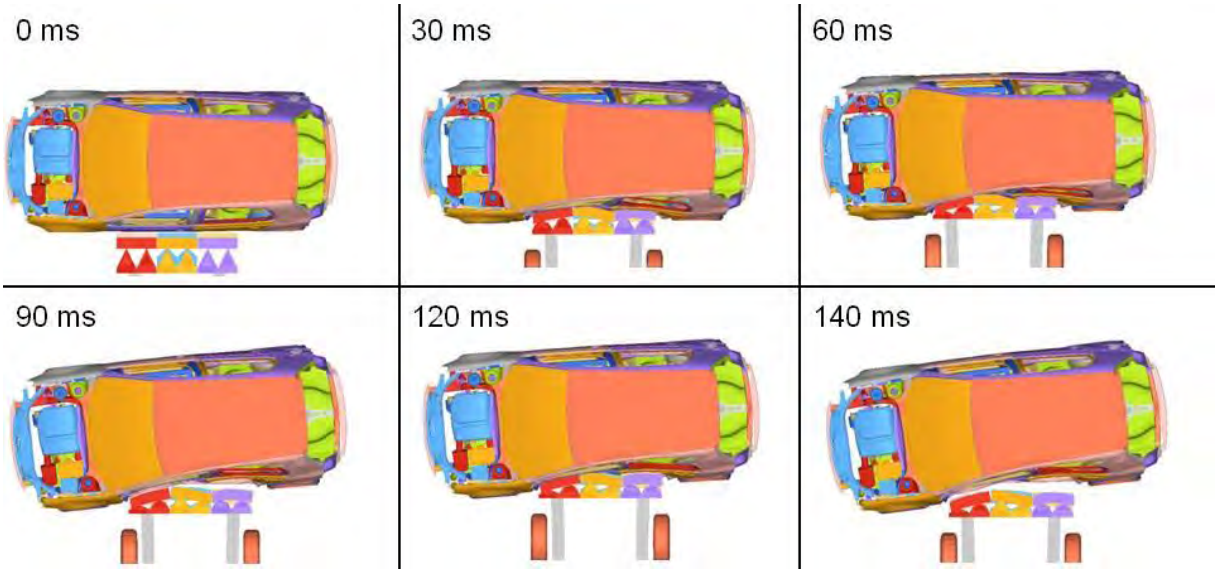

Fig. 2-10 Euro NCAP side crash progression for the crash reference model

As visible in the simulation, the moving barrier touches the vehicle on the level of the driver side doors. Due to this collision, the vehicle gets pushed into the rolling direction of the impacting barrier. As the barrier does not hit the vehicle at its centre of gravity, a slight rotation around the vehicle's yaw axis occurs. The stiffness of the rocker rail, the B pillar, the

front and rear door crash reinforcements and the floor crossbeams is decisive for the intrusion behaviour of the vehicle's side (c.f. Fig. 2-11).

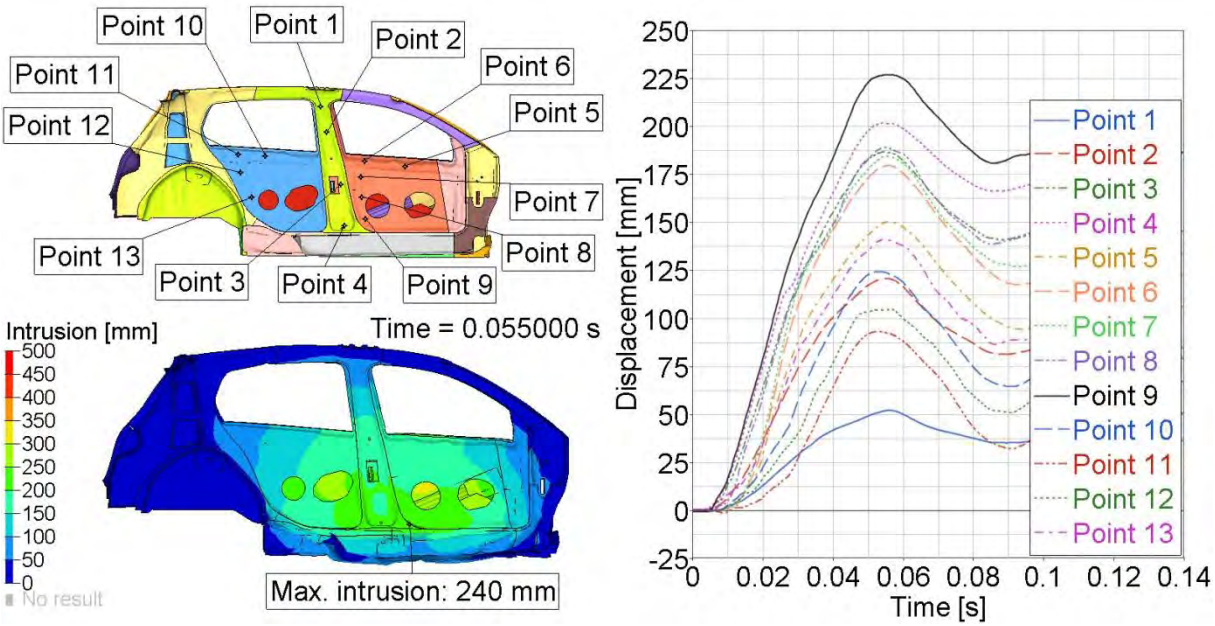

Fig. 2-11 Crash reference model – Side overview at time of maximum intrusion (low, left) and intrusion behaviour over crash duration for monitored points (right) during side crash

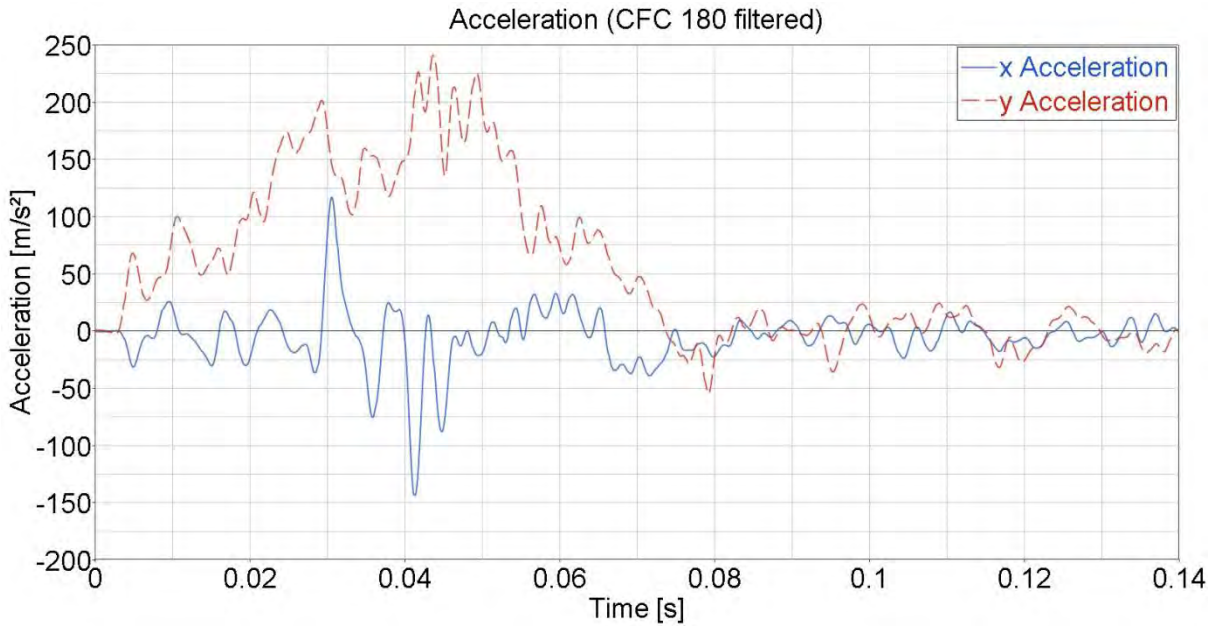

Fig. 2-12 Crash reference model – Deceleration of vehicle centre during side crash

The highest occurring intrusion reaches a level of 240 mm at the lower front door edge, while intrusion at the monitored critical points remains below a value of 230 mm. The vehicle

acceleration in y-direction (impact direction) peaks at values between 200 and 250 m/s² (c.f. Fig. 2-12).

2.1.3 Euro NCAP Pole Side Crash Behaviour of the Crash Reference Model

Fig. 2-13 shows the course of the Euro NCAP pole side crash for the crash reference model.

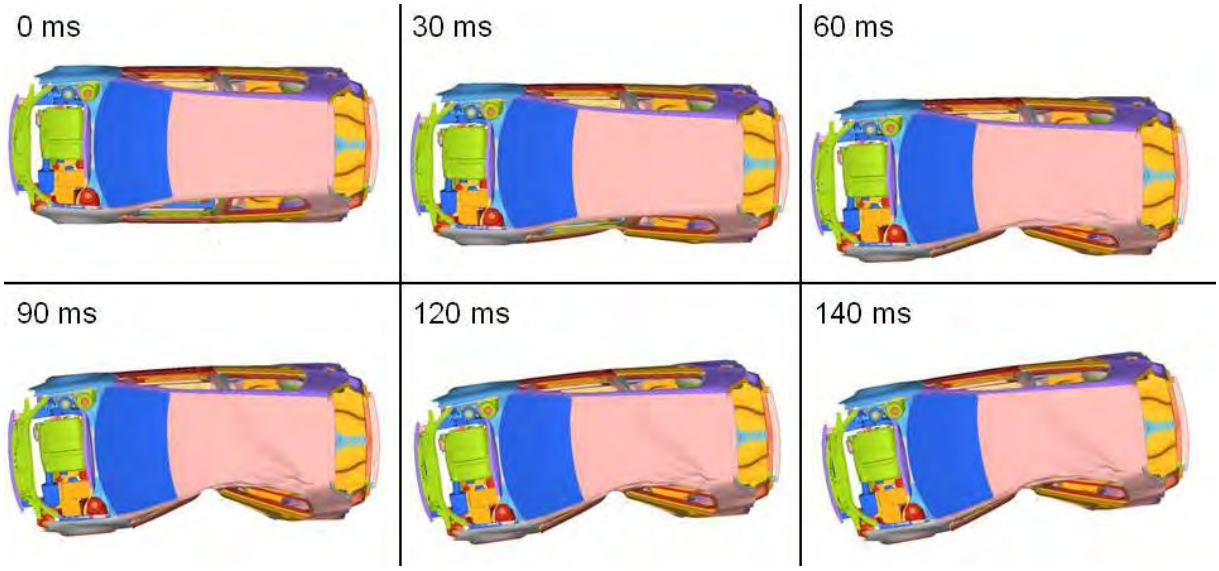

Fig. 2-13 Euro NCAP pole side crash progression for the crash reference model

The vehicle touches the rigid pole on the assumed x-axis level of the driver's head. Once in contact with the pole, the vehicle structure bends around it. The driver side doors and the B pillar elements are without significant stiffness effect.

The rocker rail and the roof rail areas and the floor crossbeam structures are decisive for the resulting intrusion of the side structure (c.f. Fig. 2-14). As the floor structure below the driver's seat should conserve its width, the occurring significant pole intrusion leads to a strong deformation of the vehicle tunnel while the driver's seat and the floor structure below mainly just get pushed aside. The collapse of the tunnel has no hazardous effect onto the powertrain, as only the exhaust system tube is situated within the tunnel in front driven gasoline vehicles. The side intrusion peaks at values of about 340 mm on the B pillar level.

Intrusions exceed 300 mm in an extended area around the peak point. Acceleration values in y-direction between 100 and 200 m/s² appear over an expanded duration (c.f. Fig. 2-15).

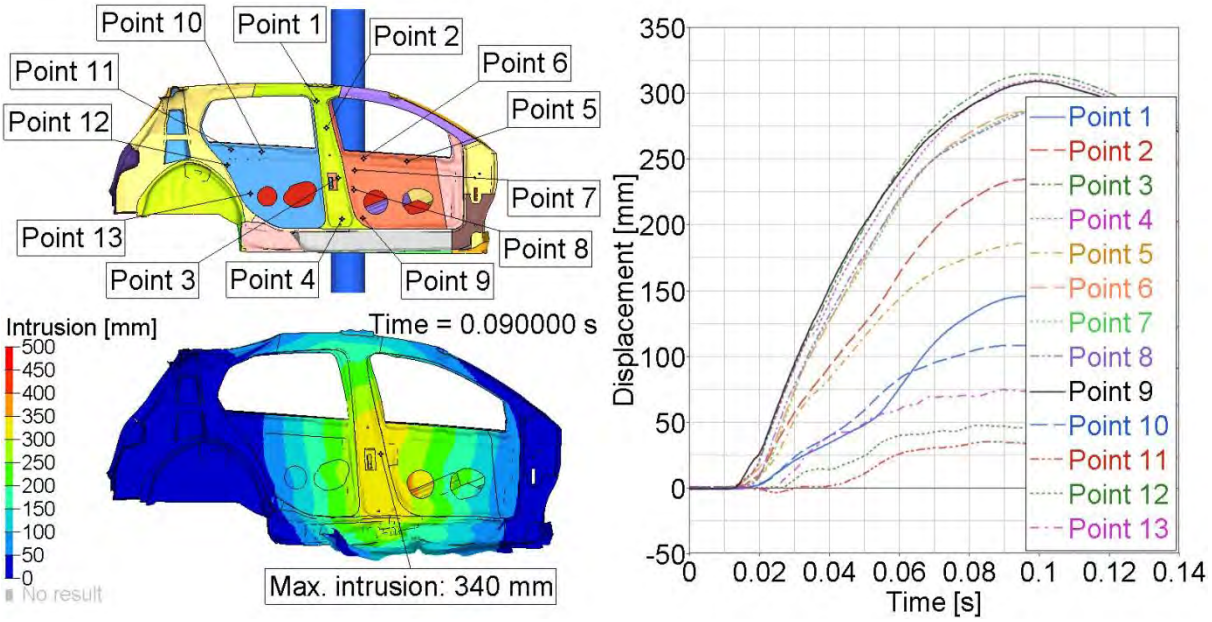

Fig. 2-14 Crash reference model – Side overview at time of maximum intrusion (low, left) and intrusion behaviour over crash duration for monitored points (right) during pole side crash

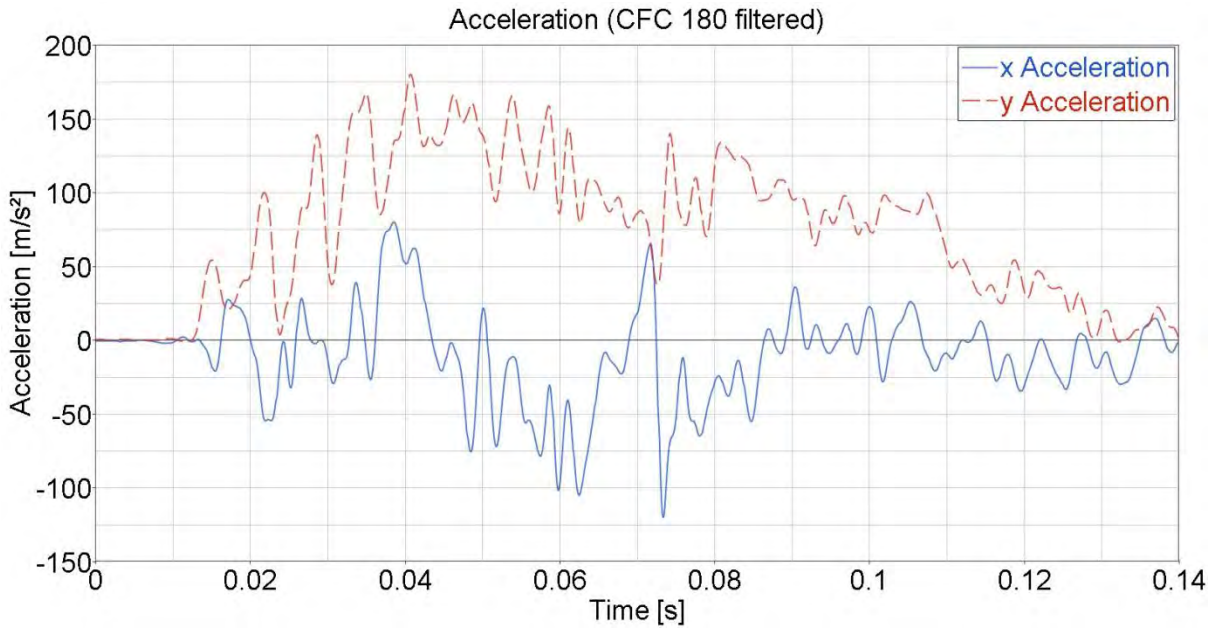

Fig. 2-15 Crash reference model – Deceleration of vehicle centre during pole side crash

2.1.4 FMVSS 301 Rear Crash Behaviour of the Crash Reference Model

Fig. 2-16 shows the course of the FMVSS 301 rear crash for the crash reference model.

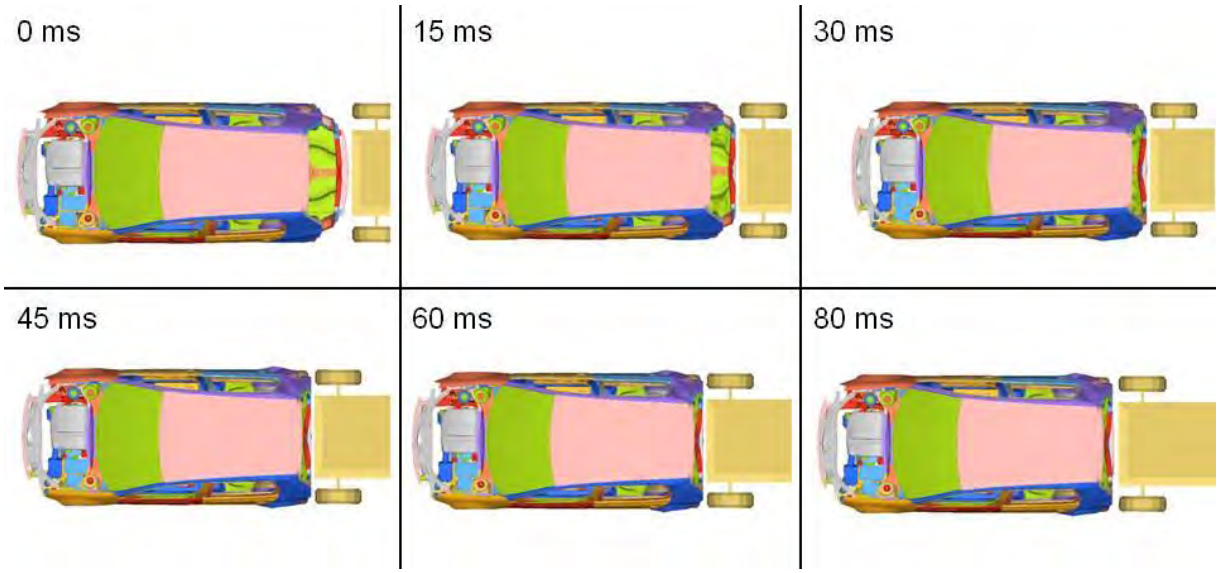

Fig. 2-16 FMVSS 301 rear crash progression for crash reference model

The moving barrier hits the rear end of the vehicle in central position. The vehicle is pushed into the barrier's movement direction. The rear end of the vehicle gets deformed until the rear wheels get into block contact with the front side of the rear wheel house. The deformation impacts the vehicle's exhaust system, but not the fuel tank (c.f. Fig. 2-17).

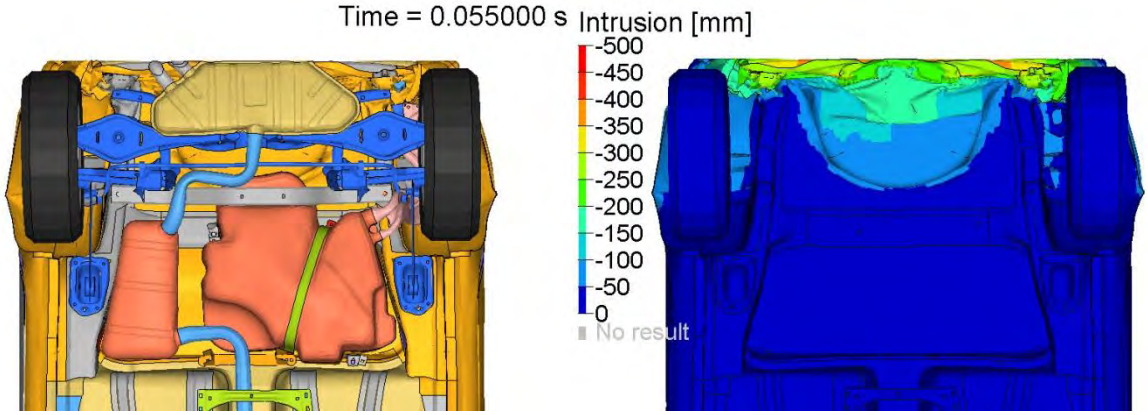

Fig. 2-17 Crash reference model – Rear crash behaviour at time of maximum intrusion

The rear end of the body-in-white suffers a maximum intrusion of 380 mm (c.f. Fig. 2-18) while maximum acceleration peaks at values between 300 and 400 m/s² (c.f. Fig. 2-19).

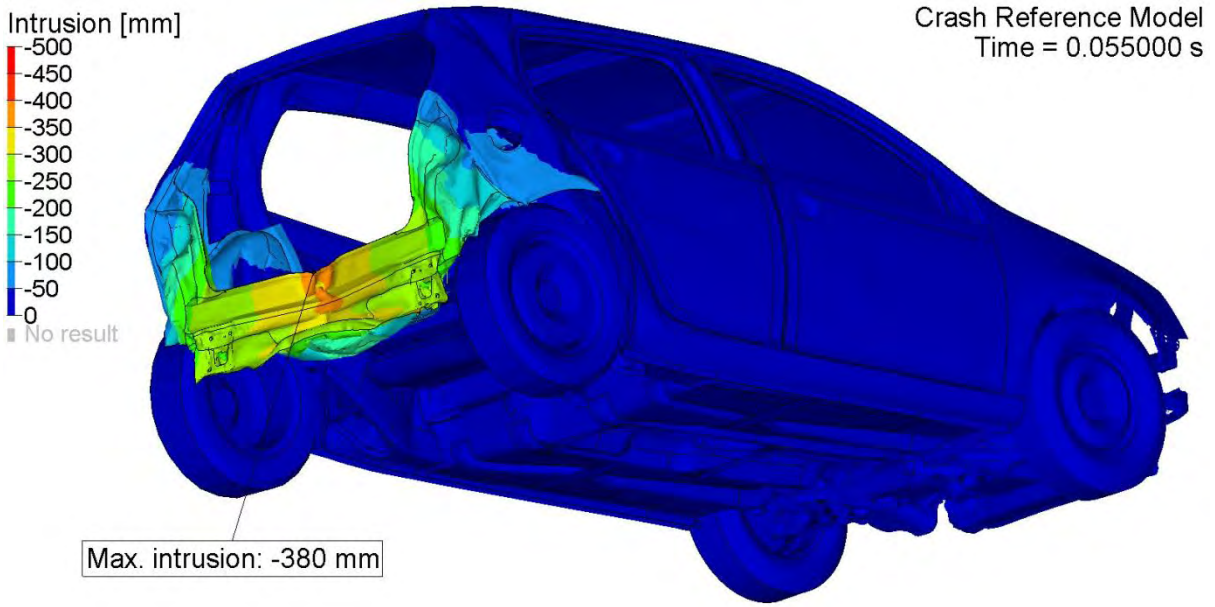

Fig. 2-18 Crash reference model – Maximum intrusion for rear crash

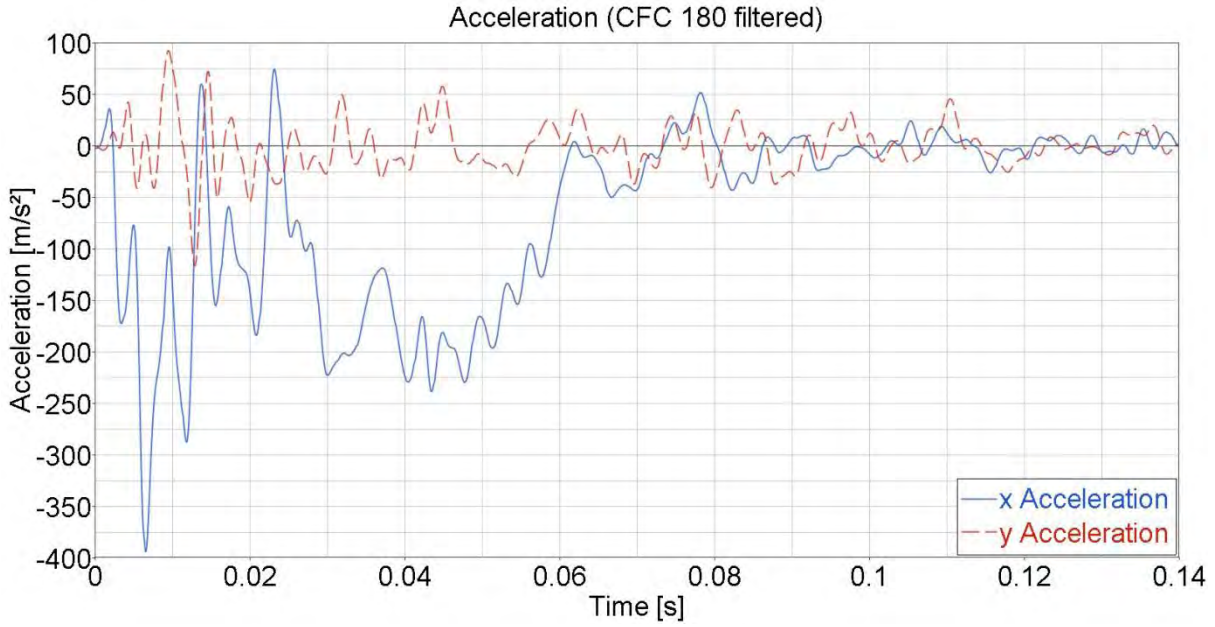

Fig. 2-19 Crash reference model – Deceleration of vehicle centre during rear crash

The described crash reference vehicle shows a crashworthiness that got rewarded with a 5 star rating in the category of adult occupant protection according to the Euro NCAP assessment standards of the year 2004 [EUR11]. One aim of the present study is to conserve the high rated crash behaviour of the crash reference vehicle while applying the different lightweight engineering measures. Other structural attributes – such as stiffness behaviour or low speed crash requirements – are as well monitored but not in the focus of the executed study steps.

3 Conversion of the Conventional to an Electric Drivetrain

In the first step of the study the transformation of the given crash reference vehicle with internal combustion engine into a full electric vehicle with 200 km driving range in the NEDC is achieved. For simplification reasons, only few modifications of the vehicle structure should be allowed. For this reason a conversion design strategy is conducted.

At first, all those internal combustion engine drivetrain (ICE) components are identified, that are not carried over to the electric vehicle. Secondly, the layout of the electric drivetrain is to be defined. Then, the structural adaptations required to integrate the electric drivetrain and to make the vehicle model meet the defined crash performance criteria are detailed.

3.1 Extraction of Conventional ICE Drivetrain Components

All drivetrain components, which do not cover any function in a full electric vehicle, can be extracted from the crash reference model (c.f. Fig. 3-1).

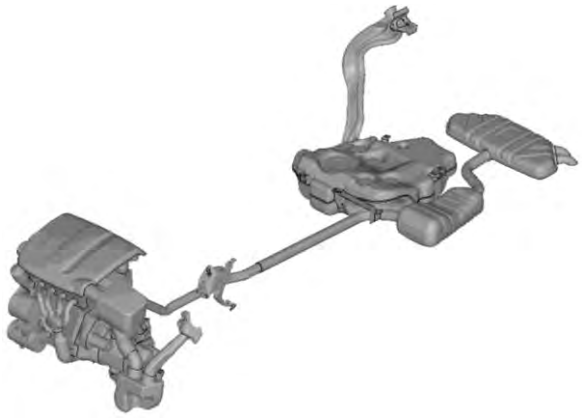

Fig. 3-1 Drivetrain components extracted from the crash reference model

This component group consists of the manual gearbox and the internal combustion engine, the fuel tank and the 90 % fuel tank fill, the clutch pedal, the exhaust system, the engine air supply system and all auxiliary components of the named parts such as brackets and fixings.

The conventional cooling system of the crash reference vehicle is maintained, as in a first approximation the same cooling system characteristics are required by the electric versions of the vehicle as by the conventional version. An additional thermal management unit for the new battery system is to be added to the vehicle separately. The weight balance of this first extraction step is detailed in Tab. 3-1.

Total weight of crash reference vehicle	**1,247 kg**
Weight of extracted powertrain, gear and peripherals	194 kg
Weight of extracted exhaust system	22 kg
Weight of extracted fuel tank system	8 kg
Weight of extracted 90 % fuel tank fill	37 kg
Vehicle weight after component extraction	**986 kg**

Tab. 3-1 Weight balance caused by the component extraction from the crash reference model

3.2 Dimensioning of the Electric Drivetrain

The goals of this dimensioning are the calculation of the electric drivetrain components layout and the evaluation of the relation between vehicle mass, energy consumption and battery capacity based on the vehicle requirements and parameters, which are defined before. The architecture of the considered driveline and all important components are illustrated in Fig. 3-2.

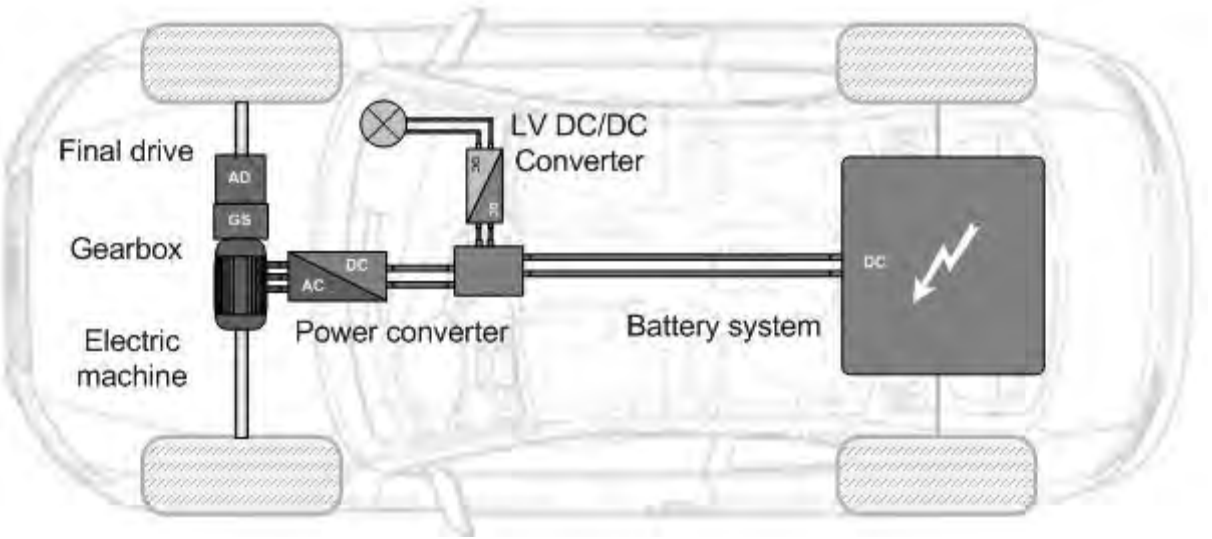

Fig. 3-2 Architecture of the battery electric driveline

The whole calculation procedure is presented in Fig. 3-3. First of all, the input parameters have to be defined. The parameters are clustered into four groups:

- Vehicle requirements
- Vehicle parameters
- Component parameters
- Driving cycle data

These parameters are then used to execute the power and range calculation. It has to be noted, that both calculations have an effect on each other, because both are mass-dependent and have an impact on the total vehicle mass.

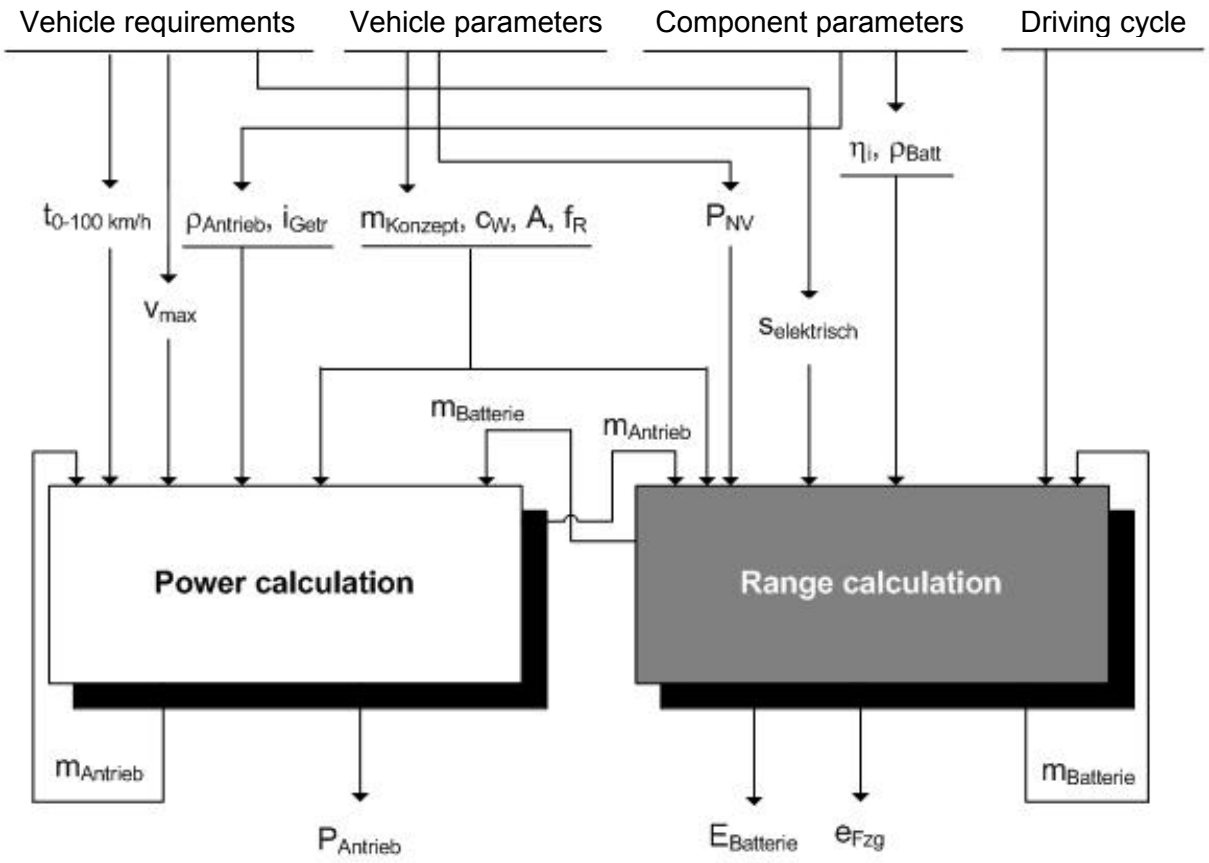

Fig. 3-3: Procedure of dimensioning the powertrain and the battery

The basic formula for all longitudinal calculations is based on the principle of conservation of force at the wheels of the vehicle:

$$\sum F_i = 0 \Leftrightarrow F_{Powertrain} - F_{Resistance} = 0 \qquad \text{Eq. 3-1}$$

$$\Rightarrow F_{Powertrain} = \left(c_d \cdot A \cdot \frac{\rho_{Air}}{2} \cdot v_{Veh}(t)^2 + \left(e_i \cdot m_{Veh} + m_{Add} \right) \cdot a_x(t) + m_{Veh} \cdot g \cdot f_r \cdot \cos \alpha_{St} + m_{Veh} \cdot g \cdot \cos \alpha_{St} \right)$$

In detail, this is the force to overcome the air resistance, the vehicle inertia while accelerating, the rolling resistance of the tires and the share caused by the road incline. The individual shares of the different driving resistances in the required driving state are defined by the vehicle-specific parameters mass, rolling resistance coefficient, drag coefficient and cross sectional area, as well as speed and/or acceleration. Except for the air resistance, all driving resistances are directly related to the vehicle mass.

The required power results from the equation above, multiplied by the driving speed:

$$P_{Demand,Wheel}(t)=\left(c_d\cdot A\cdot\frac{\rho_{Air}}{2}\cdot v_{Veh}(t)^2+(e_i\cdot m_{Veh}+m_{Add})\cdot a_x(t)+m_{Veh}\cdot g\cdot f_r\cdot\cos\alpha_{St}+m_{Veh}\cdot g\cdot\cos\alpha_{St}\right)\cdot v_{Veh}(t)$$

Eq. 3-2

Considering the efficiency of all powertrain components η_i and the electric power demand P_{LV} of the auxiliaries, the total power demand at the battery can be calculated:

$$P_{Batt}=\left(\frac{c_d\cdot A\cdot\frac{\rho_{Air}}{2}\cdot v_{Veh}(t)^2+(e_i\cdot m_{Veh}+m_{Add})\cdot a_x(t)+m_{Veh}\cdot g\cdot f_r}{\eta_i(t)}\right)\cdot v_{Veh}(t)+\frac{P_{LV}}{\eta_{DCDC}}$$

Eq. 3-3

Due to the fact, that not only static but also dynamic operations like acceleration and speed cycles are considered in this project, a longitudinal simulation model of the vehicle has to be build up. Based on the validated Matlab/ Simulink module-library of fka, the model for the battery electric vehicle is generated. This model balances the power and energy demand for different driving situations and consequently the energy consumption of the vehicle (see Fig. 3-4). Therefore it contains all relevant components of the powertrain and the battery.

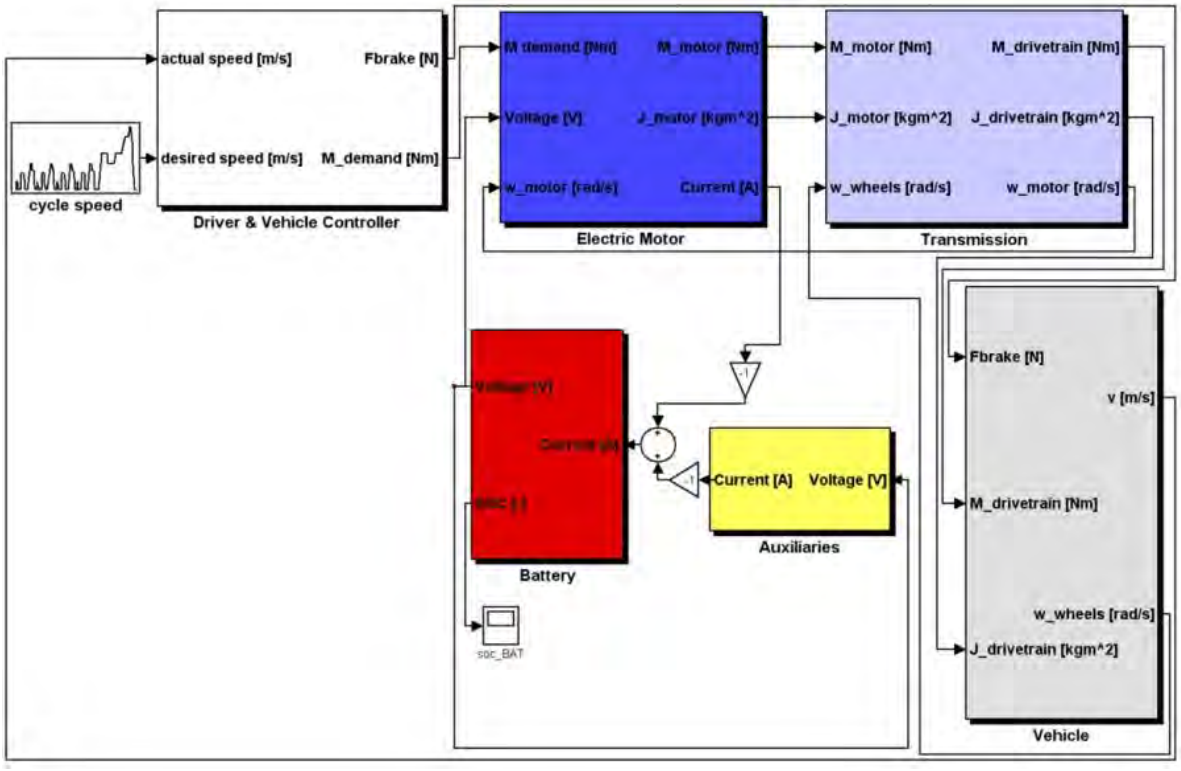

Fig. 3-4: FKA Matlab/ Simulink longitudinal simulation model

The vehicle model is implemented with a forward modeling approach. That means, that the model includes a driver model, which matches the required and actual speeds to calculate appropriate throttle and brake commands using a proportional–integral (PI) controller. The signal from throttle position is then converted to torque, which has to be supplied by the

electric machine. The torque provided by the electric machine is the input to the gearbox where the torque is transformed according to the efficiency and gear ratio. In other words, the computed torque is passed forward through the powertrain, in the direction of the physical power flow in the vehicle, until it is transformed to a traction force by the tires in the tire/road contact patch. The effects of rotational inertia are also included in the resulting acceleration calculation.

The model offers the possibility to simulate the vehicle structure with variable input parameters within different driving cycles like for example the NEDC. Furthermore, an altitude profile for the route can be assigned in order to simulate and analyze real driving cycles.

3.2.1 Definition of Boundary Conditions

Relevant requirements, parameters and input data for the drivetrain layout have to be defined.

Vehicle requirements and properties

Every product development needs certain requirements. Within a vehicle development process a lot of vehicle requirements are set at the beginning of the process. In this case we can focus on a manageable number of requirements, that will help to define the powertrain and battery attributes. This set of requirements is listed in the following:

- Range in NEDC: 200 km
- Maximum speed: 160 km/h
- Acceleration 0-100 km/h: < 10 s
- Start gradeability : 40 %

Due to the low energy density of the battery, the range goal of the vehicle is lower compared to a conventional vehicle with combustion engine. Apart from this fact the other requirements are comparable to the conventional vehicle.

Vehicle parameters

The following data set is based on the reference vehicle Volkswagen Golf V:

- Vehicle mass w/o powertrain and battery system: 997.1 kg, including on-board charger (6.2 kg) and DC/DC-converter 12 V-powernet (4.9 kg)
- Air drag coefficient c_d: 0.31
- Reference area : 2.2 m²
- Rolling resistance coefficient: 0.01
- Power demand 12 V-powernet: 250 W

Component parameters

For all considered components specific parameters for the mass-dimensioning and power-loss tables (or values) for the simulation have to be defined. Furthermore, power limits like torque limits for the electric machine and the gearbox or the maximum battery current need to be determined.

Main parts of the electric powertrain are the electric machine, the power inverter and the gearbox.

The electric machine converts the electric energy to mechanic energy and is often called "electromechanical energy converter". Depending on the vehicle concept, different electric machine models may be used. Nearly all electric machines for powertrain applications in vehicles are three-phase machines and therefore they need a power inverter, which converts the direct voltage (battery side) into an alternating voltage.

For each electric machine operating limits exist in the M/n operating chart. Here it must be differentiated between nominal and maximum values. Nominal values, such as nominal torque M_n and nominal power P_n, can be permanently requested. Whereas maximum values, such as maximum torque M_{max} and maximum power P_{max}, are only available for a short time. Limiting parameters are temperature, mechanical stability and service lifetime. If a machine is stressed beyond permitted values, thermal overload occurs due to too high currents. For example, the winding insulations melt at approx. 180°C. The complete four-quadrant operation of an electric machine is schematically illustrated in Fig. 3-5.

The torque curve is a function of the machine speed. The nominal torque is constant from 0 rpm to the nominal speed. After that the machine power is nearly constant and the torque is a function of the reciprocal of the speed (field weaking range). The maximum speed of the machine is set to 13,000 rpm. The efficiency of the electric machine is a function of input speed, torque and voltage. The losses of the inverter are included in this table.

The gearbox in the electric vehicle has to convert the torque and speed of the electric machine to the desired range at the wheels of the vehicle, so that the vehicle is able to realize large inclines and high driving speeds at the same time. Due to the high torque-utilisation and the high maximum speed of the electric machine one constant ratio is sufficient in most battery electric vehicle applications.

The efficiency of the gearbox and final drive is also a function of the operating point (speed and torque). Some efficiency lines for different input speed values of the considered gearbox are presented in Fig. 3-6.

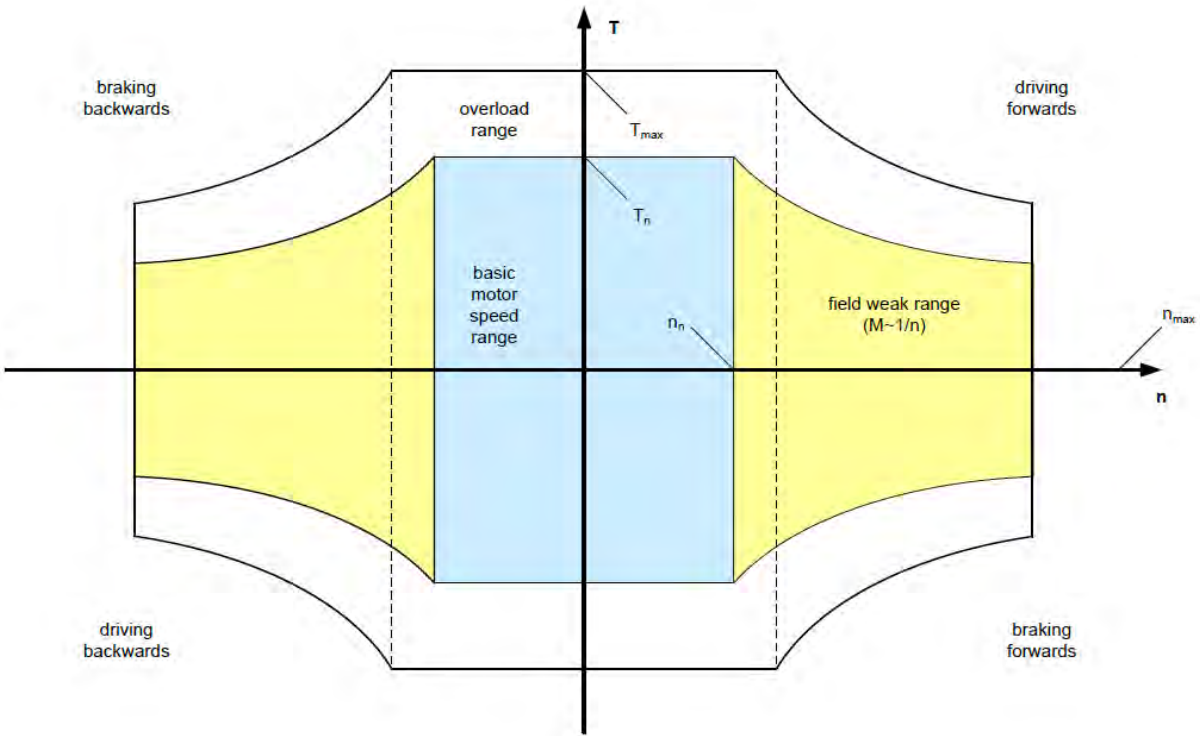

Fig. 3-5 Torque vs. speed operating map for electric machines [ECK10]

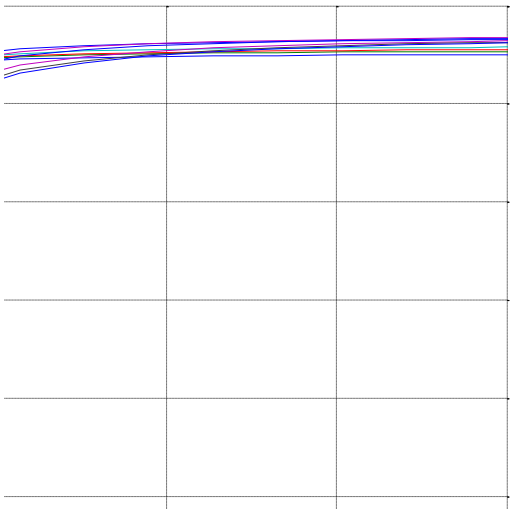

Fig. 3-6: Efficiency lines for gearbox and final drive

For the dimensioning of the powertrain components a specific power density has to be defined. Following assumptions for the power density of the powertrain components are chosen:

- Electric machine: ~1.3 kW/kg
- Power Inverter: ~10 kW/kg
- Gearbox and final drive: ~3.5 kW/kg

The base unit of a battery system is the electrochemical cell, where the conversion of chemically bound energy into electric energy (and back) takes place. This conversion is required for energy storage. A large number of different battery cell types is available with regard to shape and materials. The most promising technology nowadays with relatively high power and energy density is the Lithium-Ion battery, where lithium generates inclusion or intercalation connections with certain carbon and graphite types. If such electrodes are charged or discharged, then only the lithium ions are integrated or removed. Some of these Li-Ion battery cells are presented in a chart, where the relation between power and energy density is plotted versus the energy density of the cells (see Fig. 3-7).

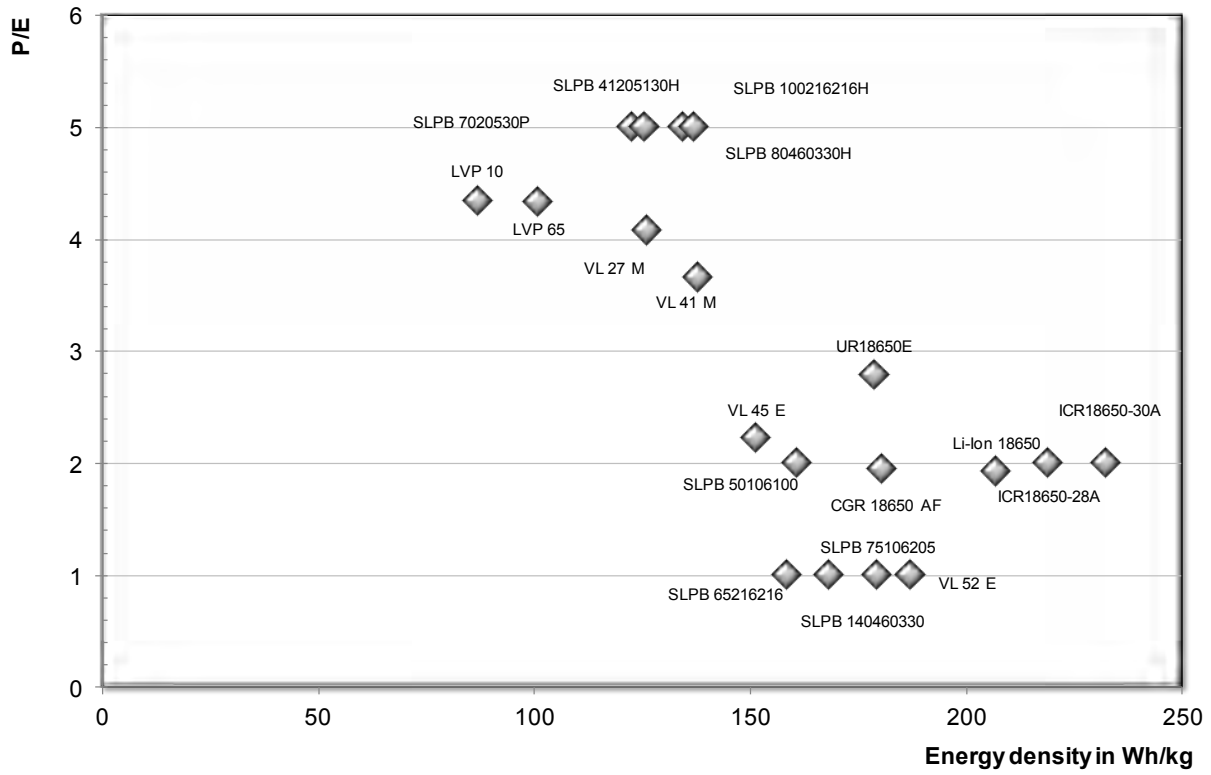

Fig. 3-7: Ragone plot for Li-Ion battery cells

Following assumptions for a possible battery cell in 2015 are made:

- Specific energy density of one battery cell: ~ 230 Wh/kg
- Nominal voltage: 3.7 V
- Nominal energy content: 244 Wh
- Cell mass (without housing): 0.94 kg

In addition to the battery cells more components are necessary to build up a battery system (see Fig. 3-8). A battery consists of serial and/or parallel connections of modules/cells of the same type and the same capacity. If several chains of cells should be connected in parallel in a battery, all the chains must contain the same number of modules/cells connected in series. Chains with different voltages may not be connected in parallel. Battery modules consist of few in series and/or parallel connected cells, which are installed in housing and surrounded by common insulation.

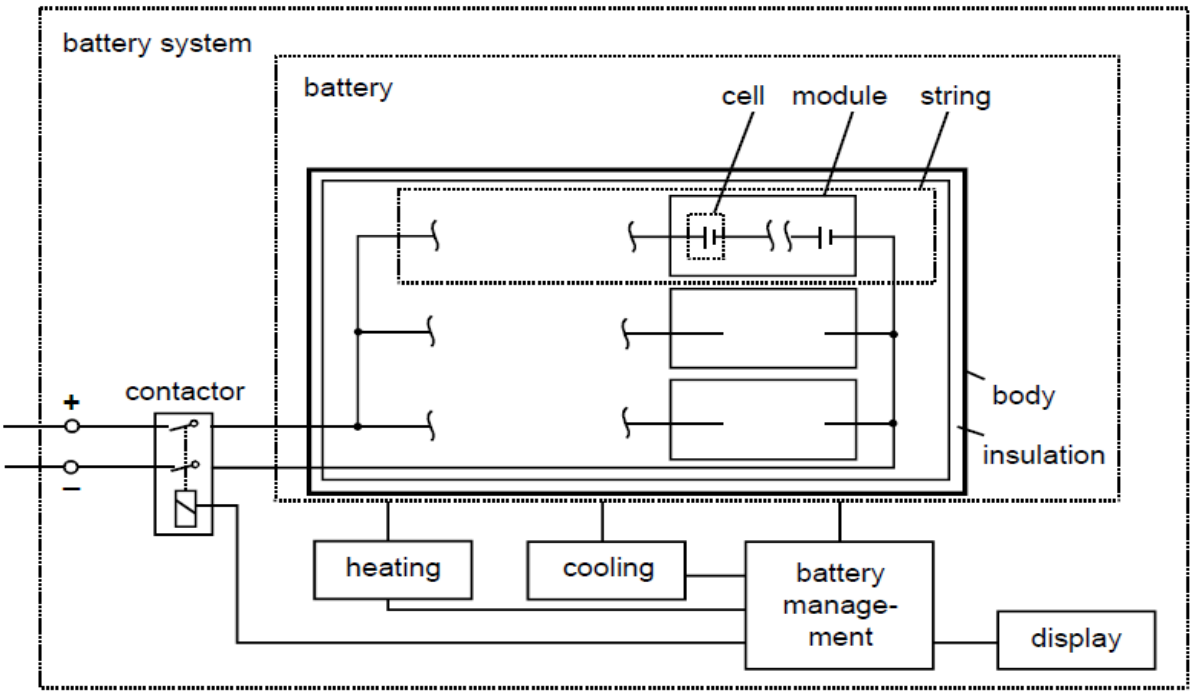

Fig. 3-8: Battery system components

A battery system consists of elements for energy storage, all peripheral equipment required for operation, such as heating and cooling aggregates, two main contactors as well as a battery management unit, which monitors the battery's conditions/states and protects the battery against overcharge and deep discharge. The periphery enables a safe and controlled usage of the battery, but increases the system mass. With regard to this periphery mass the energy density of the battery is lower compared to the battery cell. For the calculation a battery system energy density of $\rho_{ele,Batt}$=160 Wh/kg is assumed. Furthermore it is assumed, that 80 % of the total energy content of the battery system can be used.

3.2.2 Power calculation

The procedure for the power calculation is illustrated in Fig. 3-9. First of all, the gearbox ratio has to be defined and the mass of the battery system has to be assumed in order to get a reasonable vehicle mass including battery mass but excluding powertrain mass.

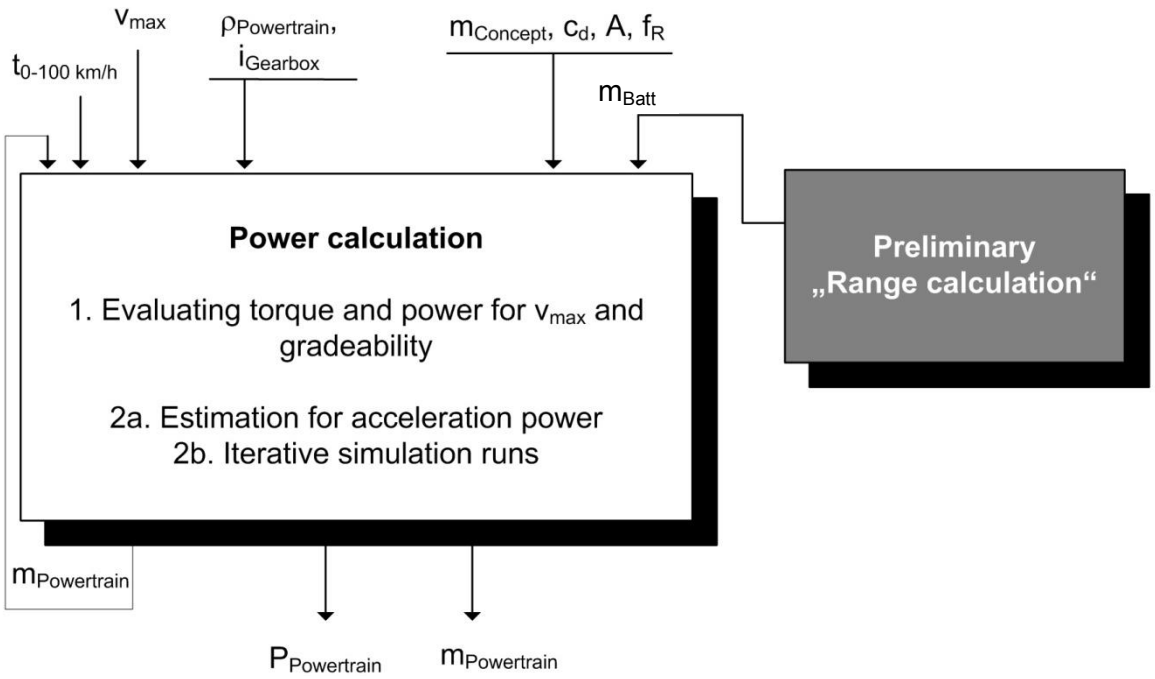

Fig. 3-9 Procedure for dimensioning of the powertrain

The gear ratio is crucial for the achievable vehicle speed. With the help of the relation between the speed of the electric machine n_{EM} and the vehicle speed

$$v_{max}=\frac{2\cdot\pi\cdot n_{EM}\cdot r_{dyn}}{i_{Gear}} \qquad \text{Eq. 3-4}$$

it is possible to calculate the gear ratio for the maximum vehicle speed of 160 km/h:

$$\Leftrightarrow i_{Gear}=\frac{2\cdot\pi\cdot n_{EM}\cdot r_{dyn}}{v_{max}}=9.5 \qquad \text{Eq. 3-5}$$

Furthermore the input vehicle mass for the power calculation m_{PC} is calculated. It is the sum of the vehicle mass without powertrain and the preliminary calculated battery mass m_{Batt^*} (for the battery mass calculation see subchapter 3.2.3):

$$m_{PC}=m_{Concept}+m_{Batt}=m_{Concept}+\frac{(a\cdot m_{Concept}+b)}{\left(\frac{\rho_{ele,Batt}\cdot x_{Batt}}{s_{ele}}-a\right)}=1{,}238\ kg \qquad \text{Eq. 3-6}$$

With this vehicle mass and the other vehicle parameters the calculation of the static requirements (maximum speed and start gradeability) is performed. A summary of this calculation is illustrated in the traction torque chart, see Fig. 3-10.

Fig. 3-10: Traction torque chart

It can be seen, that for the maximum vehicle speed of 160 km/h a nominal power of the electric machine of 45 kW is required. Furthermore the maximum torque at the wheel to procure the start gradeability of 40 % has to be 1,550 Nm. With the gear ratio of 9.5 the maximum torque at the electric machine is set to 160 Nm. Note, that this torque is only needed and available for a short time sequence (< 10 s), so it corresponds to the peak torque of the electric machine.

With these values the whole data set of the electric machine can be generated, including the torque curve (motor and generator mode) and the efficiency map (see Fig. 3-11).

In the next step the acceleration of the vehicle is calculated with the help of the simulation model. The simulation results for the full load operation of the vehicle are illustrated in Fig. 3-12.

It can be seen, that acceleration time from 0 km/h to 100 km/h is below 10 s. The results for the vehicle acceleration illustrate that within the first three seconds the electric machine is being operated with peak torque. After that the field weakening area begins, so that the torque of the machine and due to that the acceleration of the vehicle decreases. Note that the simulation is done without considering the tire slip of the vehicle.

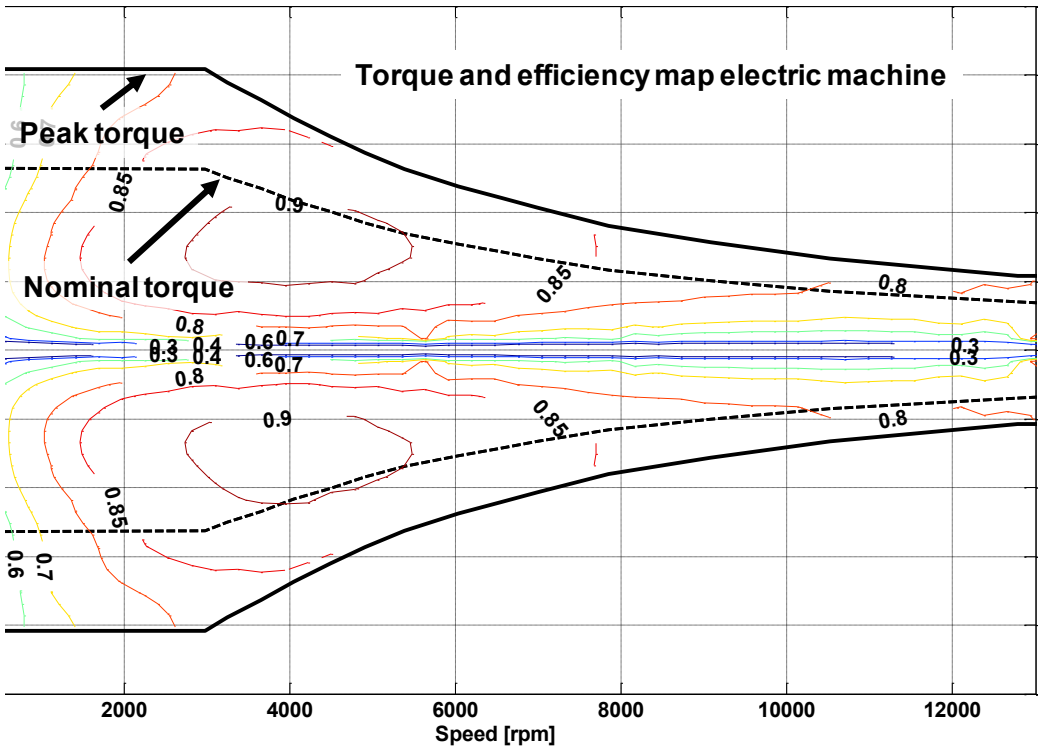

Fig. 3-11: Torque curve and efficiency map of the electric machine

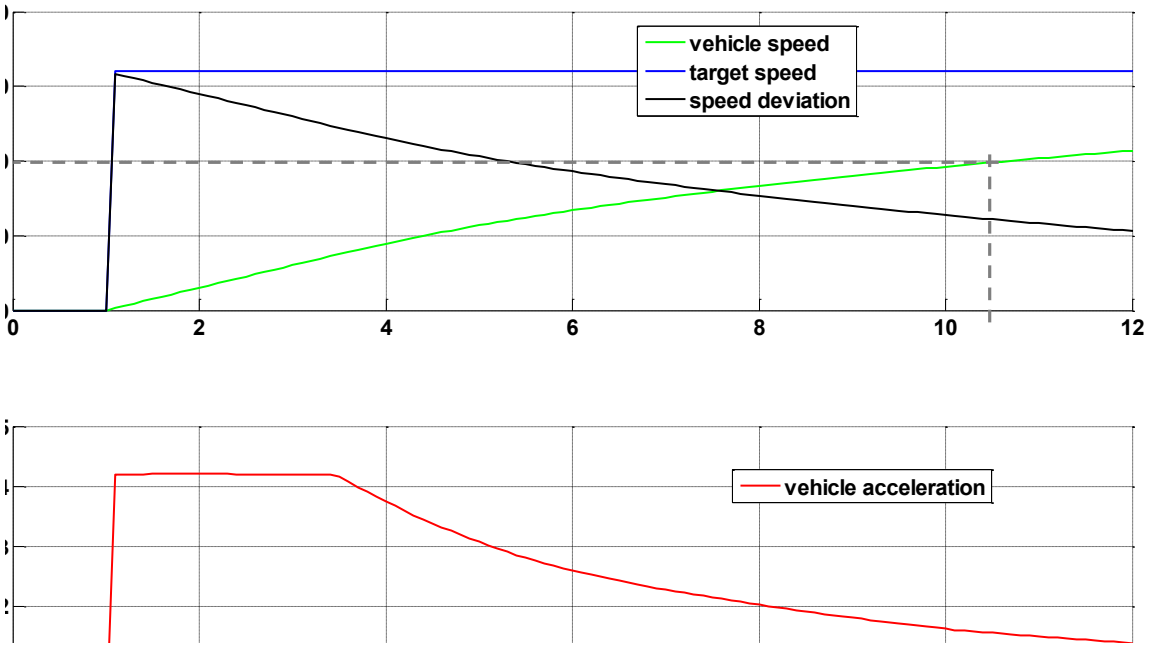

Fig. 3-12: Simulation results for full-load acceleration

The resulting powertrain has the following characteristics:

- Peak power electric machine : 66 kW
- Nominal power: 45 kW
- Max. torque at wheel: 1,550 Nm
- Max. torque of electric machine: > 160 Nm
- Mass of electric machine: 50 kg
- Gear ratio: 9.5

3.2.3 Range calculation

The procedure for the range calculation is illustrated in Fig. 3-13.

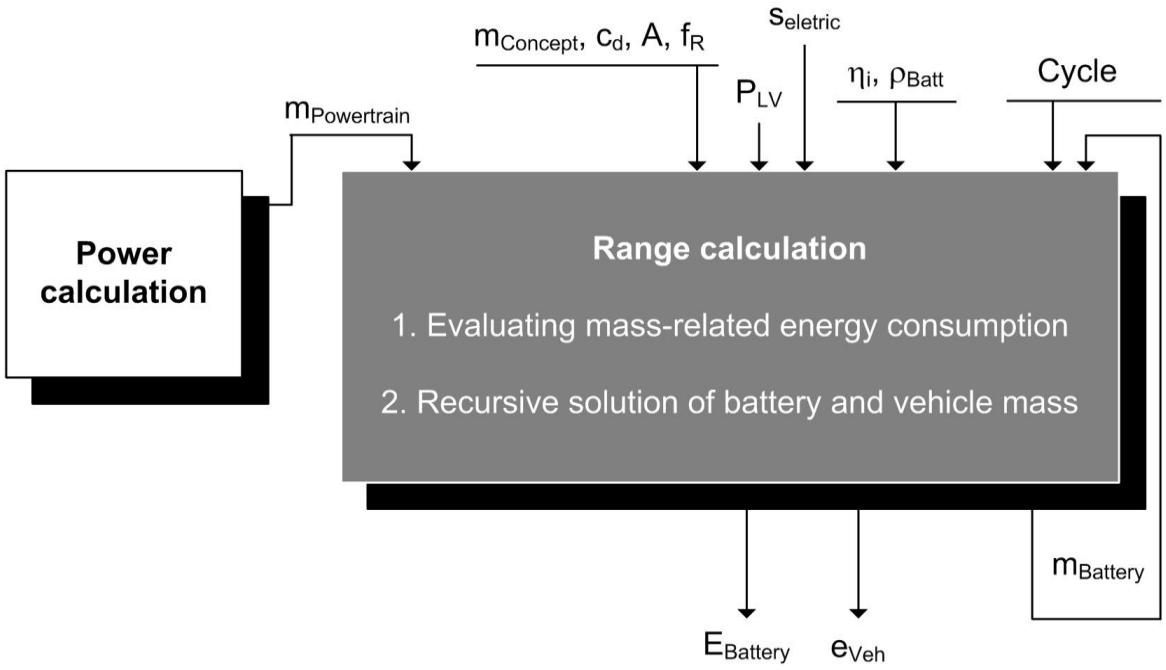

Fig. 3-13 Battery layout procedure

The basic formula for the range calculation evaluates the energy content of the battery system according to the specific energy consumption of the vehicle e_{Veh} and the desired electric range s_{ele}:

$$E_{Batt}=e_{veh} \cdot s_{ele} \qquad \text{Eq. 3-7}$$

Due to the fact that the energy consumption of the vehicle is related to the vehicle mass and that the vehicle mass includes the battery mass and therefore influences the electric range the formula can be converted in order to calculate the battery mass according to the desired range and the vehicle mass without battery:

$$m_{Batt} = \frac{e_{Veh} \cdot s_{ele}}{\rho_{ele,Batt}} \qquad \text{Eq. 3-8}$$

with $e_{Veh} = f(m_{Veh}, m_{Batt})$

First of all, the mass-related energy consumption is calculated with the simulation model. Therefore the simulation is carried out with different vehicle masses in a range from 900 kg to 1,600 kg. Besides the typical EU and US driving cycles, a representative city cycle is considered. All speed profiles are illustrated in the appendix of this report (see chapter 12.2). The resulting energy consumption in kWh/100 km for these variants for all driving cycles is illustrated in Fig. 3-14.

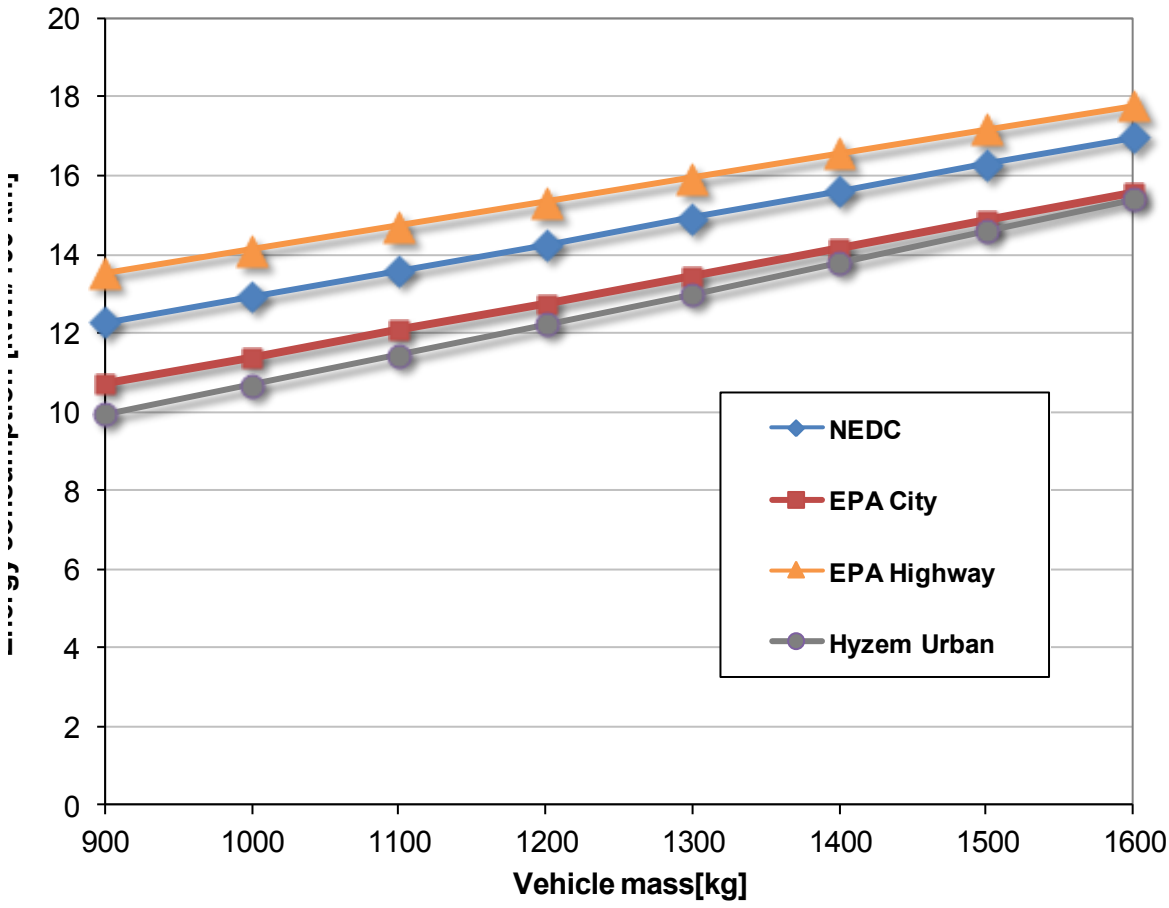

Fig. 3-14: Simulation results in different driving cycles

The energy consumption in the NEDC for a vehicle mass between 900 kg and 1,600 kg is almost linearly dependent on the vehicle mass. The gradient “a” and the intercept “b” of this function depend on the selected driving cycle and the dimensioning of the powertrain components:

$$a=\frac{(e_{Veh_2}-e_{Veh_1})}{(m_{Veh_2}-m_{Veh_1})}$$ Eq. 3-9

The y-intercept of this function for a virtual vehicle weight of 0 kg describes the basic consumption and is depending on the air resistance of the vehicle as well as the losses of the powertrain and the electric consumers:

$$b=e(m_{Veh}=0)$$ Eq. 3-10

The values for the cycle specific mass gradient a and the cycle specific basic consumption b for four different cycles are presented in Tab. 3-2.

	a	b
NEDC	0.0067 kWh/100 km/kg	6.18 kWh/100 km
EPA City	0.0069 kWh/100 km/kg	4.40 kWh/100 km
EPA Highway	0.0061 kWh/100 km/kg	8.00 kWh/100 km
Hyzem Urban	0.0078 kWh/100 km/kg	2.84 kWh/100 km

Tab. 3-2 Cycle specific energy consumption parameters

With the parameters a and b the energy consumption of the vehicle can be described as a linear function:

$$e_{veh}=a\cdot(m_{Veh}+m_{Batt})+b$$ Eq. 3-11

With this function the battery mass m_{Batt} and the energy content E_{Batt} can be evaluated:

$$m_{Batt}=\frac{(a\cdot m_{Veh}+b)}{\left(\frac{\rho_{ele,Batt}\cdot x_{Batt}}{s_{ele}}-a\right)}$$ Eq. 3-12

$$E_{Batt}=m_{Batt}\cdot\rho_{ele,Batt}=\frac{(a\cdot m_{Veh}+b)}{\left(\frac{x_{Batt}}{s_{ele}}-\frac{a}{\rho_{ele,Batt}}\right)}$$ Eq. 3-13

With:

- a Cycle-specific mass gradient
- b Cycle-specific absolute consumption
- m_{Veh} Vehicle mass w/o battery
- s_{ele} Electric Range
- x_{Batt} Useable SOC-range
- $\rho_{ele,Batt}$ Specific battery energy density

With the desired range of 200 km in the NEDC and the specific parameters of the battery system, that were presented before, the mass of the battery system is 232 kg and the resulting energy content 37.6 kWh.

With the total vehicle mass of 1,328 kg including the powertrain mass and the mass of the battery system, the energy consumption and the resulting electric range in all cycles can be evaluated. The results for the driving range are illustrated in Fig. 3-15.

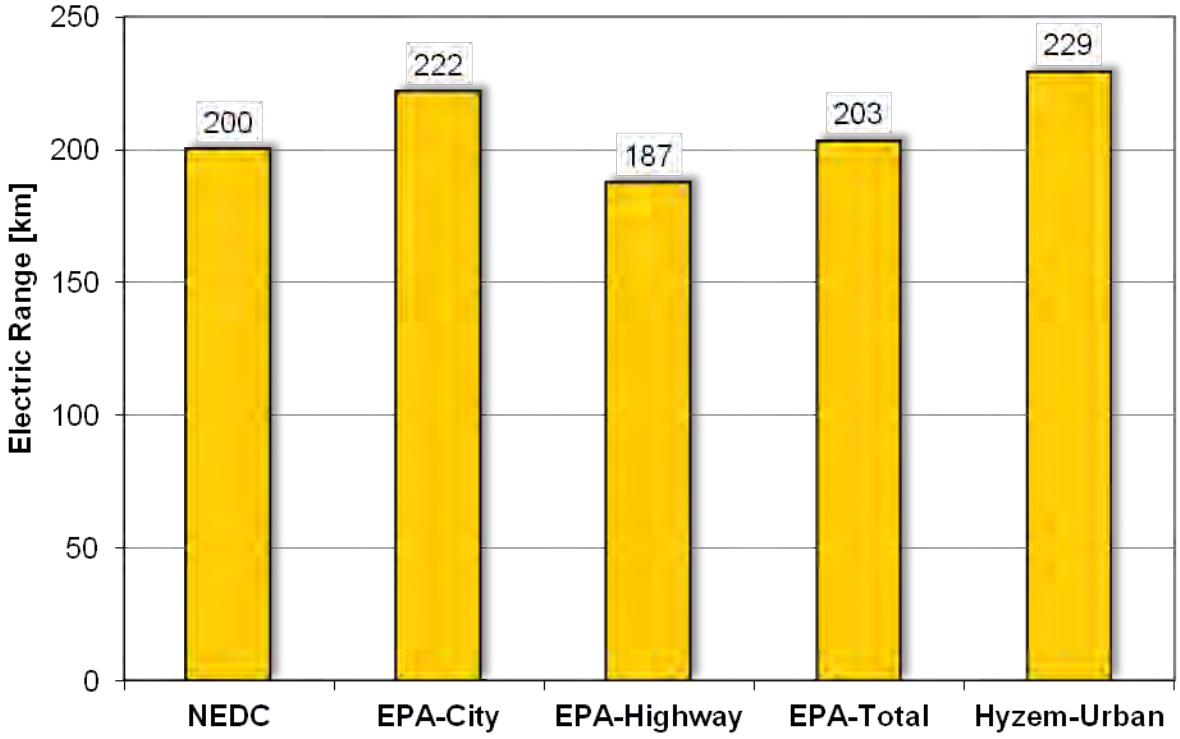

Fig. 3-15 Driving range of the electric reference vehicle in different driving cycles

Due to lower specific energy consumptions in the cycles “EPA-City” and “Hyzem-Urban”, the range in these cycles is higher than the NEDC-range. Solely the range in the EPA Highway is lower because of the higher average vehicle speed. The total EPA range, which is an average value of the city and highway part, is quiet comparable to the NEDC range.

3.2.4 Resulting Battery System

With the given battery integration space and the imperative of avoiding too many modifications to the vehicle’s structural parts, standard size battery cells in cylindrical form are chosen. With this cell form a maximum number of cells can be installed within the vehicle with very little structural modifications. The resulting battery system has the following energetic features:

- Energy content: 37.6 kWh
- Nominal power: 58.4 kW

- Number of cells: 154
- Electric connection: 2 parallel, 77 in series
- Cylindrical cell dimensions: diameter 54 mm, length 222 mm
- Total cell mass: 165 kg
- Total battery system mass: 232 kg
- Nominal battery voltage: 294 V

3.3 Geometrical Design of the Electric Drivetrain

According to the dimensioning for a 200 km drive range in the NEDC, 154 cylindrical battery cells have to be arranged within the vehicle without a significant reduction of the usable space for passengers and luggage. At the same time other requirements, such as crash safety and thermal management, have to be considered.

The extraction of the unused conventional drivetrain components leaves significant space within the vehicle tunnel and below the rear seats. These volumes, situated below the passenger survival space, offer the highest safety against deformation [SCH11]. For this reason a T-shaped arrangement of the battery cells within the tunnel and the former fuel tank space is chosen (c.f. Fig. 3-16). To increase the safety against intrusion into the battery pack in the tunnel area in case of side crash impacts, a gap of 110 mm length is included on the x-axis level of the front seat crossbeams.

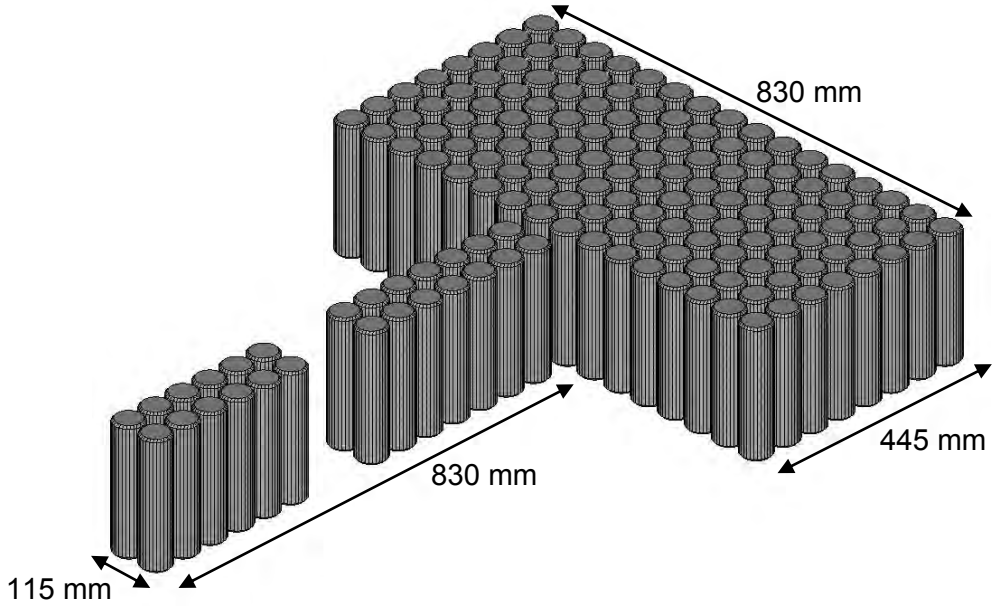

Fig. 3-16 Arrangement of the 154 cylindrical battery cells

The battery cells are included in a steel frame with holes at every cell top for cooling reasons. To stabilise the cells within the frames, a plastic inner structure in honeycomb form is integrated into the steel frame (c.f. Fig. 3-17). The cell holding frames are sat under pretension by crossed steel plates.

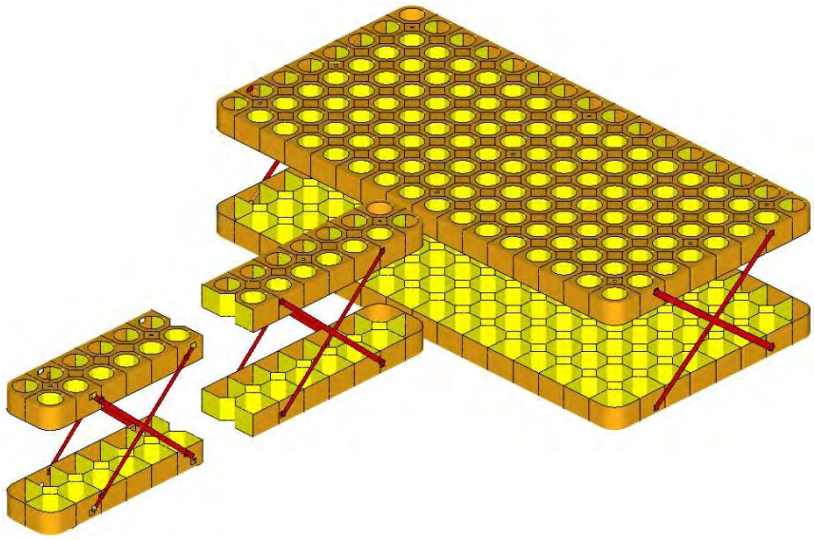

Fig. 3-17 Battery system – Inner cell holder system

The inner cell holder system is put onto a cooling plate and the whole assembly is fixed on an even aluminium plate closing the tunnel space and the former fuel tank space against the exterior. The battery management electronic components are situated in front of the battery cells. The structure is covered by a plastic housing. An extruded aluminium framework is bolted to the even ground plate at the rear end and the floor to attach the system to the central floor and the rear axle crossbeam of the vehicle (c.f. Fig. 3-18).

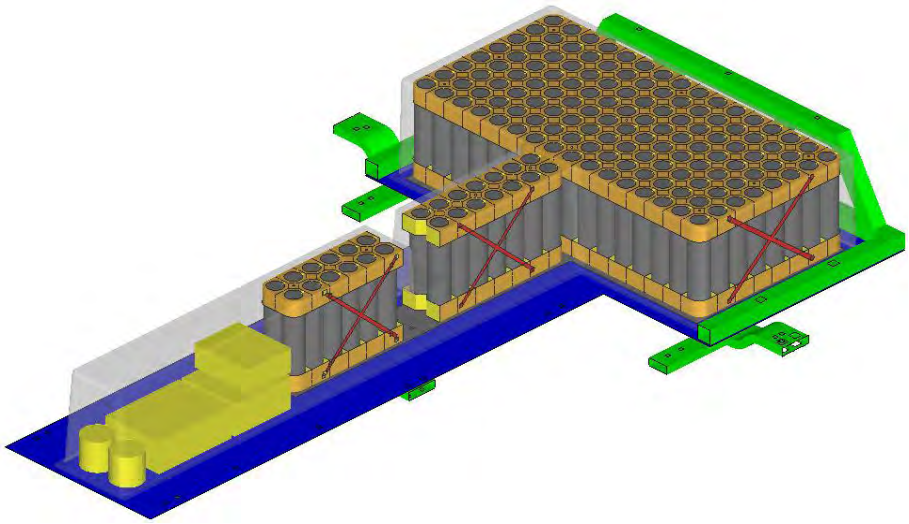

Fig. 3-18 Complete battery system

The presented battery system design is frozen throughout the study. The weight characteristics of the battery system are described in Tab. 3-3.

Total weight of battery system	**232 kg**
Weight of 154 battery cells	165 kg
Weight of system peripheries (electronics, cooling)	23 kg
Weight of battery system structure	44 kg

Tab. 3-3 Weight of the battery system of the electric reference vehicle

The electric engine-gear unit chosen to fulfil the defined driving task is integrated into the vehicle's front using the mounting components of the crash reference model. With the help of a profile framework electronic components required for the management of the electric powertrain are mounted onto the top of the engine-gear-unit (c.f. Fig. 3-19). Other new periphery components are fixed to the bulkhead near the brake booster, the engine mounting and the subframe near the battery system's front end. The weight characteristics of the new front vehicle components are listed in Tab. 3-4.

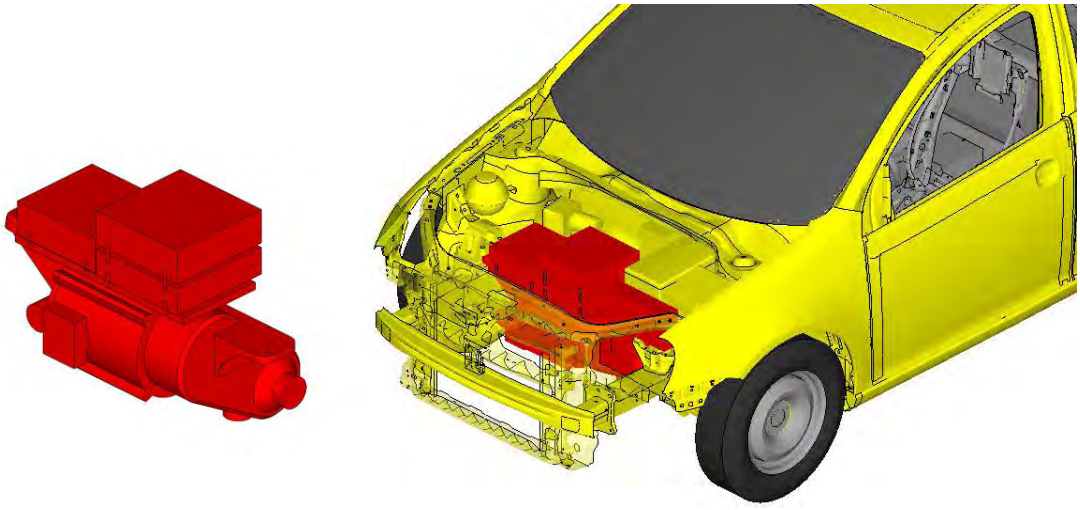

Fig. 3-19 Electric engine-gear unit and engine electronics (left) and the vehicle front of the electric reference vehicle (right)

Total weight of new front vehicle components	**99 kg**
Engine-gear-unit	70 kg
Powertrain electronics (switchbox)	2 kg
Powertrain electronics (frequency converter)	7 kg
Powertrain electronics (battery charger)	6 kg
Powertrain electronics (DC/DC converter)	5 kg
Vacuum pump	3 kg
PTC heater module	2 kg
Additional mounting and fixing elements	4 kg

Tab. 3-4 Weight of new front vehicle components

3.4 Structural Integration of the Battery System into the Vehicle

Although a conversion design strategy is followed in this study, decent modifications of the floor structure appear necessary to integrate the battery system into the vehicle. Due to the given dimensions of standardised cylindrical battery cells and the additional proportions of the battery system periphery and structural elements, some overlaps with the crash reference vehicle's floor structure occur (c.f. Fig. 3-20).

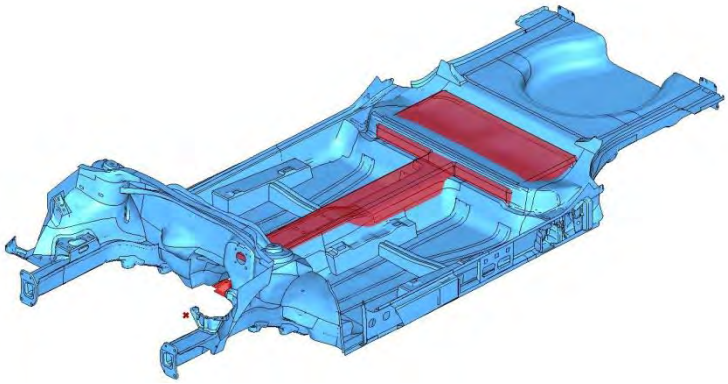

Fig. 3-20 Overlaps of the crash reference model with the battery system

To remove these conflicts, the upper cover of the tunnel has to be elevated by 15 mm to the front and by 65 mm to the rear segment. No enlargements to the side are necessary, so the modifications do not impact the front seats or the seat mounting systems. The back seat cover has to be elevated by 27 mm. In this way a new floor architecture with modified floor sheets and reinforcement panels is created (c.f. Fig. 3-21).

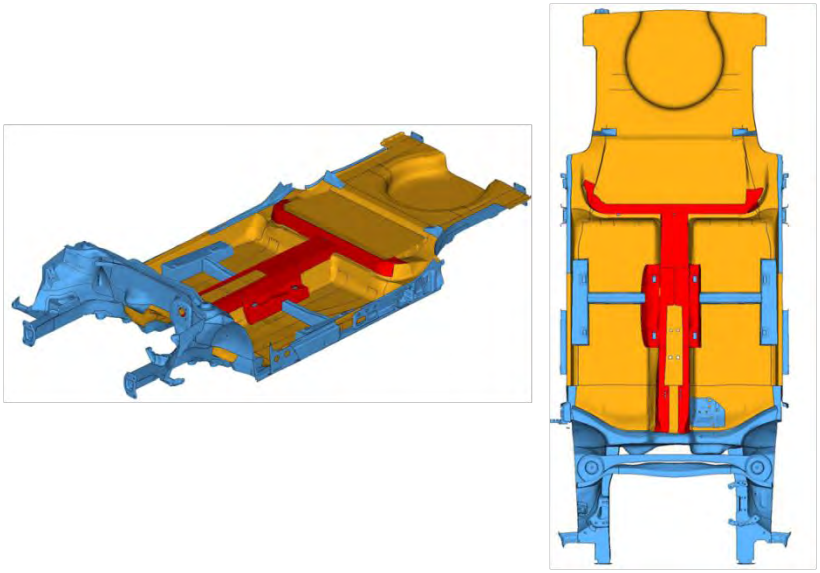

Fig. 3-21 Modified floor sheets (yellow) and reinforcement sheets (red) for battery system integration

To reach the high crashworthiness standards of the crash reference vehicle and at the same time to protect the battery cells from any deformation, additional structural floor elements are necessary (c.f. Fig. 3-22). New hat-profile longitudinal beams on the level of the rocker rail are required to reduce the global intrusion of side barriers into the vehicle side. In addition, a central crossbeam is mounted on B pillar level, to stiffen the floor structures below the front seats and the tunnel. Finally a reinforcement element is added to the top of the tunnel and into the battery cell gap to hinder front seat crossbeams from intruding into the tunnel space. These strong modifications, representing additional structural weight of 12 kg, are necessary to change the response nature of the crash reference vehicle's floor structure in case of side impacting, which originally was based on a significant deformation of the tunnel.

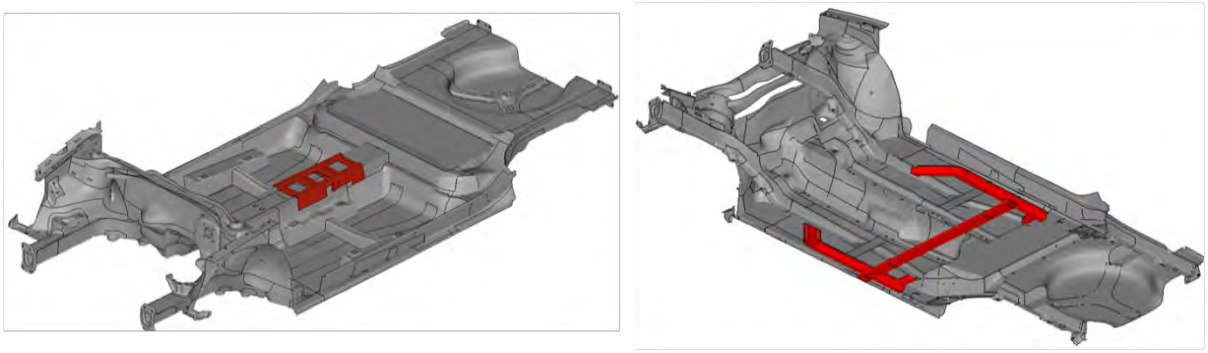

Fig. 3-22 Electric reference vehicle floor with crash related adaptations (red)

3.5 Final Summary of the Electric Reference Vehicle's Characteristics

The electric reference vehicle finally achieved resulting from the study's first step has the following features:

- Total vehicle mass: 1,328 kg
- Axle load distribution (front/rear): 55/45
- Weight of body-in-white structure (steel unibody): 272 kg

With the structural design completed, the crashworthiness of the electric reference vehicle can be assessed.

3.6 Analysis of the Electric Reference Vehicle's Crash Performance

In a similar way as for the crash reference vehicle, the crash behaviour of the electric reference model is simulated for the four analysed crash loadcases. In addition to the already described intrusion and acceleration aspects, also the protection of the battery cells against deformation is monitored. Euro NCAP rating standards do not provide any specific assessment criteria for electric vehicles. The same standards as for gasoline vehicles are applied [EUR10].

3.6.1 Euro NCAP Front Crash Behaviour of the Electric Reference Model

Fig. 3-23 shows the progression of the Euro NCAP crash test simulated for the electric reference vehicle. As the vehicle front package is different, also the intrusion behaviour on the bulkhead level into the passenger compartment changes. For the critical intrusion points (according to Fig. 3-24), the experienced intrusion values remain on a level of under 50 mm (c.f. Fig. 3-25). Concerning this aspect, the crash behaviour of the crash reference version is fully conserved.

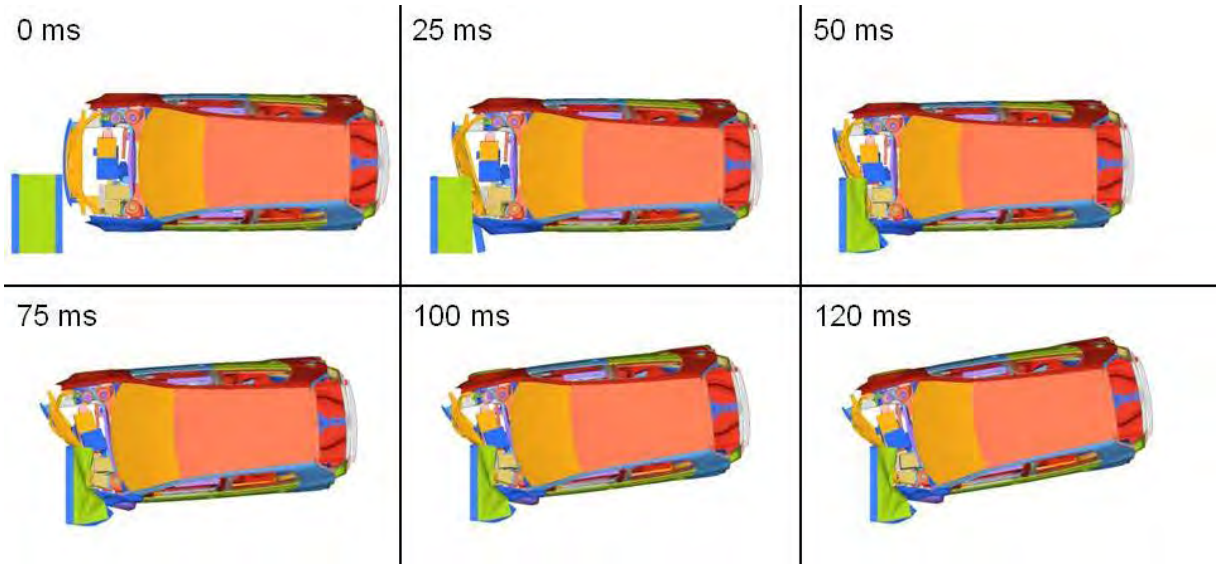

Fig. 3-23 Euro NCAP front crash progression for the electric reference model

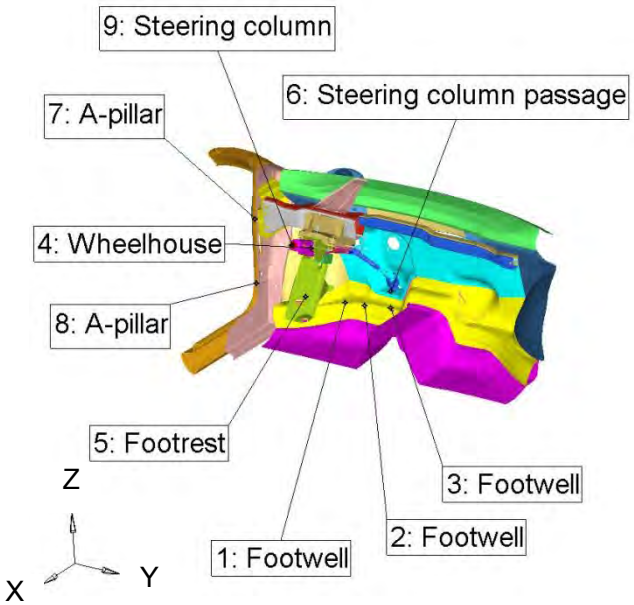

Fig. 3-24 Tracked points for intrusion in case of offset front crash (Euro NCAP)

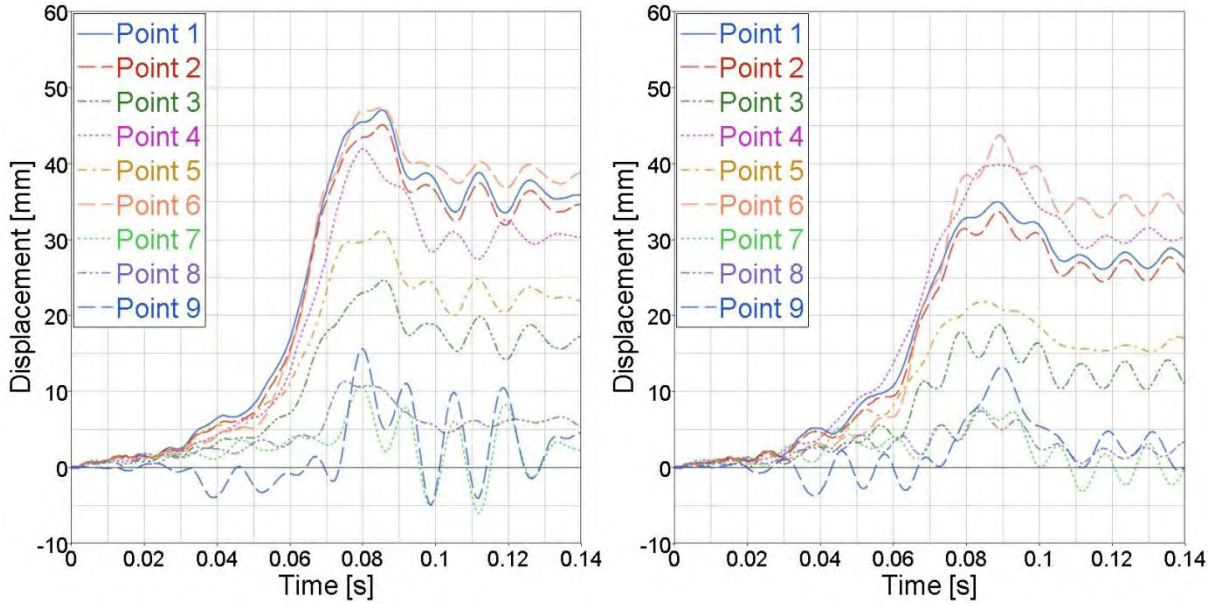

Fig. 3-25 Intrusion at evaluation points during front crash – comparison of crash reference (left) to electric reference vehicle (right)

As the front package components have changed in position, dimension and shape, a different general intrusion picture can be detected (c.f. Fig. 3-26).

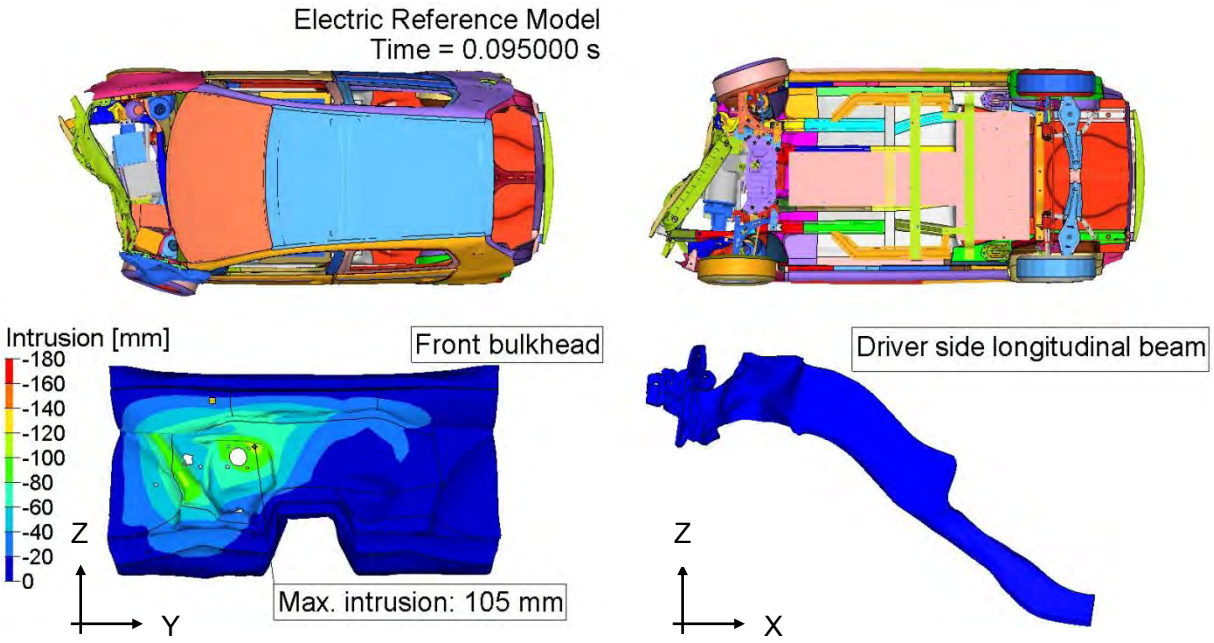

Fig. 3-26 Electric reference model – Front crash behaviour at time of maximum intrusion

For the vehicle with electric powertrain the highest intrusions can be detected in a central bulkhead position, near the brake booster hole. Although major components of the body structure remain unchanged, the deceleration behaviour during the crash progression

changes, as the total vehicle mass changes together with other inertia properties (c.f. Fig. 3-27). Deceleration in x-axis direction appears more stretched and therefore softer.

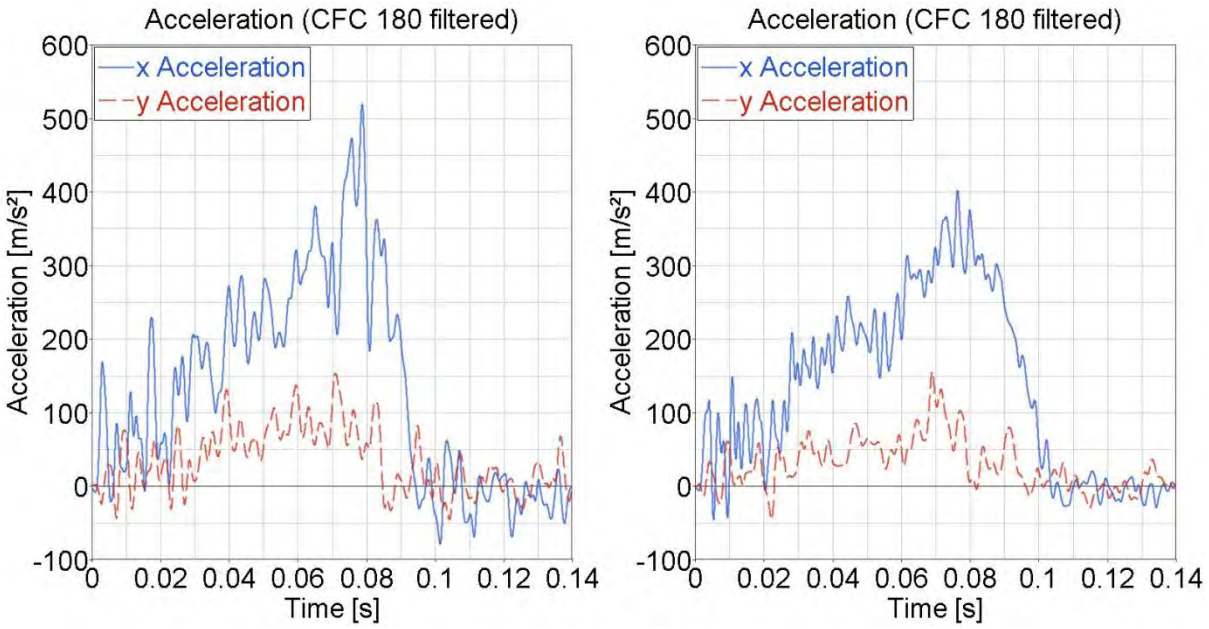

Fig. 3-27 Comparison of deceleration of vehicle centre during front crash for crash reference (left) and electric reference model (right)

The battery system position was chosen at a place of generally low deformation danger, therefore no deformation risk for the cells can be detected. As the front crash is performed at highest crash speed (64 km/h), the battery cells have to be fixed against inertia related movements.

3.6.2 Euro NCAP Side Crash Behaviour of the Electric Reference Model

The side crash performed with the electric reference vehicle clearly shows the effects of the side stiffening measures applied to protect the tunnel space against deformation and collapse (c.f. Fig. 3-28 and Fig. 3-29).

As the comparison for the monitored intrusion points shows (c.f. Fig. 3-30), intrusion values drop significantly to a level generally below 180 mm. Meanwhile accelerations in y-axis direction remain on the same level (c.f. Fig. 3-31).

For this loadcase as also for the pole side crash loadcase, battery cell protection imperatives overrule all other possible indicators. Thus side stiffening measures that appear exaggerated regarding general intrusion and even resulting in higher acceleration values are justified.

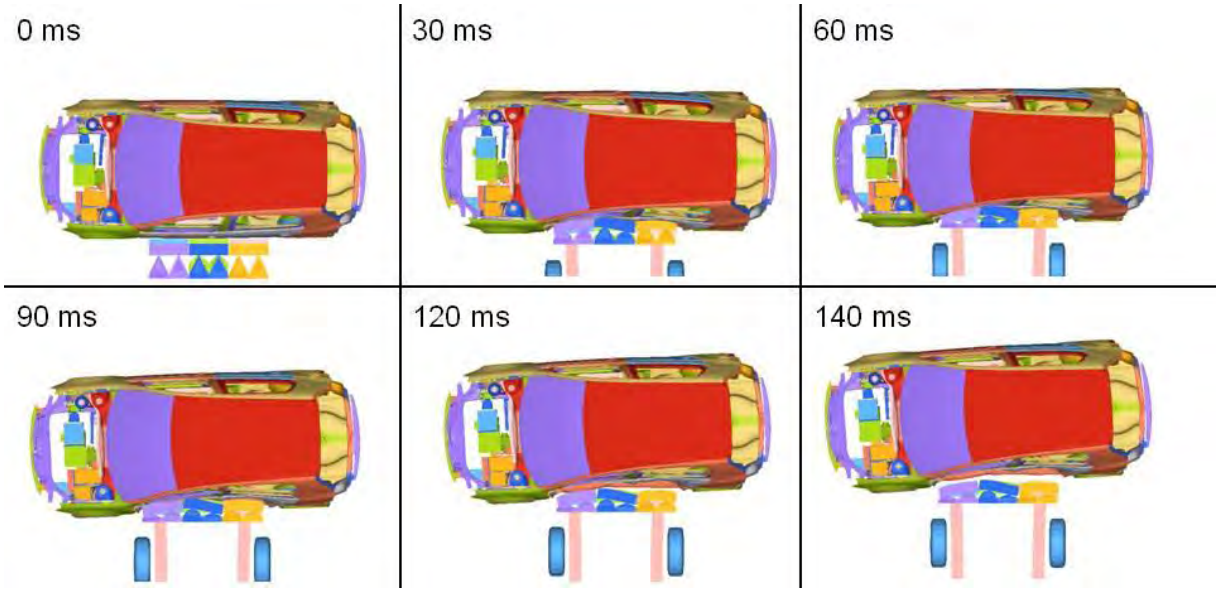

Fig. 3-28 Euro NCAP side crash progression for the electric reference model

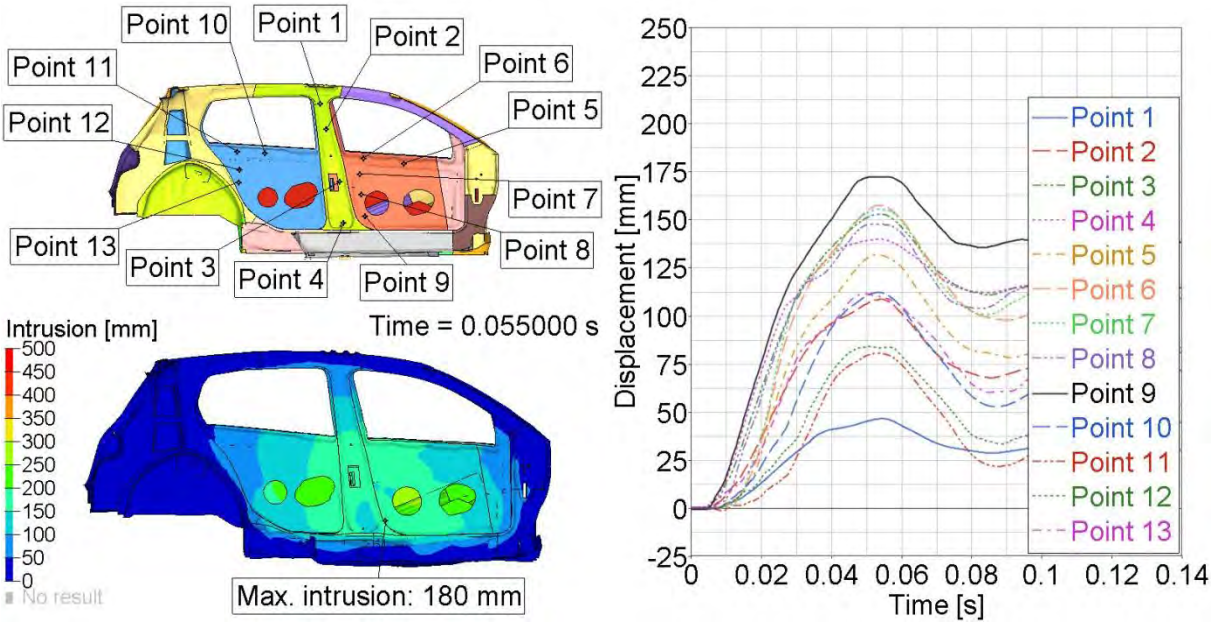

Fig. 3-29 Electric reference model – Side overview at time of maximum intrusion (low, left) and intrusion behaviour over crash duration for monitored points (right) during side crash

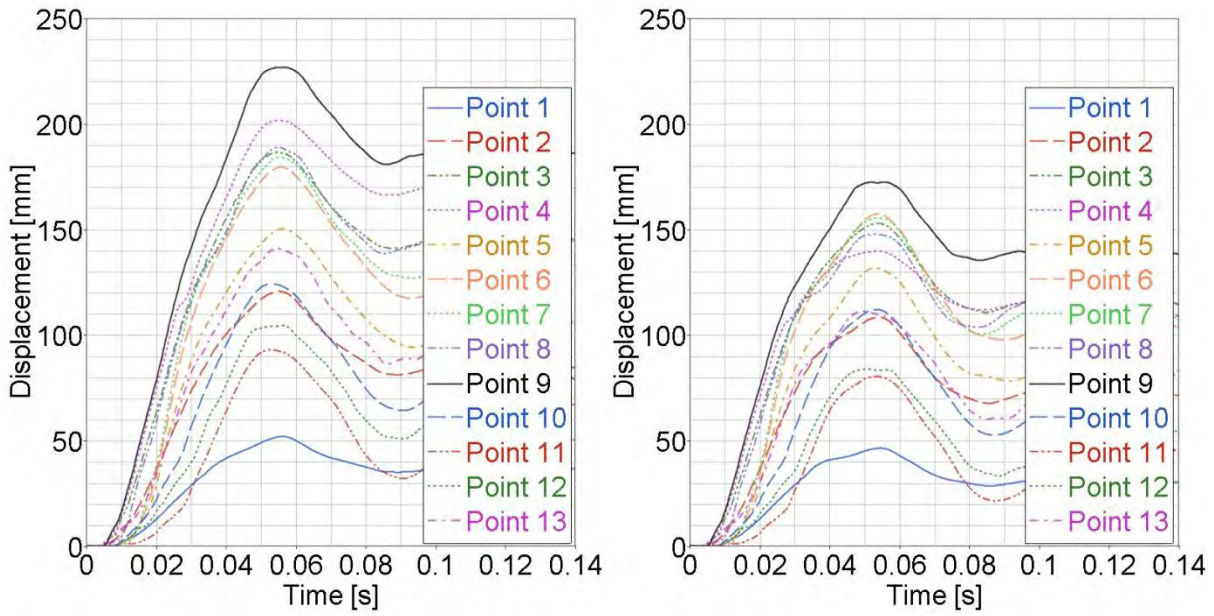

Fig. 3-30 Intrusion at evaluation points during side crash – Comparison of crash reference (left) to electric reference vehicle (right)

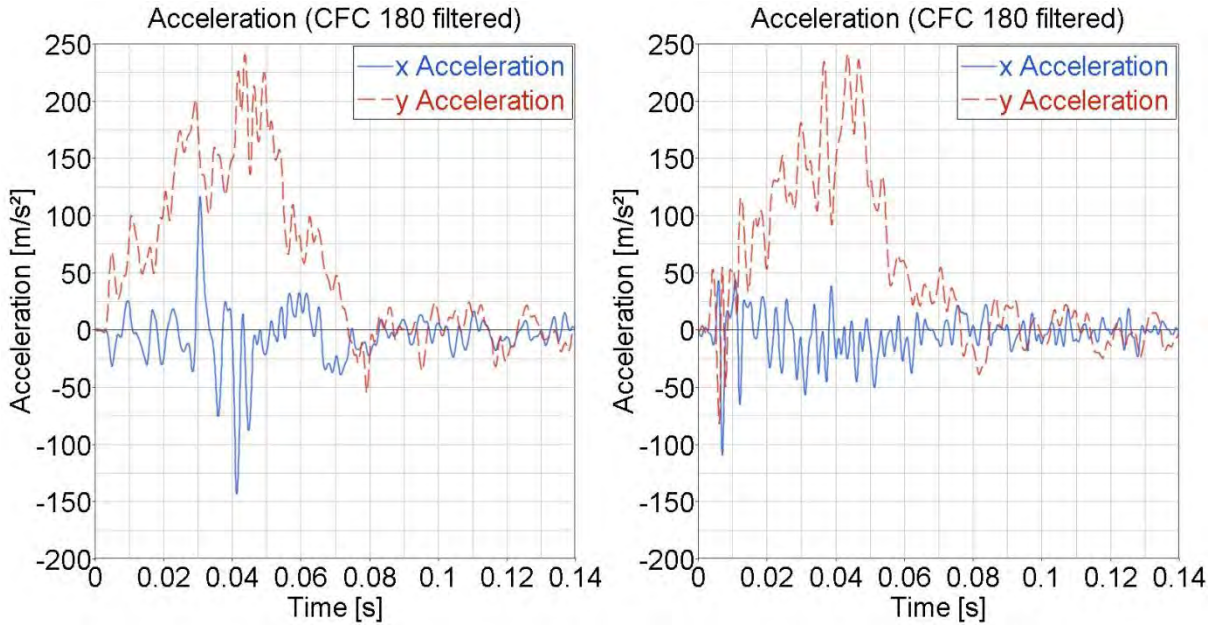

Fig. 3-31 Vehicle centre acceleration during side crash – Comparison of crash reference (left) to electric reference vehicle (right)

3.6.3 Euro NCAP Pole Side Crash Behaviour of the Electric Reference Model

The effects already detected during the side crash are visible in even more evident form for the pole side crash (c.f. Fig. 3-32 and Fig. 3-33).

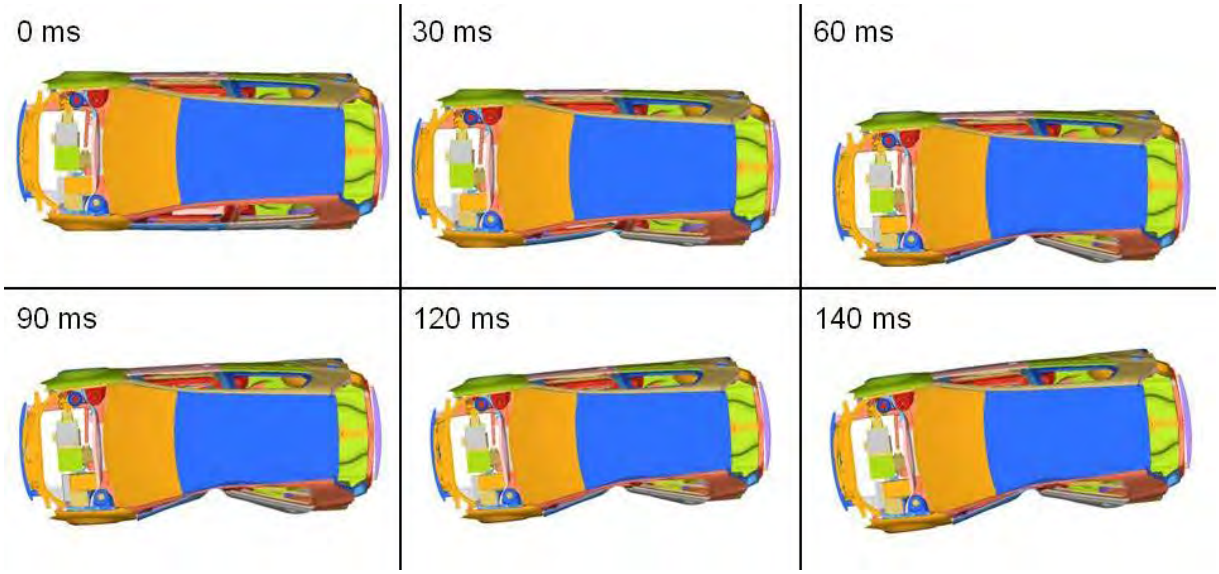

Fig. 3-32 Euro NCAP pole side crash progression for the electric reference model

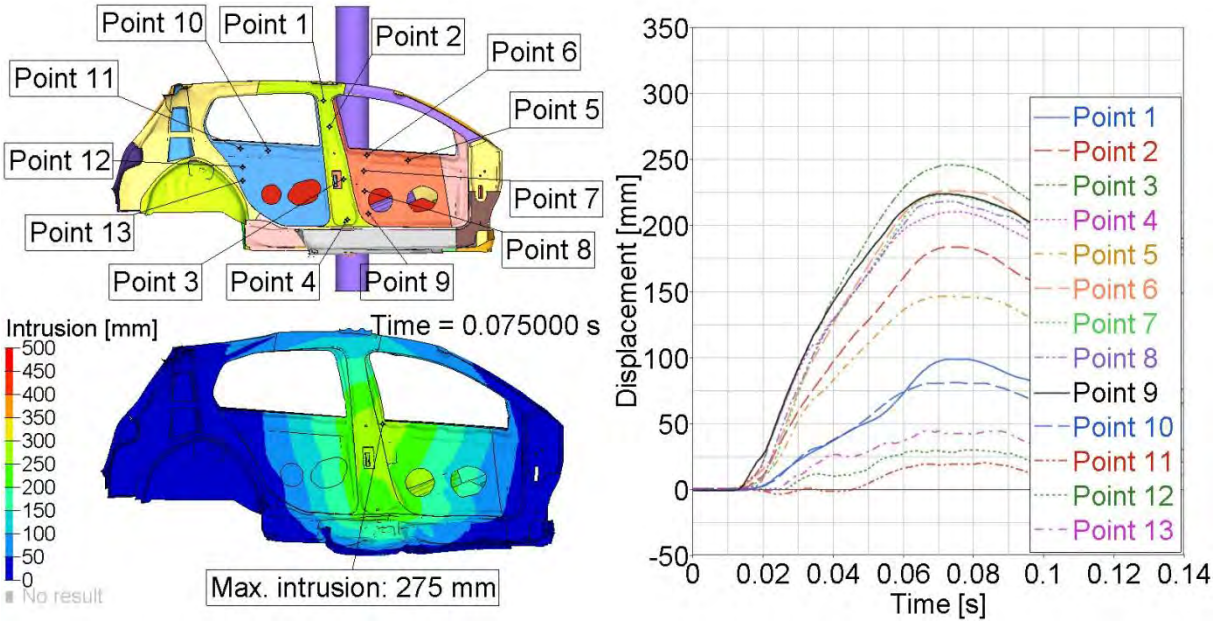

Fig. 3-33 Electric reference model – Side overview at time of maximum intrusion (low, left) and intrusion behaviour over crash duration for monitored points (right) during pole side crash

As the comparison for the monitored side intrusion points shows (c.f. Fig. 3-34), intrusion values drop by over 50 mm to values below 250 mm. At the same time the acceleration peak affecting the vehicle nearly doubles (c.f. Fig. 3-35).

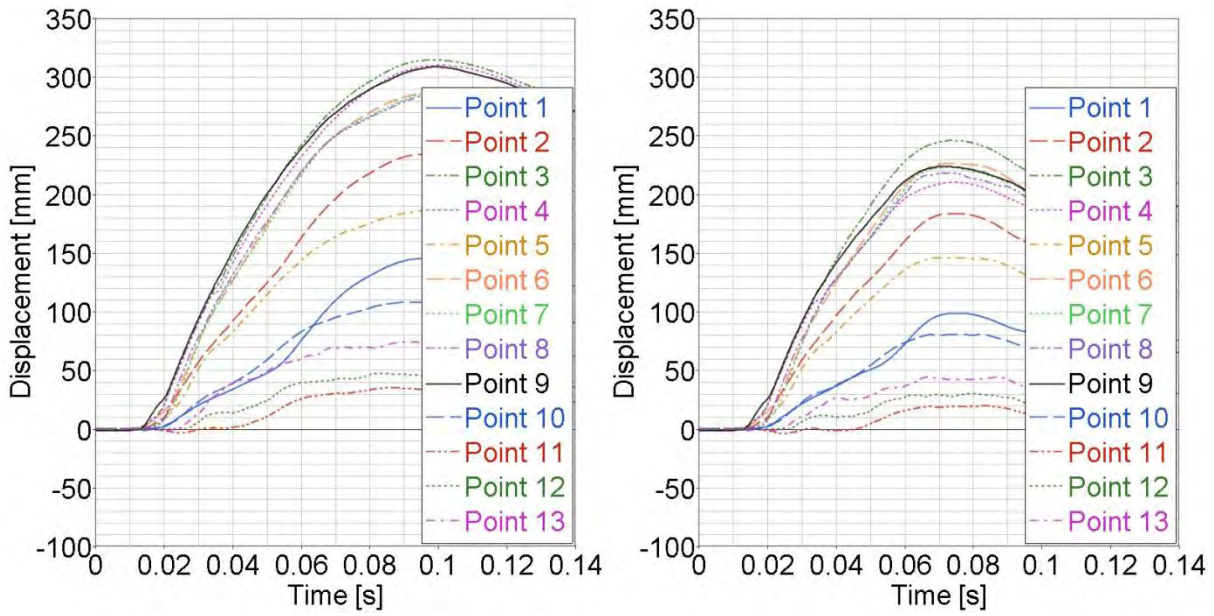

Fig. 3-34 Comparison of intrusion alongside crash progression for discrete evaluation points (left – crash reference vehicle, right – electric reference vehicle)

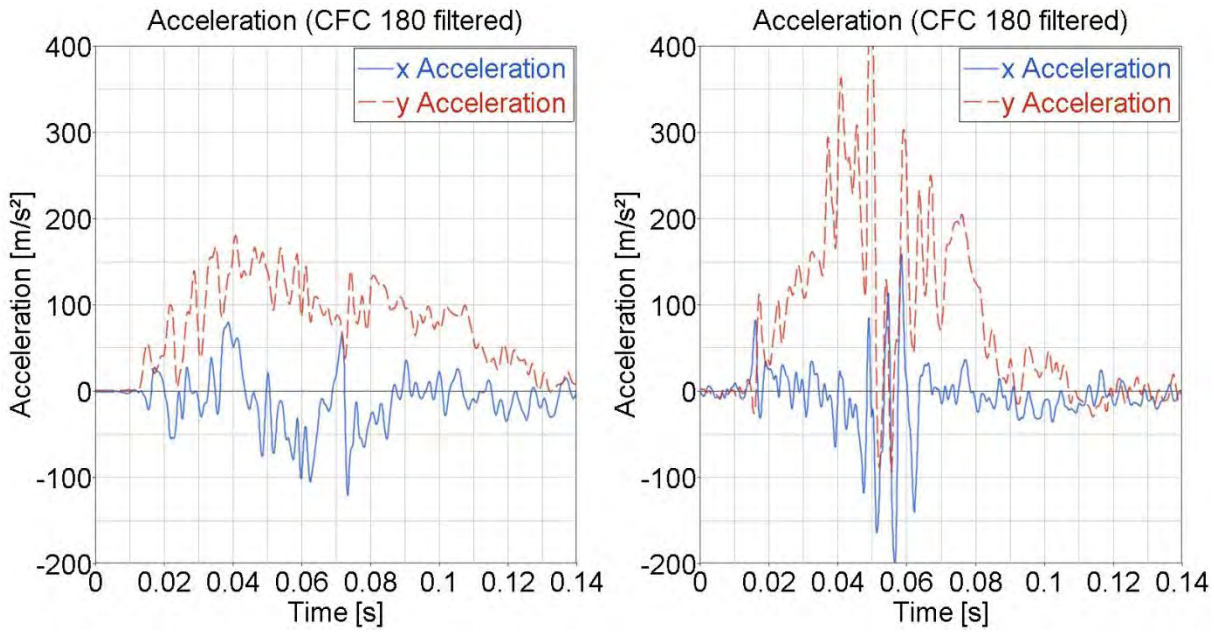

Fig. 3-35 Vehicle centre acceleration during pole side crash – Comparison of crash reference (left) to electric reference vehicle (right)

This loadcase shows in an even more emphasizing manner the imperative of battery cell protection given that current battery cells and modules do not allow deformation. The high intrusions and deformations of the tunnel space resulting from the unfavorably thin shape of the rigid pole barrier can only be reduced by the above described additional reinforcement measures leading to higher acceleration levels.

3.6.4 FMVSS 301 Rear Crash Behaviour of the Electric Reference Model

Rear crash can be regarded as not problematic for the electric reference vehicle (c.f. Fig. 3-36).

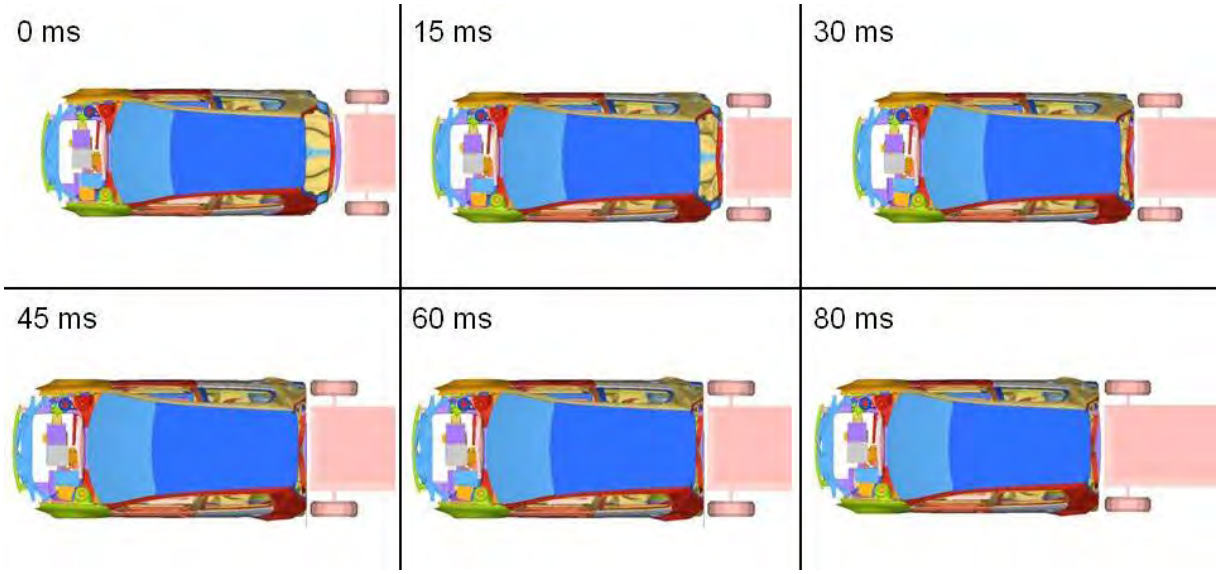

Fig. 3-36 FMVSS rear crash progression for the electric reference model

As Fig. 3-37 shows rear end deformations do not reach the level of the battery cells even though maximum intrusion increases slightly (c.f. Fig. 3-38). Meanwhile no significant change in acceleration behaviour can be detected (c.f. Fig. 3-39).

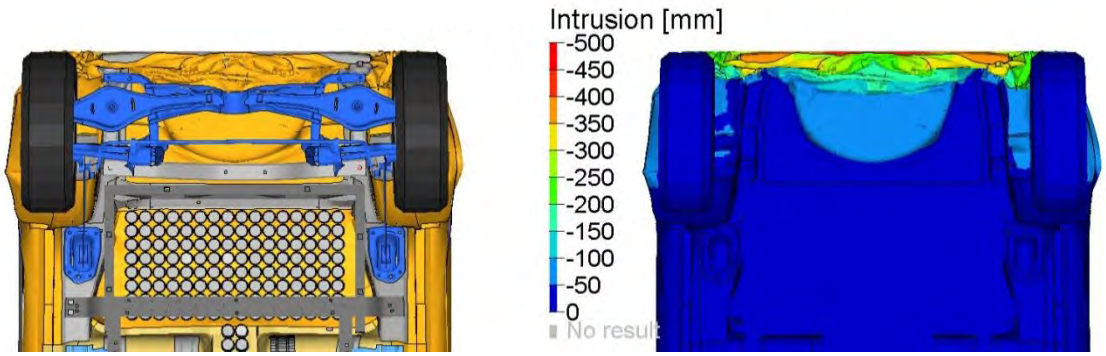

Fig. 3-37 Electric reference model– Rear crash behaviour at time of maximum intrusion

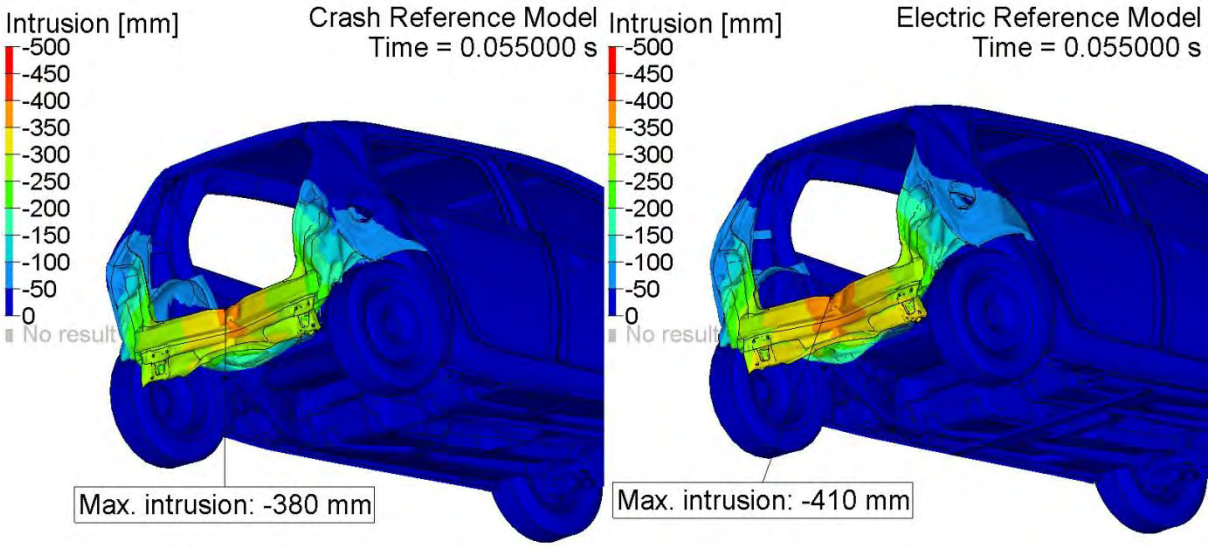

Fig. 3-38 Maximum intrusion at rear crash – Comparison of crash reference (left) and electric reference vehicle (right)

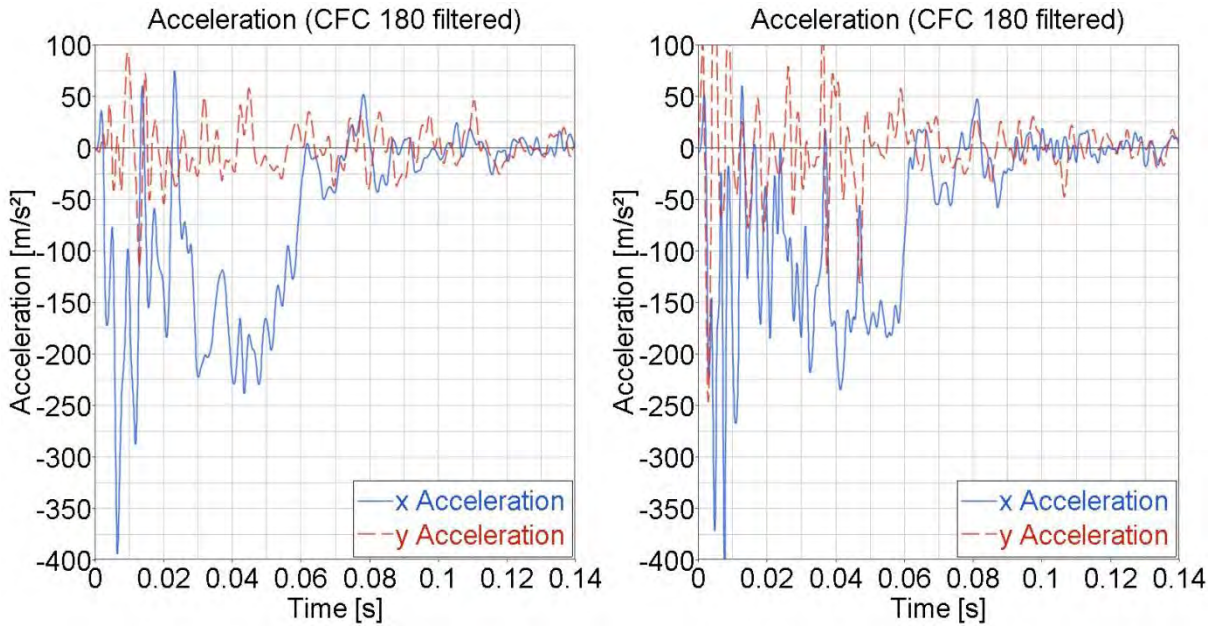

Fig. 3-39 Comparison of deceleration of vehicle centre in the x-y-plane during FMVSS 301 rear crash for the crash reference model (left) and the electric reference model (right)

In summary, the switch of powertrain concepts from the crash reference to the electric reference vehicle following a conversion design strategy is possible concerning the aspect of crashworthiness. Nevertheless especially the side crash loadcases require weight intensive reinforcement measures.

4 Application of Lightweight Measures

In the second step of the presented study, the transformation of the electric reference vehicle with steel unibody design into a vehicle with full aluminium structure is performed. The material substitution effort includes all components of the body-in-white, the front and rear armatures and the hang-on parts such as doors, closures and front fenders. The powertrain design chosen for the electrified reference model is conserved. Nevertheless, downsizing measures concerning the battery system are executed to keep the desired 200 km drive range in the NEDC, after the structural weight of the aluminium design vehicle is determined. Engine component downsizing and other secondary weight reduction measures are not regarded. Again, the crashworthiness of the vehicle under the described loadcases is analysed.

4.1 Aluminium Materials for a Full-Aluminium Vehicle Structure

For the different structural tasks different aluminium part manufacturing methods and a large range of aluminium alloys can be chosen. The material selection used for application in this study step is described in Tab. 4-1.

Alloy	Function	$R_{p0.2}$ value
5xxx	Structural sheet	150 MPa
6xxx	External skin sheet	250 MPa
6xxx	Structural sheet	200 MPa
6xxx	Structural sheet	250 MPa
7xxx	Structural sheet	400 MPa
6xxx	Extrusion for beam parts	280 MPa
6xxx	Extrusion for beam parts	320 MPa
6xxx	Extrusion for crushed parts	200 MPa
6xxx	Extrusion for crushed parts	280 MPa
AlSi10Mg	Die casting	140 MPa

Tab. 4-1 Overview of used aluminium alloys

4.2 The Full-Aluminium Vehicle Structure of the Target Vehicle Model

With the aimed production volume of 100,000 cars per year several aluminium structural designs are selectable for the body realisation. In this study step a mixed space frame design approach is chosen.

4.2.1 Body-in-White

The body-in-white designed as space-frame structure is using a combination of extrusion parts, complex casting nodes and sheet parts (c.f. Fig. 4-1).

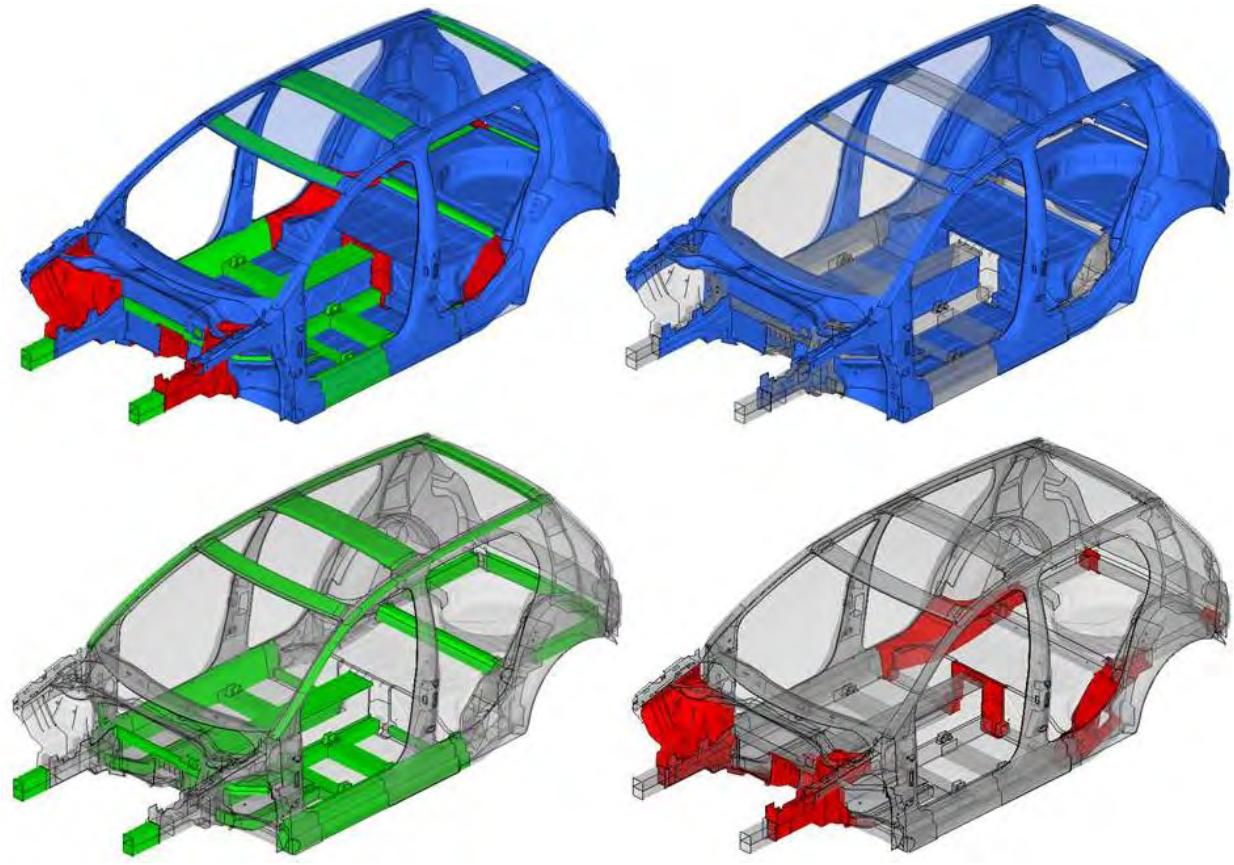

Fig. 4-1 Application of aluminium manufacturing methods to the target vehicle model (blue: sheet, green: extrusion, red: casting)

To reduce the complexity of the design task, the exterior skin surface of the crash reference vehicle is conserved as well as a maximum amount of sheet parts. Only their part thickness is modified to adapt the parts to the different strength properties of aluminium in comparison to steel (c.f. Fig. 4-2).

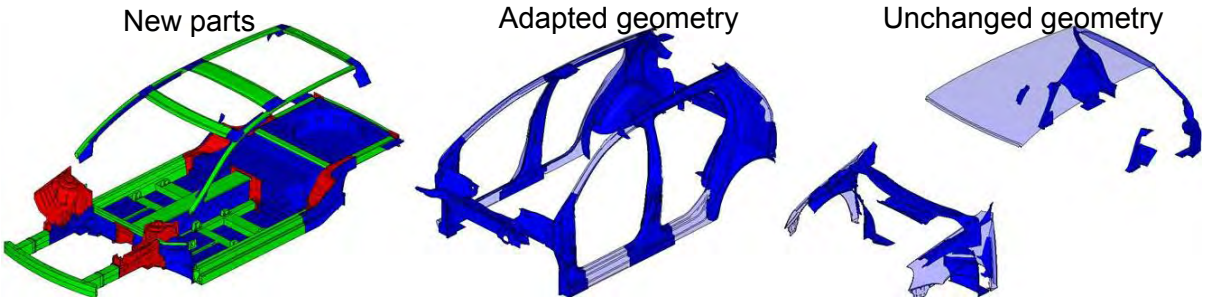

Fig. 4-2 Re-design part overview

New components and shapes appear in the vehicle's roof and floor structure and the front vehicle as a space frame design is realized. The floor (c.f. Fig. 4-3) consists of extruded longitudinal beams and crossbeams arranged around the tunnel space. High stiffness

against side crash intrusions is guaranteed by the solid rocker rail design as well as by the double crossbeam structure below the front seats.

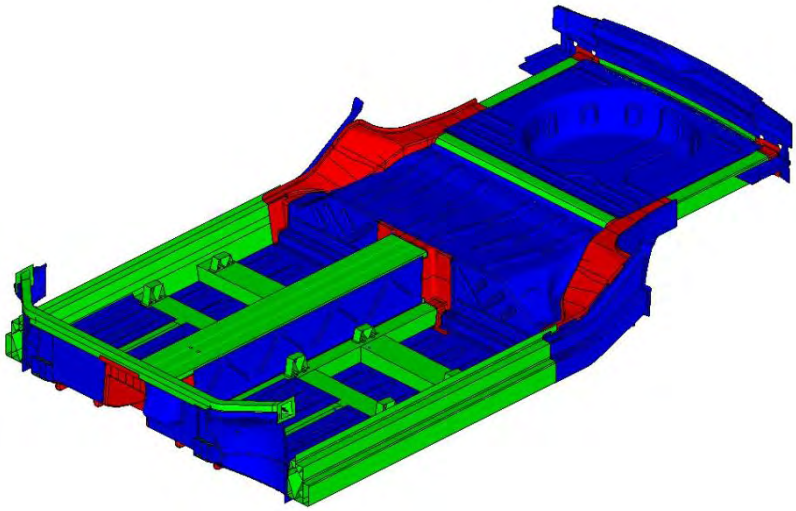

Fig. 4-3 Target vehicle model floor

The roof structure consists of one hydro formed roofrail running from the A to the C pillar, assuring good stiffness properties together with the extruded roof crossbeams (c.f. Fig. 4-4).

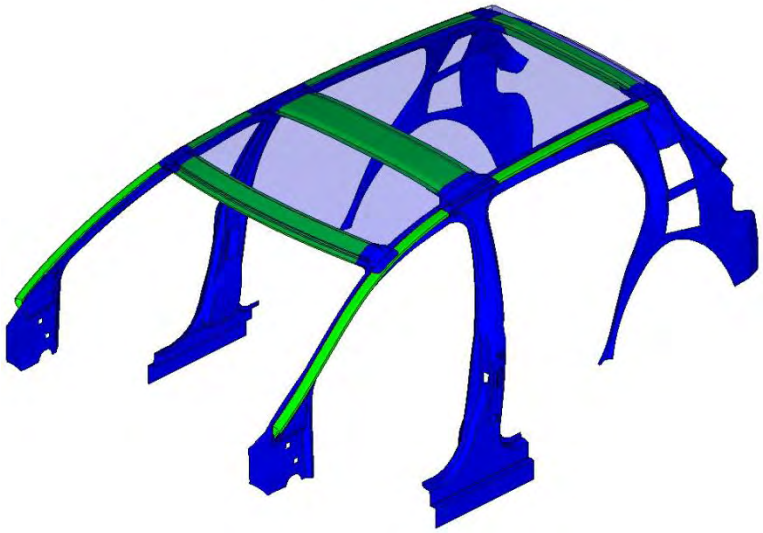

Fig. 4-4 Target vehicle model roof

In the chosen space frame design the longitudinal crashbeams in the front vehicle move closer to the vehicle's centre. These straight shaped crash elements offer good energy absorption properties together with low weight involvement. The front armature is realized as stick-in concept directly mounted to the longitudinal crash beams of the body-in-white front (c.f. Fig. 4-5).

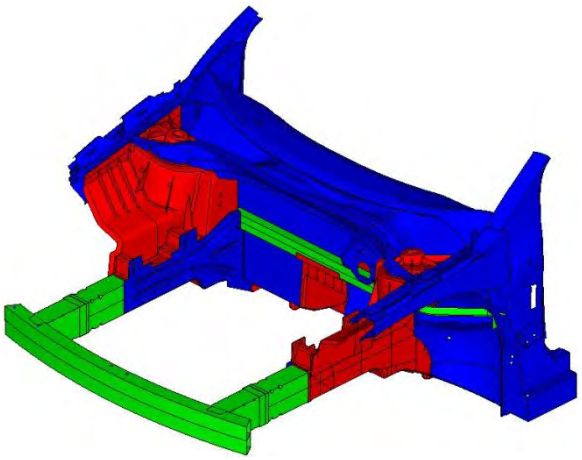

Fig. 4-5 Target vehicle model front

For specific parts within the described structure, a sheet or an extrusion/sheet design could also be considered to replace the die casting node elements, potentially offering additional cost and weight advantages. Alternative designs are however not a focus of this study.

The joining strategy followed for the body-in-white is detailed in Fig. 4-6. To increase the body-in-white's stiffness, flow drill screwing (FDS) and punch riveting is applied in combination with additional adhesive bonding.

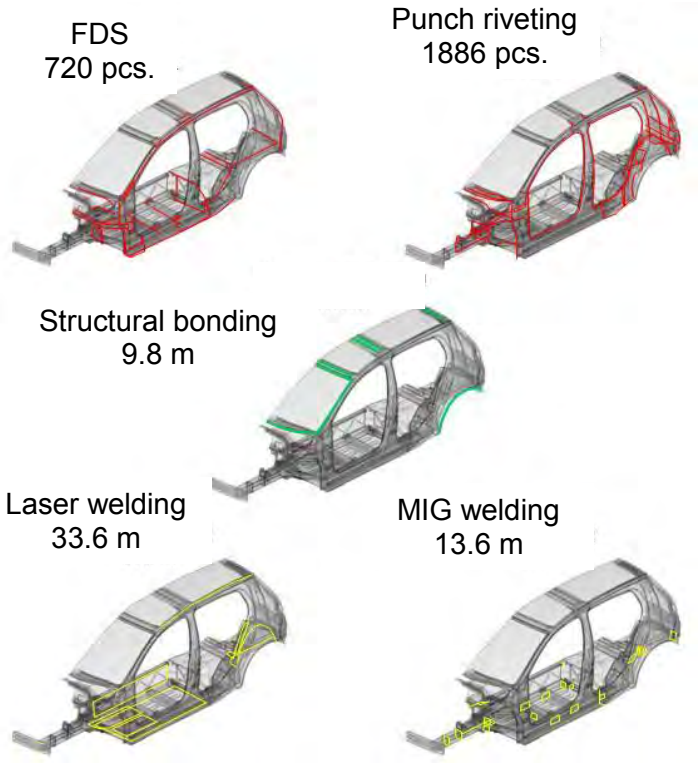

Fig. 4-6 Joining methods involved in full body-in-white assembly

4.2.2 Front and Rear Armatures

While the front armature is realized in a stick-in design, the rear armature is realized as complex hydro formed monobeam structure with crash absorption inlay elements included at its side ends (c.f. Fig. 4-7).

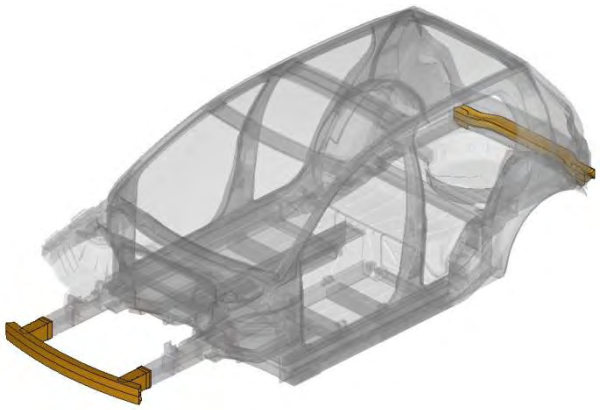

Fig. 4-7 Target model front and rear armature

4.2.3 Front and Rear Doors

The design of the doors is not changed. Only thickness increases and slight proportion changes are applied to adopt the structure to aluminium properties (c.f. Fig. 4-8).

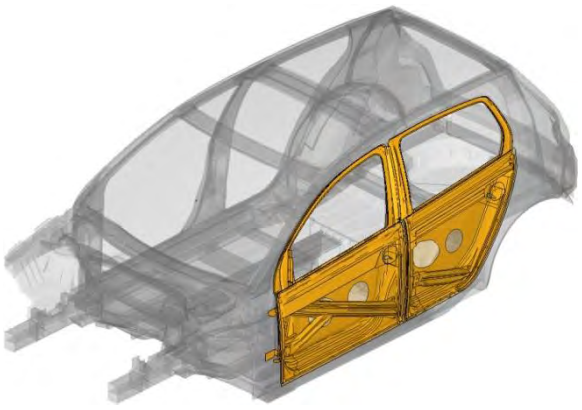

Fig. 4-8 Target model front and rear door

4.2.4 Fenders

A similar approach is followed for the fenders. Here again sheet thickness increases while the geometry remains unchanged (c.f. Fig. 4-9)

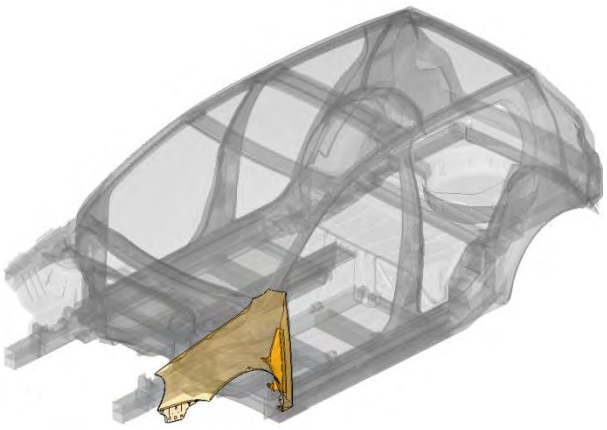

Fig. 4-9 Target model front fenders

4.2.5 Closures (Hood and Tailgate)

These elements of the vehicle are not part of the design model as the necessary FE data is missing from the crash reference model used as basis for all study design tasks. Nevertheless weight reductions of over 40 % for the closure structures (e.g. without tailgate glazing) are assumed by material substitution from steel to aluminium.

4.3 Driving Performance and Battery System Downsizing Measures

With the defined aluminium body structure the relation between body lightweight measures and energy consumption, battery mass and energy content is analysed. The energy consumption for the lightweight concept has to be evaluated at first. The same energy consumption calculation is performed after the battery pack has been downsized to meet the NEDC range of 200 km.

As discussed in Chapter 3.2.3, the correlation between the total vehicle mass and the vehicle's energy consumption can be described with the cycle-specific parameters a and b:

$$e_{veh}=a\cdot(m_{Veh}+m_{Batt})+b \qquad \text{Eq. 4-1}$$

The battery energy content and mass, which is determined by the desired electric vehicle range as well as different battery system parameters, can be described as a straight proportional function of the vehicle mass (without battery mass):

$$m_{Batt}=\frac{(a\cdot m_{Veh}+b)}{\left(\frac{\rho_{ele,Batt}\cdot x_{Batt}}{s_{ele}}-a\right)} \qquad \text{Eq. 4-2}$$

$$E_{Batt}=m_{Batt}\cdot\rho_{ele,Batt}=\frac{(a\cdot m_{Veh}+b)}{\left(\frac{x_{Batt}}{s_{ele}}-\frac{a}{\rho_{ele,Batt}}\right)} \qquad \text{Eq. 4-3}$$

With these functions the energy consumption for the lightweight concept and consequently also the new range of the vehicle can be calculated. In the next step the new battery energy content and mass for a range of 200 km can be evaluated. All results are summarised in Tab. 4-2.

	Electric reference model	**Target vehicle model without downsizing**	**Target vehicle model with downsizing**
Vehicle mass w/o battery	1096 kg	933 kg	933 kg
Energy consumption	15.1 kWh/100 km	13.9 kWh/100 km	13.7 kWh/100 km
Battery energy	37.6 kWh	37.6 kWh	34.3 kWh
Battery mass	232 kg	232 kg	207 kg
Range	200 km	216 km	200 km

Tab. 4-2 Results for the electric reference and the aluminium target vehicle models

4.4 Aluminium Alloy Attribution to the Target Vehicle Model Structure

The following aluminium alloy attribution is performed for the modelled vehicle structure (c.f. Fig. 4-10). In addition, the exterior skin is made out of 6xxx sheet alloy with a yield stress level of $R_{p0.2}$ = 250 MPa.

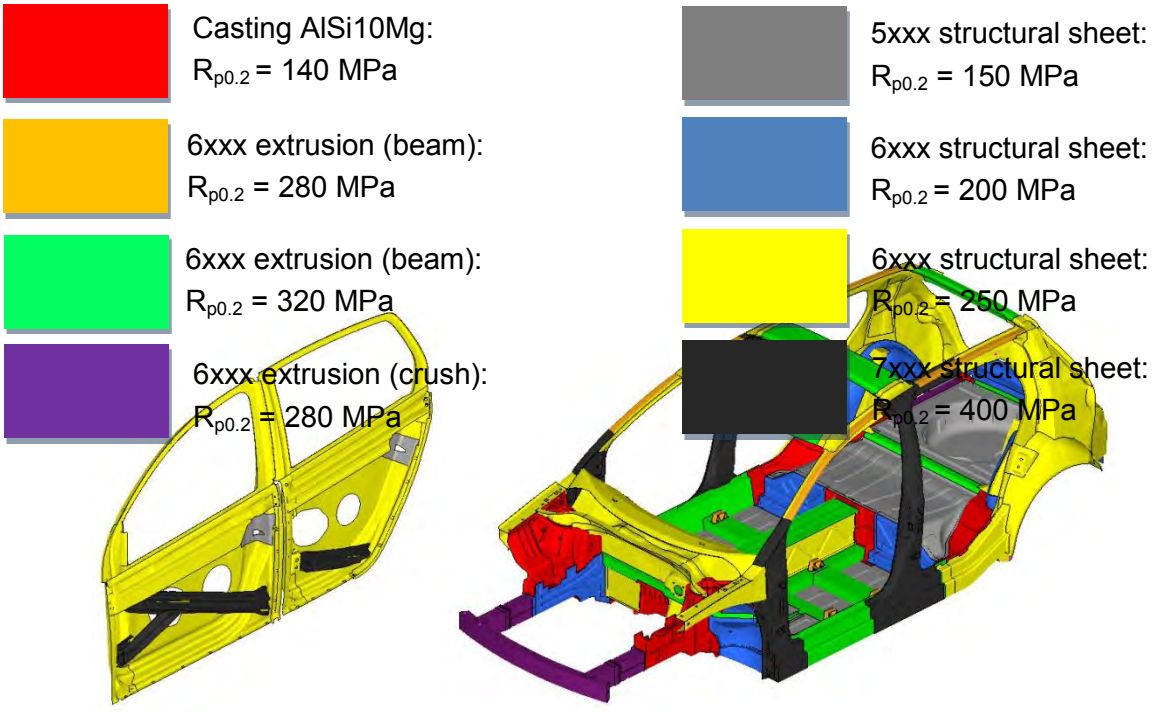

Fig. 4-10 Material attribution to body-in-white, armatures and doors for target vehicle model

4.4.1 Target Vehicle Model's Characteristics

The target vehicle model shows the following features:

- Total vehicle weight (after powertrain downsizing): 1,140 kg
- Axle load distribution after downsizing (front/rear): 57/43
- Weight of body-in-white structure (full-aluminium): 151 kg

The complete body structure involves 213 kg of aluminium, distributed over the different aluminium manufacturing methods (c.f. Fig. 4-11).

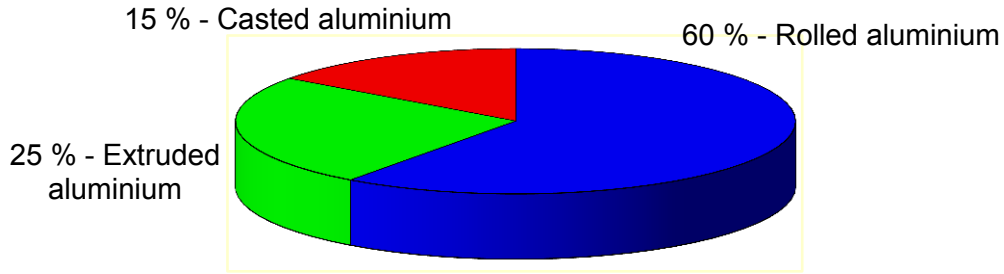

Fig. 4-11 Distribution of aluminium manufacturing methods over the target vehicle body

Resulting weight reductions compared to the electric reference vehicle are listed in Tab. 4-3. Significant weight reductions of around 40 % can be achieved in all structural regions of the vehicle's body. It shall be noted that the current project only considers a limited number of structural properties of the aluminium target vehicle (strongly focused on crash load cases). If other load cases would also be considered, it is fair to assume that the weight of the aluminium target vehicle would be somewhat higher.

	Electric reference vehicle	**Target vehicle model**	**Weight reduction [%]**
Body-in-white	272 kg	151 kg	-44 %
Doors (one side)	30.2 kg	19.2 kg	-36 %
Fenders (one side)	2.40 kg	1.28 kg	-47 %
Armatures	12.5 kg	7.53 kg	-40 %
Closures	24.8 kg	14.0 kg	-43 %
Total body structure	375 kg	213 kg	-43 %

Tab. 4-3 Involvement of steel in electric reference and of aluminium in target vehicle structure

4.5 Analysis of the Aluminium Target Vehicle's Crash Performance

The same crashworthiness evaluation loadcases as for the two vehicle models before are simulated for the aluminium target vehicle model.

4.5.1 Euro NCAP Front Crash Behaviour of the Aluminium Target Model

The evaluation of the front crash simulation results for the target vehicle model follows the known description scheme (c.f. Fig. 4-12 to Fig. 4-16).

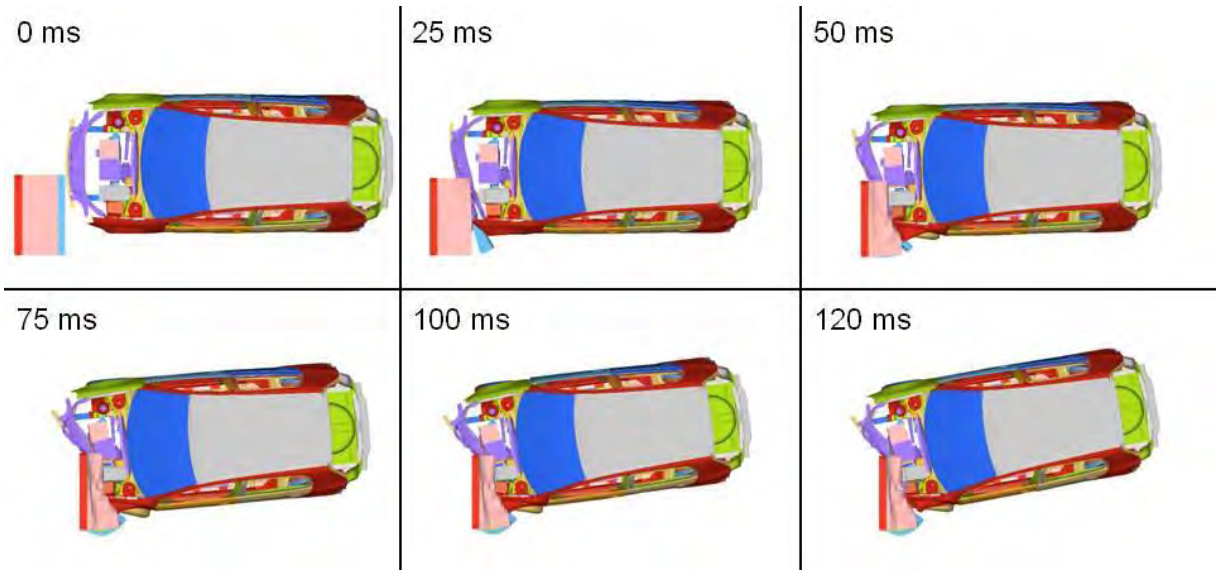

Fig. 4-12 Euro NCAP front crash progression for the target vehicle model

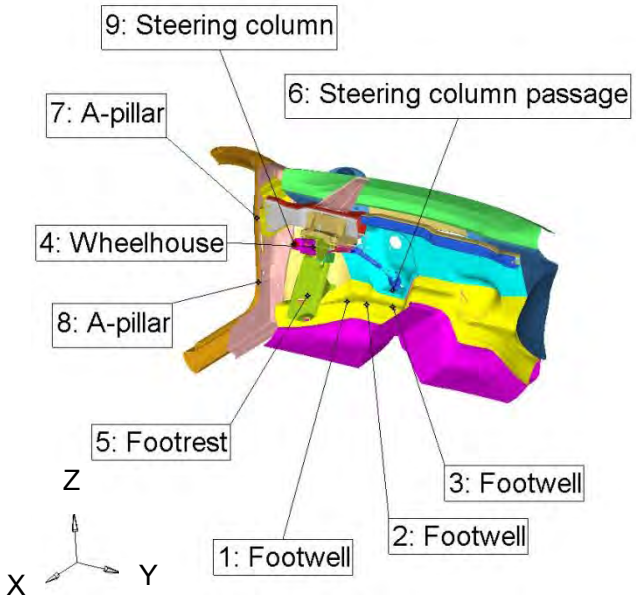

Fig. 4-13 Tracked points for intrusion in case of offset front crash (Euro NCAP)

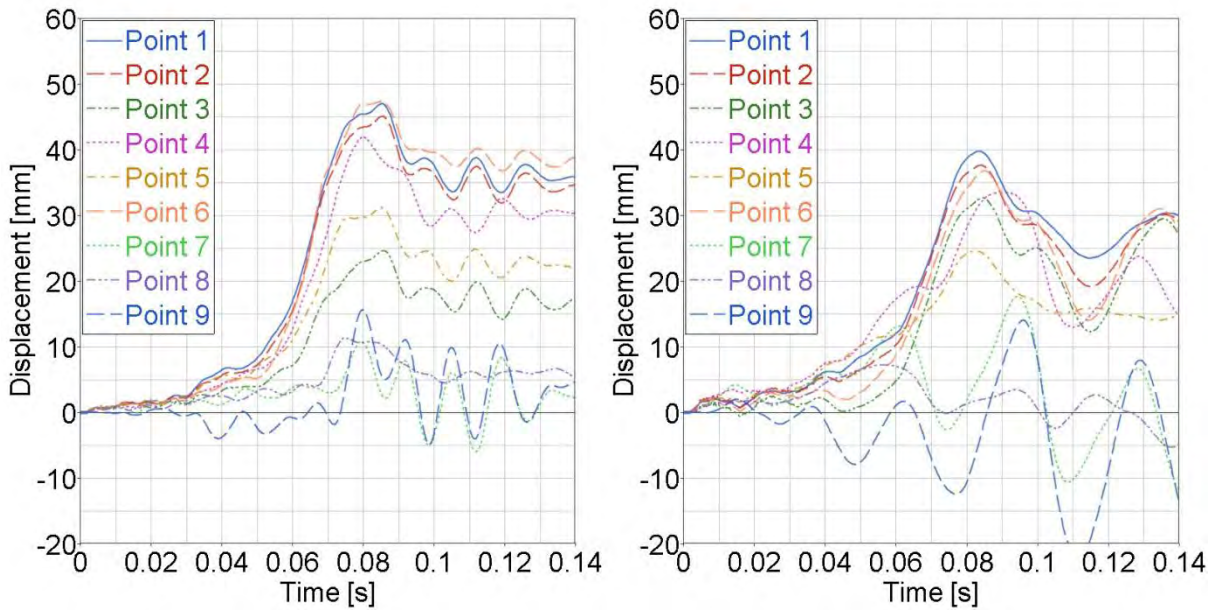

Fig. 4-14 Intrusion at evaluation points during front crash – Comparison of crash reference (left) to target vehicle model (right)

The only major structural change applied to the target vehicle model on the bulkhead level is the new bulkhead crossbeam. This stiffening component helps to reduce the general intrusion peak value to the crash reference level of under 85 mm. Similarly, the intrusions detected for the specially monitored nine points remain on the level below 50 mm.

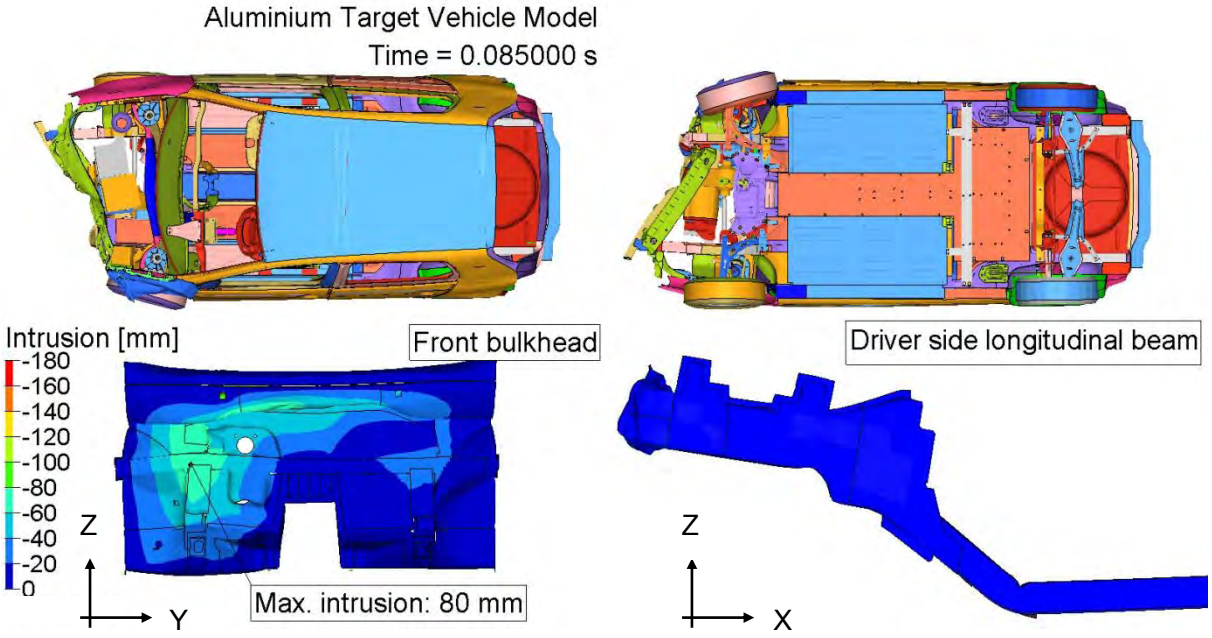

Fig. 4-15 Target vehicle model – Front crash behaviour at time of maximum intrusion

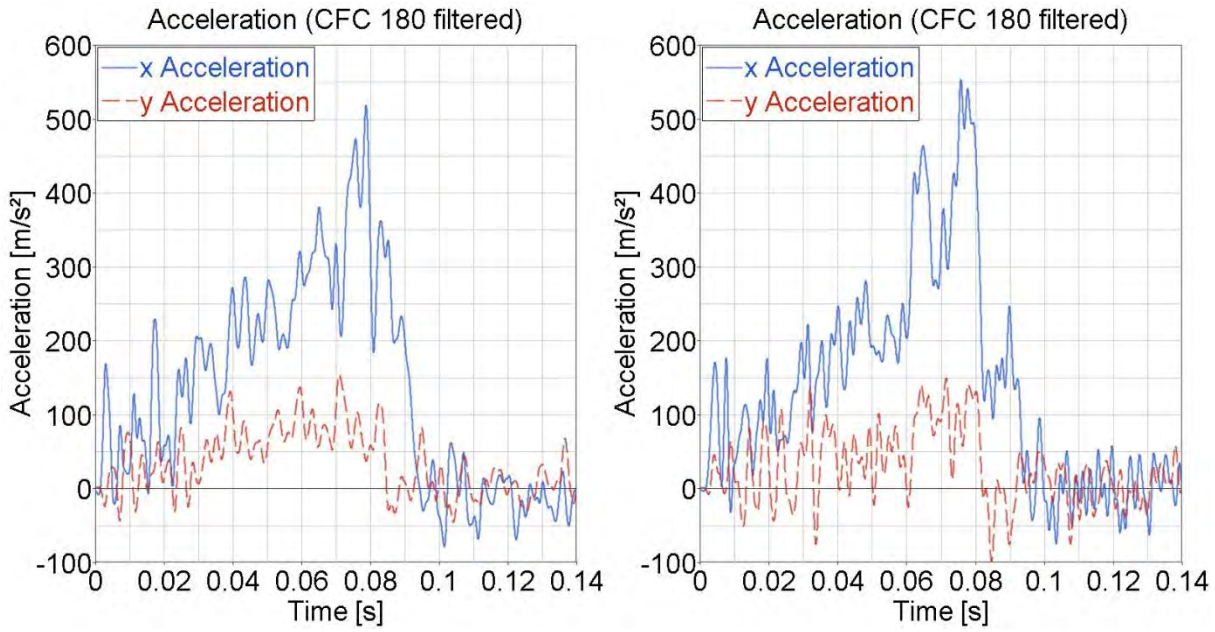

Fig. 4-16 Vehicle centre acceleration during front crash – Comparison of crash reference (left) to target vehicle model (right)

No significant change in the deceleration behaviour can be detected in comparison to the crash reference behaviour.

4.5.2 Euro NCAP Side Crash Behaviour of the Aluminium Target Model

The examination of the side crash simulations for Euro NCAP side crash and pole side crash shows that the new vehicle structure design also accomplishes the primary task of battery system protection (c.f. Fig. 4-17 to Fig. 4-20).

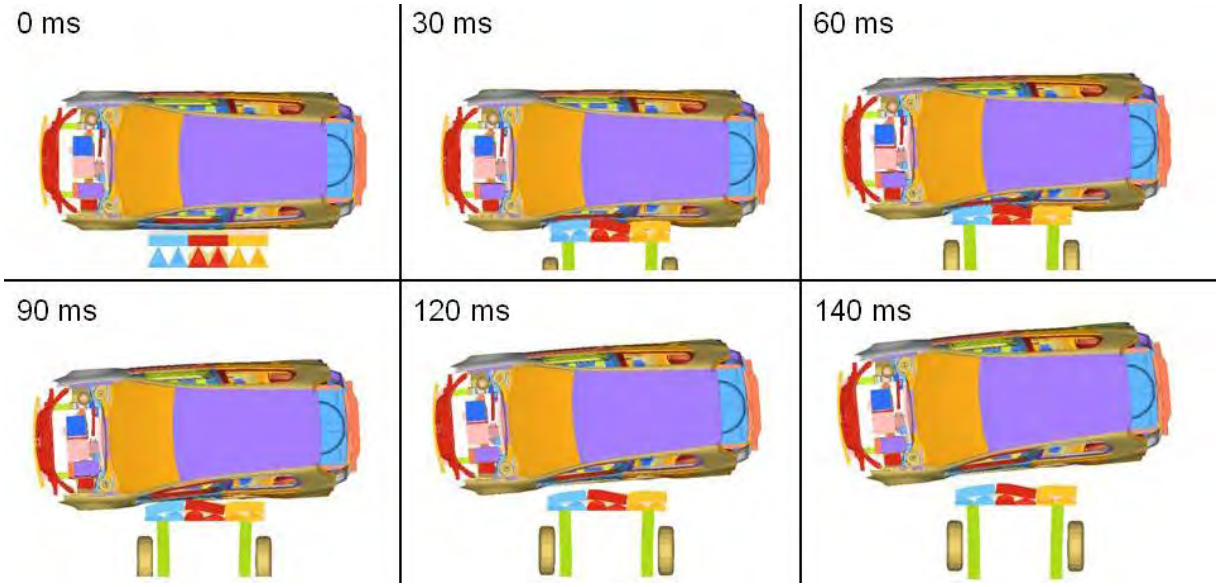

Fig. 4-17 Euro NCAP side crash progression for the target vehicle model

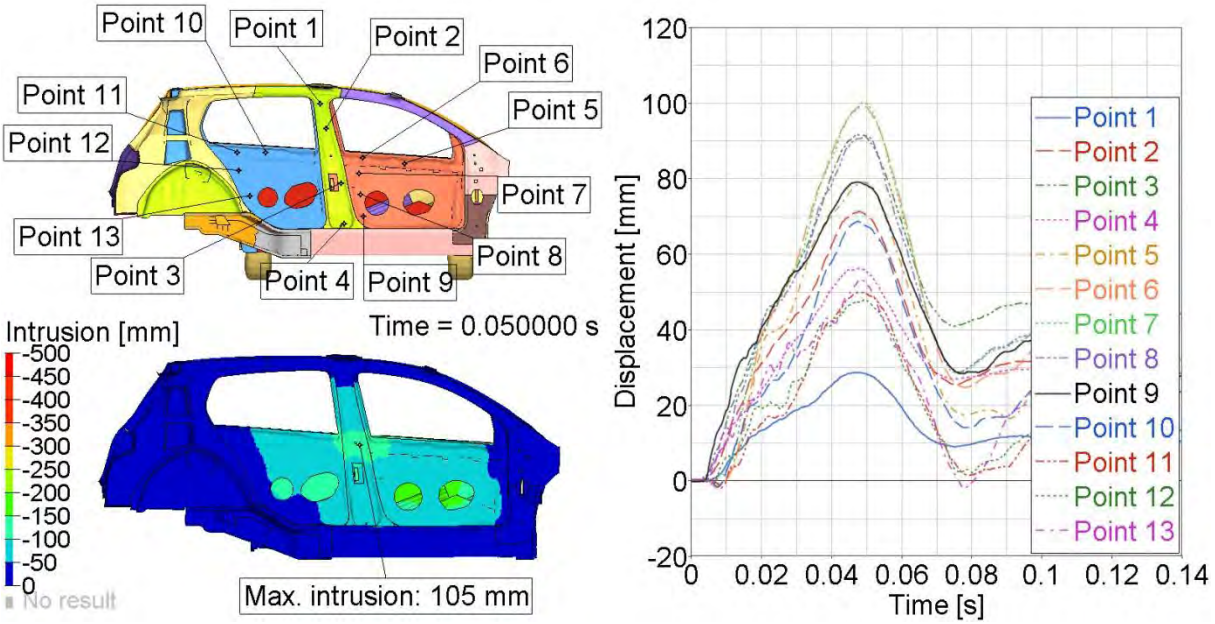

Fig. 4-18 Target vehicle model – Side overview at time of maximum intrusion (low, left) and intrusion behaviour over crash duration for monitored points (right) during pole side crash

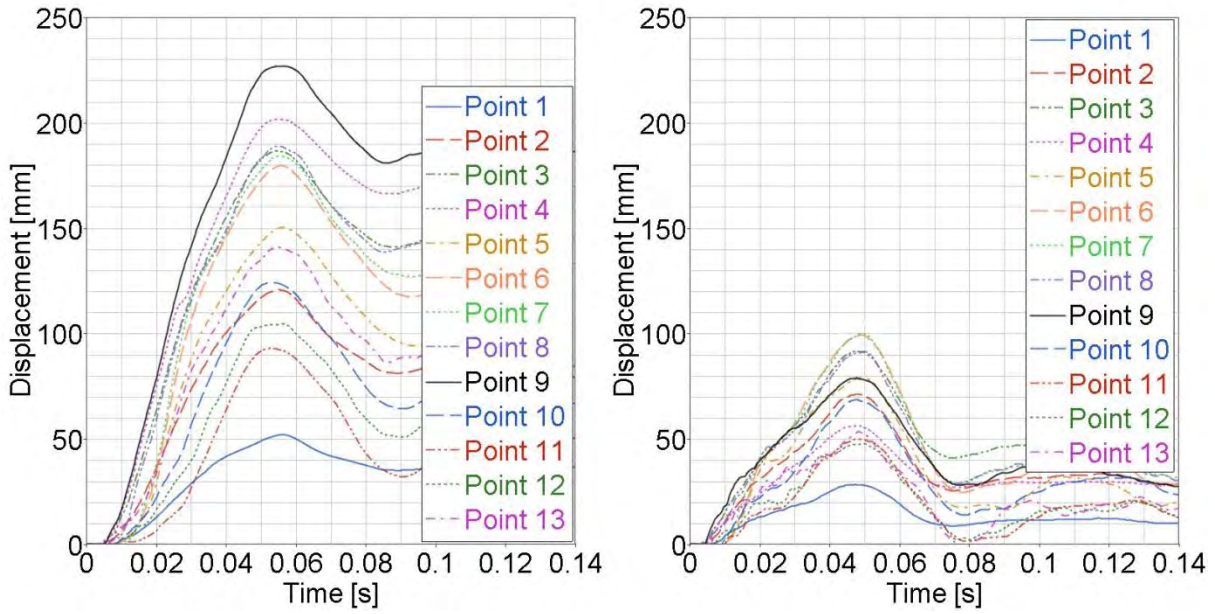

Fig. 4-19 Intrusion at evaluation points during side crash – Comparison of crash reference (left) to target vehicle model (right)

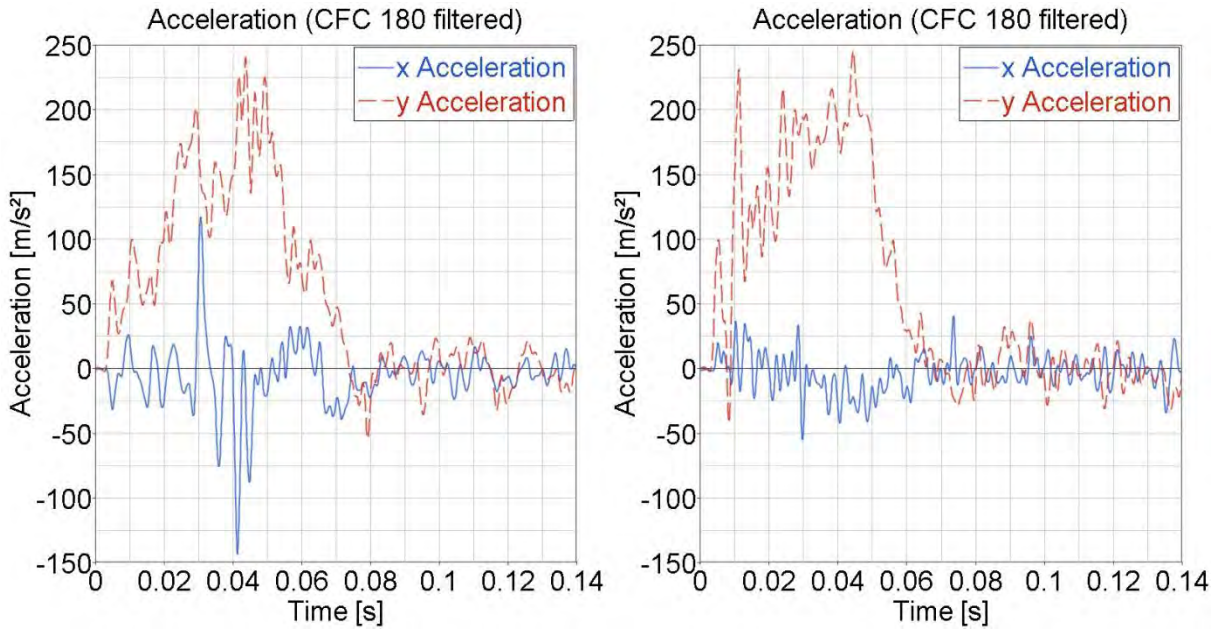

Fig. 4-20 Vehicle centre acceleration during side crash – Comparison of crash reference (left) to target vehicle model (right)

Again, a significant reduction of the general side intrusion is achieved. This time, the stiffening effects of the rocker rail and the front seat crossbeams are sufficient to reach the low intrusion levels. No additional reinforcement elements are required.

4.5.3 Euro NCAP Pole Side Crash Behaviour of the Aluminium Target Model

The effects already identified for the Euro NCAP side crash can also be detected in the pole side crash simulation (c.f. Fig. 4-21 to Fig. 4-24).

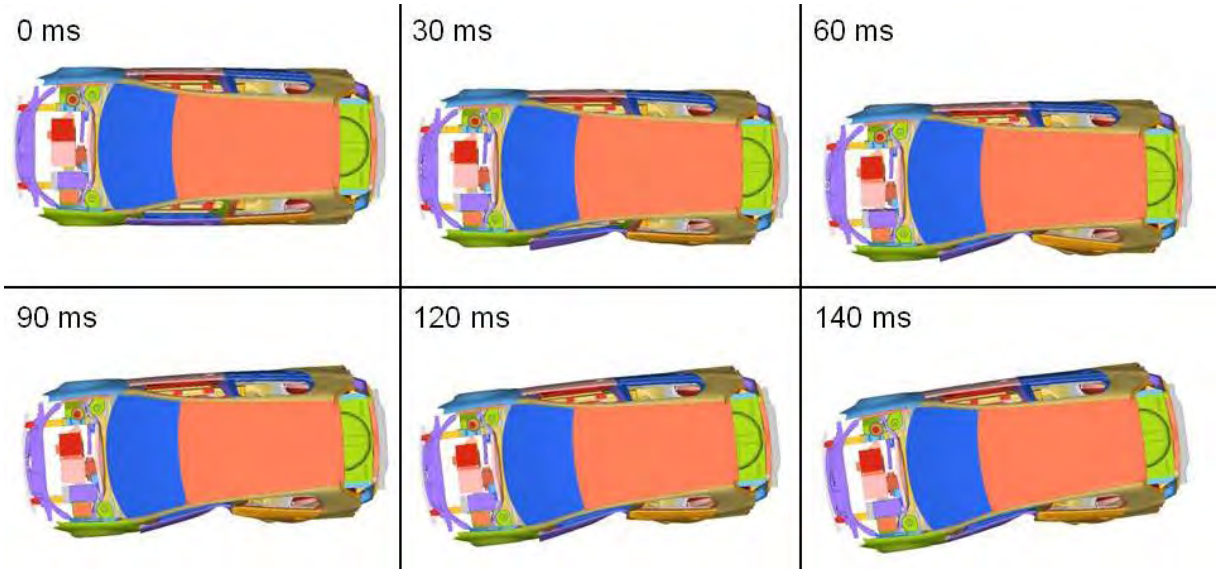

Fig. 4-21 Euro NCAP pole side crash progression for the target vehicle model

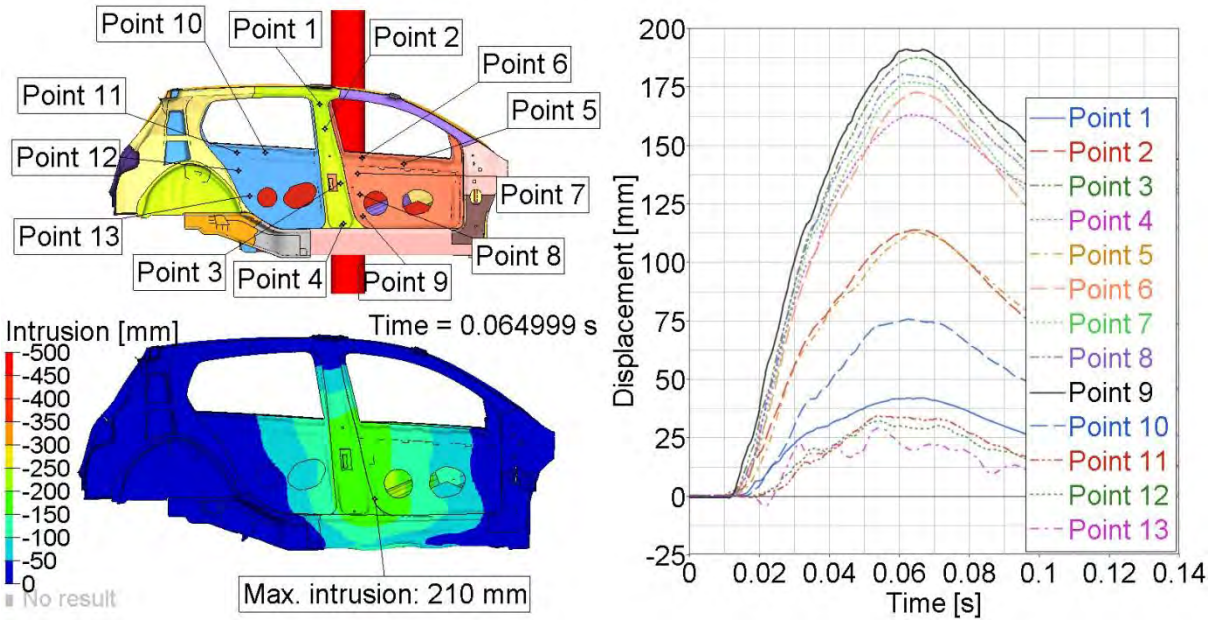

Fig. 4-22 Target vehicle model – Side overview at time of maximum intrusion (low, left) and intrusion behaviour over crash duration for monitored points (right) during pole side crash

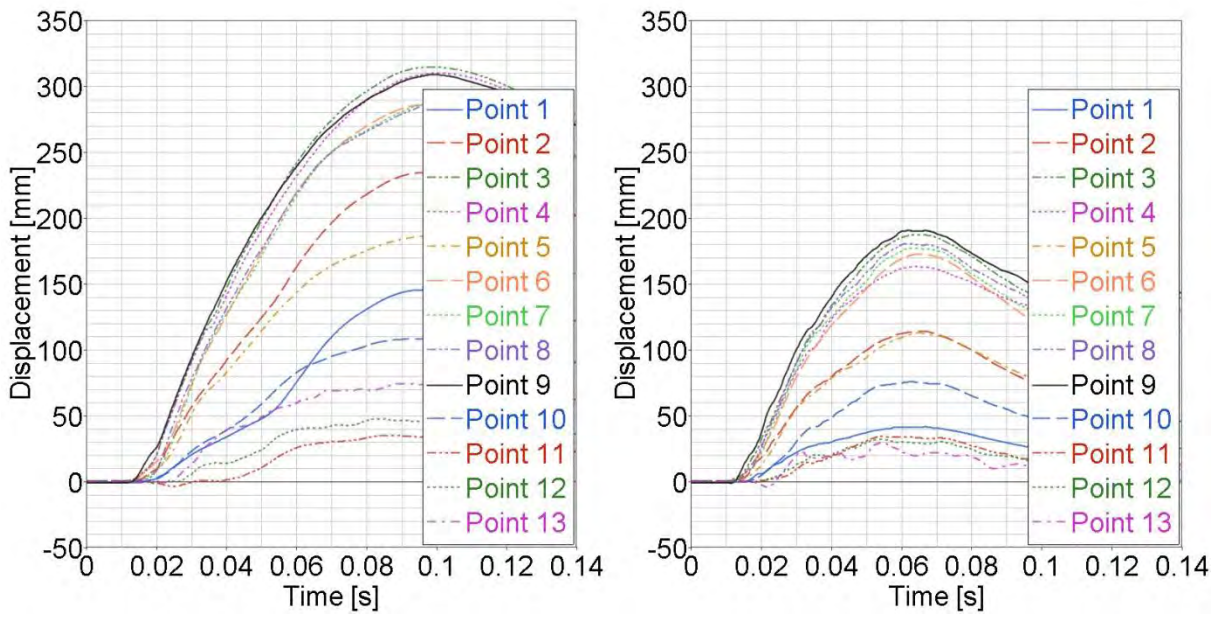

Fig. 4-23 Intrusion at evaluation points during pole side crash – Comparison of crash reference (left) to target vehicle model (right)

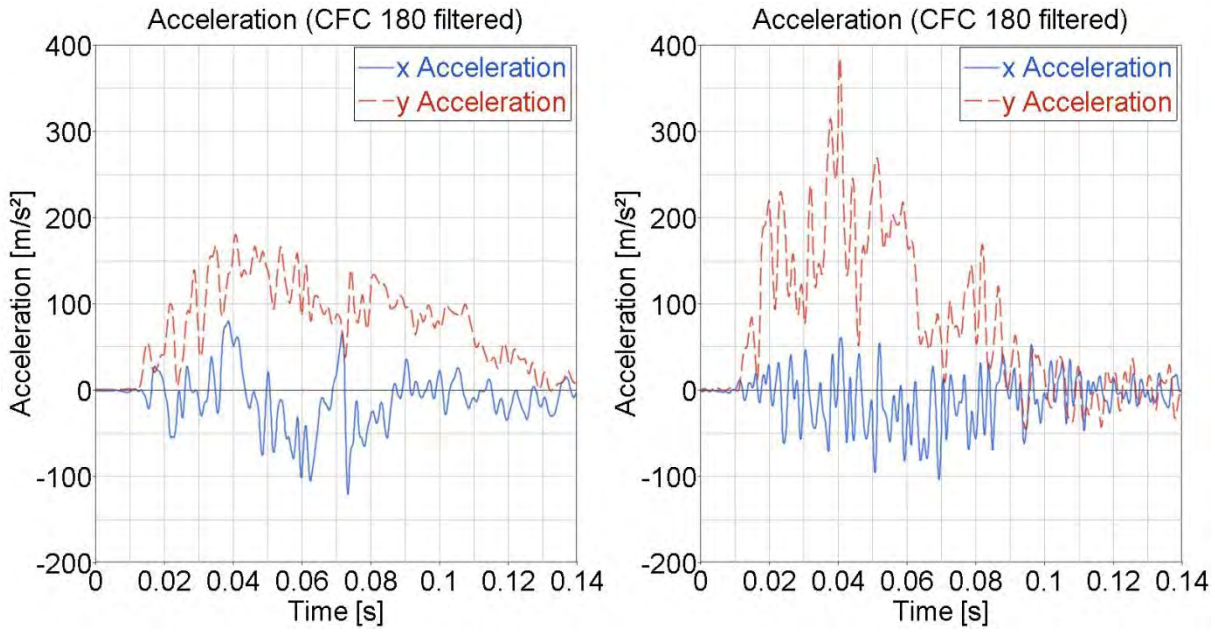

Fig. 4-24 Vehicle centre acceleration during pole side crash – Comparison of crash reference (left) to target vehicle model (right)

The side intrusions decline significantly to reach the desired battery system protection level. The negative effect of vehicle deceleration amplitude increase also occurs. Again, well performing restraint systems are mandatory.

4.5.4 FMVSS 301 Rear Crash Behaviour of the Aluminium Target Model

The rear impact simulation proofs the reproduction of the good crash reference behaviour (c.f. Fig. 4-25 to Fig. 4-28).

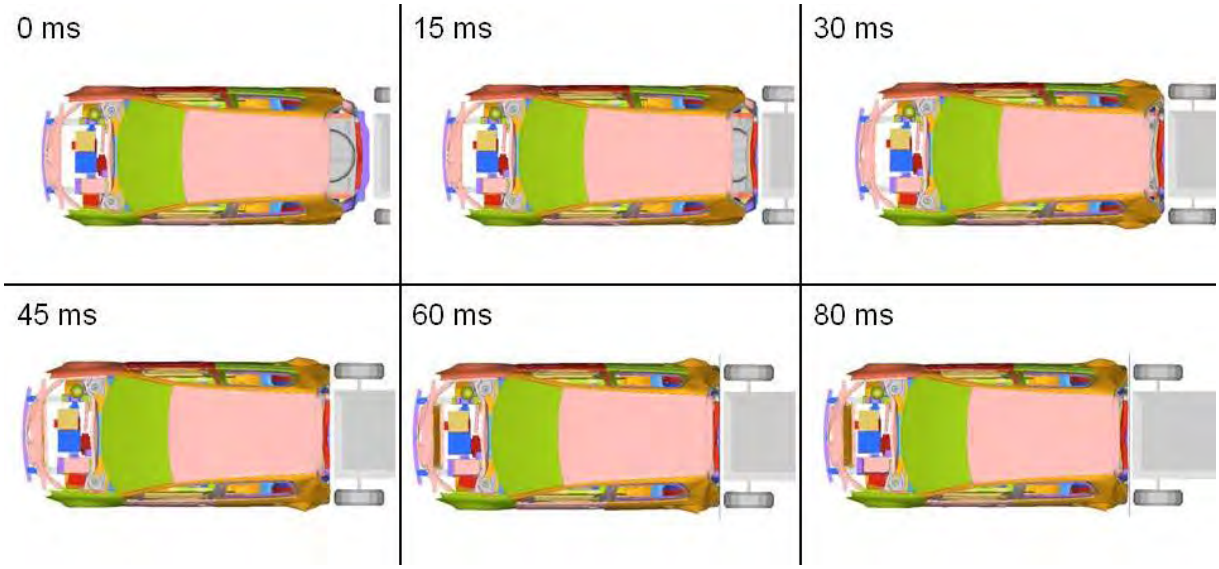

Fig. 4-25 FMVSS 301 rear crash progression for the target vehicle model

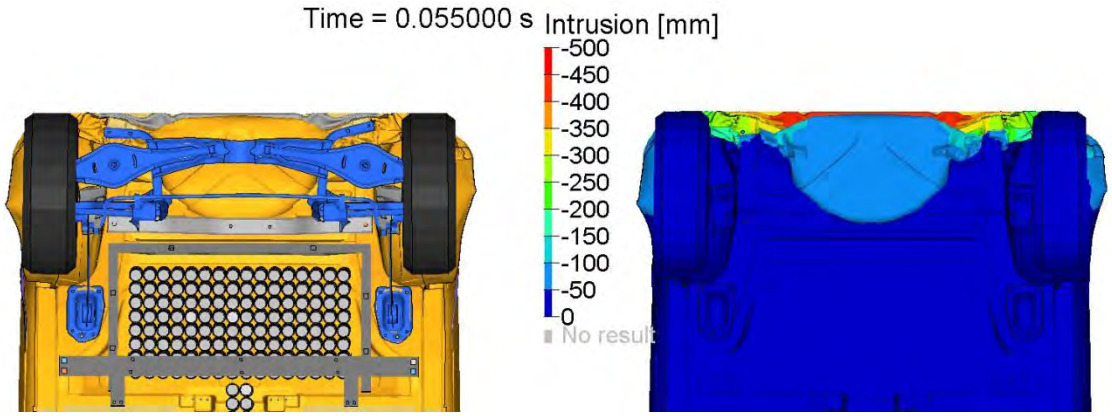

Fig. 4-26 Target vehicle model – Rear crash behaviour at time of maximum intrusion

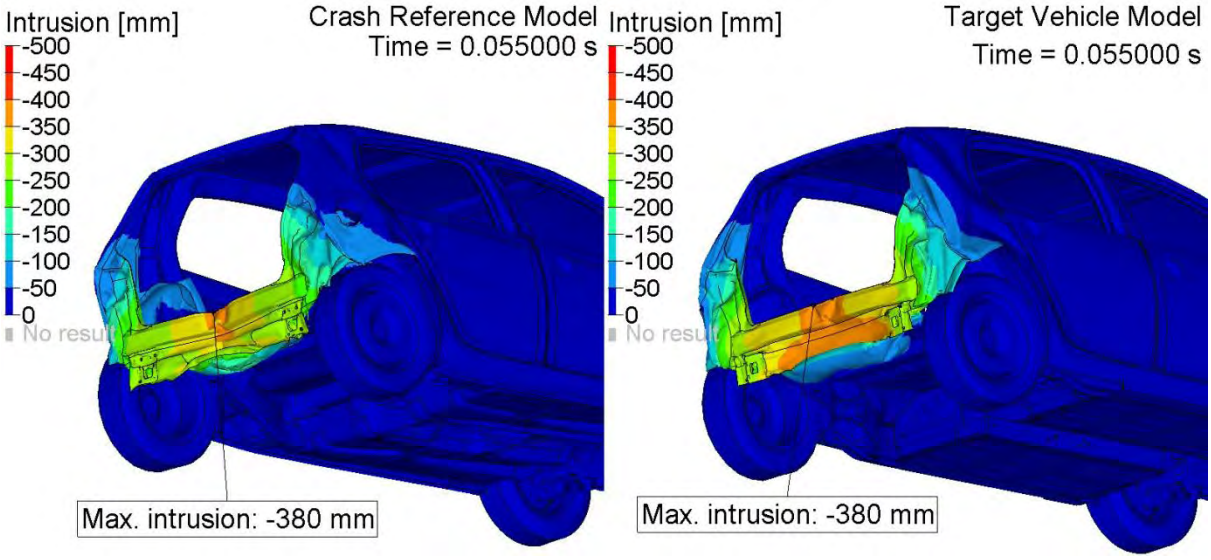

Fig. 4-27 Maximum intrusion at rear crash – Comparison of crash reference (left) and target vehicle model (right)

The battery system remains undeformed, while general deformation reaches the known reference levels. At the same time, the acceleration peaks remain on a level comparable to the reference.

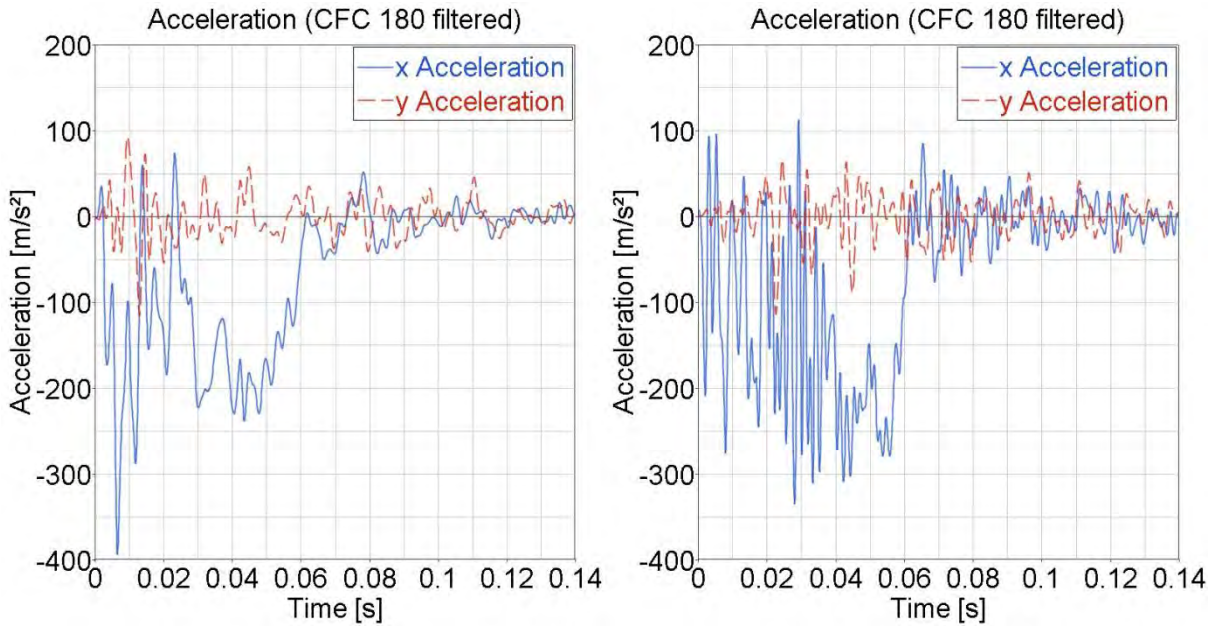

Fig. 4-28 Vehicle centre acceleration during rear crash – Comparison of crash reference (left) to target vehicle model (right)

5 Cost Investigations

With the structural design tasks accomplished, all cost effects of the lightweight strategy can be quantified in detail. First of all, the additional lightweight costs for replacing the steel unibody structure of the electric reference with the aluminium space-frame structure of the target vehicle model are analysed. Secondly, the modelled cost savings due to downsizing of the battery system after reduction of the structural weight can be evaluated. As the technical scenario of the year 2015 analysed in this study covers uncertainties concerning the development of costs for full electric vehicles, a cost tool is defined allowing the flexible modification of several cost parameters.

5.1 The Lightweight Costs of the Aluminium Target Model

The part costs of structural components are modelled using a fka in-house cost tool, based on material costs estimated for the year 2015 (assumed London Metal Exchange[1] price of 2,500 $ at an exchange rate of 1.00 € = 1.42 $ and additional alloy depending material conversion costs) and the manufacturing effort in function of the part geometry, material properties and the required tooling machines. The machine cost rates for the tooling machines forming the basis of the calculation tool result from cost estimations made by experts from the machine manufacturing and the supplier branch. The part cost calculations assume a production volume of 100,000 vehicles per year. Joining costs are calculated according to average cost modelling for the respective joining technology and the involved joining partners.

The resulting total body costs are presented in Fig. 5-1. The comparison of costs for the electric reference vehicle and the aluminium target vehicle model is summarized in Tab. 5-1.

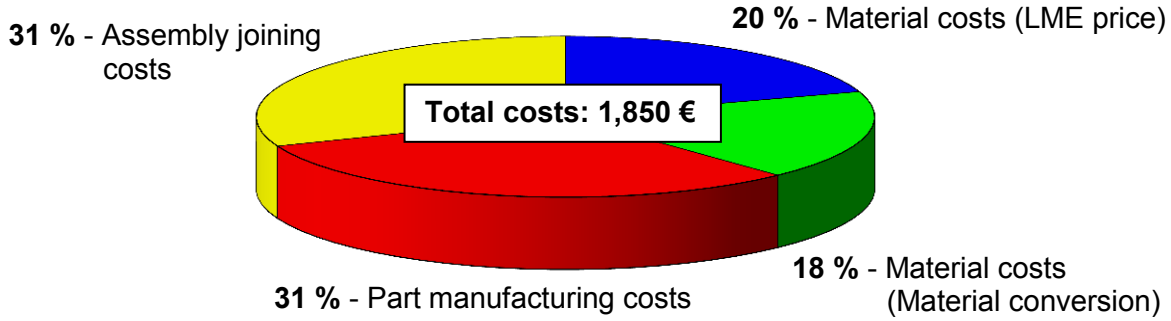

Fig. 5-1 Total body costs of the target vehicle model

[1] http://www.lme.com/aluminium.asp

Electric reference vehicle		Target vehicle model	
Total part costs modelled	520.00 €	Total part costs modelled	1,270.00 €
Total joining cost for biw	315.00 €	Total joining cost for biw	580.00 €
Δ total part costs from electric reference to target vehicle model			+750.00 €
Δ total joining costs from electric reference to target vehicle model			+265.00 €
Δ total assembly cost from electric reference to target vehicle model			+1,015.00 €

Tab. 5-1 Lightweight cost summary for electric reference and target vehicle models

The investigation focusing on the downsizing of the battery system presented in the following shows under which conditions the additional lightweight costs of 1,015 € can be compensated.

5.2 Cost Effect of Battery System Downsizing

Tab. 5-2 shows the comparison between the electric reference vehicle's battery system and the battery system of the target vehicle after downsizing.

Electric reference vehicle		Target vehicle model	
Battery system weight	232 kg	Battery system weight	207 kg
Number of battery cells	154	Number of battery cells	140
On-board capacity	37.6 kWh	On-board capacity	34.3 kWh

Tab. 5-2 Battery system dimensioning data for electric reference and target vehicle model

The exercised battery downsizing measures reduce the on-board battery capacity of the vehicle to reach the aimed 200 km driving range in the NEDC by 3.3 kWh.

Based on various investigations concerning the development of battery system prices an assumed price of 500 €/kWh in the year 2015 would lead to a total battery cost reduction by 1,650 € [KAL07], [LUN10] and [MAT05]. Compared to the additional cost for the lightweight design of 1,015 €, it can be concluded that the benefit due to the lower battery cost more than outweigh the additional cost for the lightweight aluminium vehicle.

It shall be noted that some parts represent a rather high specific lightweight cost (€/kg lightweighting) in order to achieve a full aluminium design. This increases of course the average specific lightweight cost. With a battery system cost of 500 €/kWh a full aluminium design is however still cost efficient. It is important to understand that even with a lower battery price in the future, the lightweighting of a large number of parts will still be cost efficient. A future study could look at this issue in detail.

5.3 Use Phase Economies of the Battery System Downsizing

In addition to the reduced investment costs a lighter vehicle also consumes less energy during its use phase.

Assuming a total mileage of 150,000 km in the NEDC, reducing the vehicle's weight by 188 kg results in a use phase energy consumption reduction (as from grid) by 2.10 MWh. Calculating with an exemplary electricity price of 0.19 €/kWh, this induces an additional life time cost saving of 400 €.

5.4 Cost Tool

The aim of the cost tool is the basic estimation of the cost effects and change in energy demand by lightweight measures. The tool, which is implemented in Microsoft Excel, provides a basic functionality in order to calculate several important values for the battery electric vehicle. Furthermore it is possible to compare two vehicle settings.

The tool is based on the analysed electric reference vehicle, so that following parameters are predefined and not variable:

- Air drag coefficient c_d: 0.31
- Reference area : 2.2 m²
- Rolling resistance coefficient: 0.01
- Power demand 12 V-powernet: 250 W
- Maximum speed: 160 km/h
- Life time mileage: 150,000 km

The input parameters for the tool and their admissible/reasonable values are listed in Tab. 5-3.

Tool input parameters	Admissible value range
Vehicle mass w/o battery system [kg]	600 – 2,000
Range in NEDC [km]	100 – 400
Energy density of battery system [Wh/kg]	80 – 200
Specific battery costs [€/kWh]	200 – 1,000

Tab. 5-3 Input parameter range of fka cost tool

The values for the energy density and the specific costs of the battery systems are known values for today's battery systems. The other limits are assumptions for a possible SOP in 2015. These values are based on several publications [LUN10], [MAT05] and [KAL07].

With these input parameters and the formulas from Chapter 3.2.3 a set of output parameters is calculated in the tool. These values are:

- Specific energy consumption in kWh/100km
- Total vehicle mass in kg
- Battery capacity in kWh
- Battery mass in kg
- Battery costs in €
- Specific battery cost savings in €/kg
- Life-time electricity costs in €

In addition to the formulas from Chapter 3.2.3, the cost-function for the battery system costs K_{Batt} has to be defined:

$$K_{Batt}=E_{Batt}\cdot k_{Batt}=\frac{(a\cdot m_{Veh}+b)}{\left(\frac{x_{Batt}}{s_{ele}}-\frac{a}{\rho_{ele,Batt}}\right)}\cdot k_{Batt} \qquad \text{Eq. 5-1}$$

With k_{Batt} as the specific battery costs in €/kWh

The derivative of the cost-function – the growth rate of the battery costs versus the basic vehicle mass – allows the quantification of the cost saving potential by lightweight measures in electric vehicles, considering the driving cycle, the electric range and the usable specific energy density of the battery system:

$$\frac{\Delta K_{Batt}}{\Delta m_{Veh}}=\frac{a\cdot k_{Batt}}{\left(\frac{x_{Batt}}{s_{ele}}-\frac{a}{\rho_{ele,Batt}}\right)} \qquad \text{Eq. 5-2}$$

6 Life Cycle Analysis[2]

The life cycle analysis aims at comparing the GHG life cycle emissions of the two electric cars compared in this project (the electric reference vehicle and the aluminium target vehicle), also called their respective carbon footprint. The carbon footprint calculation will focus on the following aspects of the various car life cycle steps:

- Production and manufacturing

The life cycle calculation will focus on the aluminium and steel parts of the two electric vehicle body structures and on the difference between their battery packs. It is assumed that the GHG intensity of the battery production corresponds to 20 kg GHG/kg of battery cell [FRI11]. All other parts of the vehicles will be considered as identical in the two concepts. In particular, the two electric engines are supposed to be the same and only the difference in the battery packs will be considered.

It should be noted that such simplification is slightly detrimental to the aluminium vehicle since a downsizing of some other components could take place due to the lighter total weight of the aluminium vehicle. For the vehicle structures, the metal supply for the steel parts as well as for the aluminium parts is supposed to correspond to the European average, i.e. 40 % from recycling and 60 % from primary production for both metals. The assessment considers production and semi-finishing processes but does not include fabrication steps like forming, cutting or joining operations.

- Use phase

A total mileage of 150,000 km is assumed, corresponding to 1,000 charging cycles with an average discharge level of 75 % of the maximum useful capacity of the batteries. The GHG calculation of the electricity is based on today's EU-25 average grid mix, i.e. 525 kg of GHG emission/MWh of electric energy [PEI11]. Additionally, a sensitivity analysis is done with the assumption that the GHG intensity of this grid mix can be reduced by 50 %.

- End of life

Only the recycling of the two vehicle structures is considered. The additional benefits resulting from the end of life recycling are calculated on basis of 90 % recycling rate considering that a full substitution can take place for both metals. These benefits are calculated for the net flow of recycled metal, i.e. after deduction of the recycled metal already considered at the production stage.

[2] This LCA section has been developed by the EAA LCA team and integrated into the report by fka

6.1 Basic Data used for the Life Cycle Analysis Calculations

Tab. 6-1 to Tab. 6-4 list the basic data used for the life cycle analysis calculations.

Mass and composition of the vehicle structures		**Composition (%)**			
		Steel	Aluminium		
	Total mass (kg)	Flat carbon steel	Rolled aluminium	Extruded aluminium	Cast aluminium
Electric reference vehicle	375	100 %			
Aluminium target vehicle	213		60 %	25 %	15 %

Tab. 6-1 Considered body mass and material data for electric reference and target vehicle model

Battery system characteristics	**Electric reference vehicle**	**Aluminium target vehicle**	**Difference**
Number of battery cells	154	140	14
Total battery energy content [kWh]	37.6	34.3	3.3
Total weight of battery cells [kg]	165	150	15
Energy consumption / 200 km ride [kWh]	30.0	27.4	2.6
Energy extracted from grid (charging) [kWh]	33.3	30.5	2.8
Energy consumption at grid level [kWh/km]	0.1665	0.1525	0.014

Tab. 6-2 Battery system data for electric reference and target vehicle model

Process	**GHG intensity (kg CO_2-equiv/kg)**	**Source**
Primary aluminium	9.7	EAA data [EAA08]
Aluminium recycling	0.5	
Primary steel	2	Autosteel model [WAS09]
Recycled steel	0.4	

Tab. 6-3 LCA basic calculation data for production and recycling of aluminium and steel

Semi-finishing processes	**Flat carbon steel**	**Rolled aluminium**	**Extruded aluminium**	**Cast aluminium**
GHG intensity (kg CO_2-equiv/kg)	0.6	0.6	0.7	0.3
Sources	Autosteel	EAA data		

Tab. 6-4 LCA basic calculation data for semi-finishing process of aluminium and steel

6.2 Life Cycle Analysis Results

Tab. 6-5 and Tab. 6-6 show the results of the calculations based on the input data detailed before. Fig. 6-1 traces the greenhouse gas emission curve over the complete use phase of the compared vehicle models.

GHG intensity for the 2 vehicles (kg CO_2-Equiv)		**Electric reference vehicle**	**Aluminium target vehicle**
Indicators for the vehicle body structure			
	Production	735 kg	1,405 kg
	End of life (EoL) benefits	-300 kg	-980 kg
	Total	435 kg	425 kg
Indicators for the battery production (only for the difference)		0.0 kg	-300 kg
Indicators for the electricity consumption (use phase impact)		14,086 kg	12,901 kg

Tab. 6-5 GHG emission balance for structure and battery system of the electric reference and the aluminium target model

Results for the full life cycle		**Electric reference vehicle**	**Aluminium target vehicle**	**Difference**
GHG intensity (kg CO_2-Equiv)	Production	735 kg	1,105 kg	+370 kg
	Use	14,086 kg	12,901 kg	-1,185 kg
	EoL benefits	-300 kg	-980 kg	-680 kg
	Total	**14,521 kg**	**13,026 kg**	**-1,495 kg**

Tab. 6-6 GHG emission balance summary for the electric reference and the aluminium target model

Even if benefits from the end of life stage of the vehicle are not considered, the break even point is at about 47,000 km, meaning that the higher greenhouse gas intensity resulting from the production phase of the aluminium target vehicle is rapidly recovered over the use phase, due to the lower energy consumption than for the heavier electric reference vehicle.

But as the share of full electric vehicles on the European markets is supposed to increase, the greenhouse gas emission of electricity production within the European Union is also likely to decrease. To consider this tendency, the following sensitivity analysis quantifies the effect of a possible greenhouse gas intensity reduction of electricity production by 50 %.

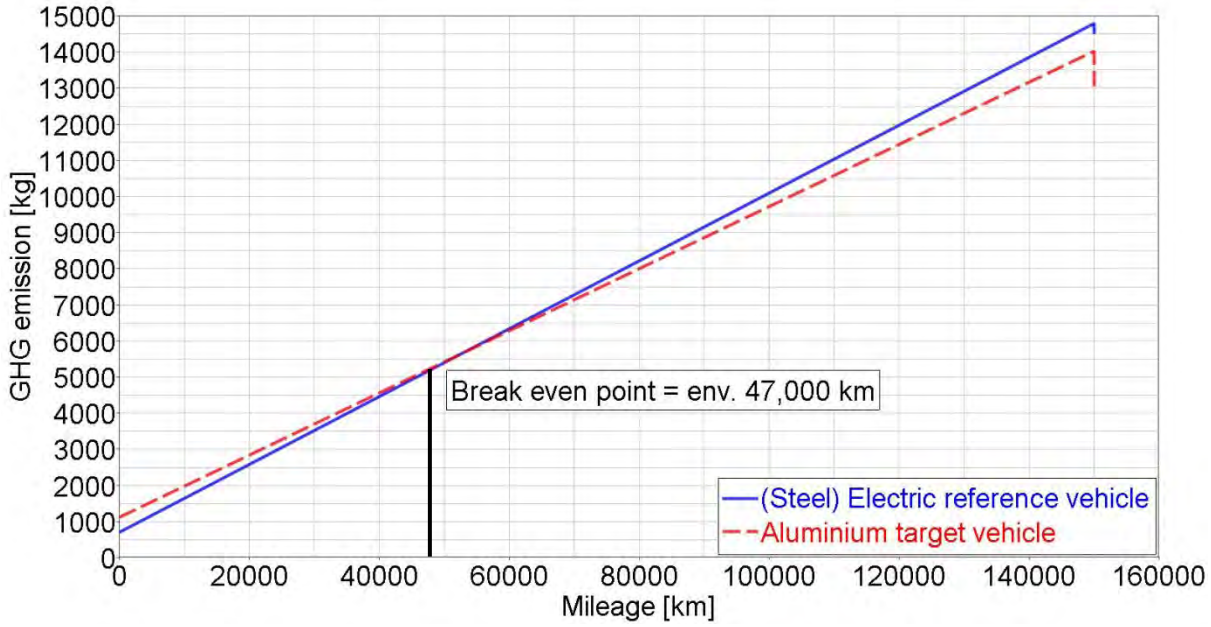

Fig. 6-1 Comparison of GHG emission over full life cycle for aluminium target and electric reference vehicles

6.3 Sensitivity Analysis

To study the impact of a greener EU-25 grid mix, the described LCA calculations are repeated with a modelled 50 % reduction of greenhouse gas intensity of electricity production. Tab. 6-7 and Fig. 6-2 show the differing results.

Results for the full life cycle		**Electric reference vehicle**	**Aluminium target vehicle**	**Difference**
GHG intensity (kg CO_2-Equiv)	Production	735 kg	1,105 kg	+370 kg
	Use	7,043 kg	6,451 kg	-592 kg
	EoL benefits	-300 kg	-980 kg	-680 kg
	Total	**7,478 kg**	**6,576 kg**	**-902 kg**

Tab. 6-7 GHG emission balance summary for the electric reference and the aluminium target model after 50 % reduction of use phase GHG intensity

If the GHG intensity of the electricity production is reduced by 50 %, the break even point between the aluminium target and the electric reference vehicle is delayed to mileage values around 94,000 km, i.e. corresponding to double the distance. Still, the advantage of intensive aluminium use in electric vehicle's structure is visible already during the vehicle's use phase.

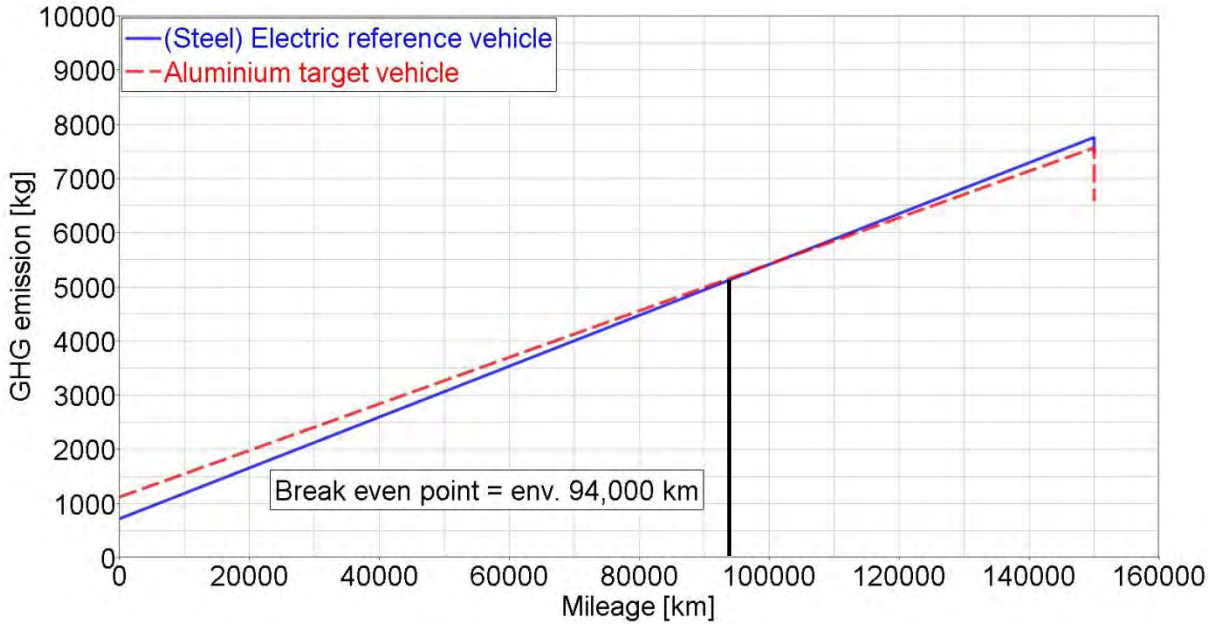

Fig. 6-2 Comparison of GHG emission over full life cycle for aluminium target and electric reference vehicles with 50 % emission reduction over use phase

6.4 Life Cycle Analysis Conclusion

If the additional benefits of the end of life stage are considered, the aluminium electric vehicle appears certainly better in terms of overall greenhouse gas life cycle emission since savings of about 1.5 tonnes of GHG are calculated for the baseline scenario and 0.9 tonnes for the scenario with the lower GHG grid mix intensity. These calculations show that additionally to cost savings, the aluminium intensive vehicle is also a better option in terms of carbon footprint over the life cycle of the vehicle.

7 Summary

The main objective of this study was to determine the cost trade-off point between aluminium lightweight engineering and powertrain downsizing for electric vehicles. As basis of this study a C segment reference vehicle with steel unibody and internal combustion engine was chosen. The mass and crashworthiness properties of this vehicle were analysed in four Euro NCAP and FMVSS 301 highspeed loadcases. The structural behaviour was to be conserved by all following vehicle designs modelled.

In the first step of the study, the crash reference vehicle was converted into a full electric vehicle using a conversion design strategy. The steel unibody structure was conserved and an electric powertrain was designed, assuming battery technology features available in the year 2015.

In a second step, the full-steel body structure of the electric reference vehicle was replaced by a full-aluminium space frame structure. While reaching the defined crashworthiness targets, weight reduction by 162 kg over the body structure compared to the electric reference with steel-unibody could be realized. As a secondary effect, the battery system capacity could be downsized by 3.3 kWh maintaining the intended driving range of 200 km.

After the accomplishment of the design tasks, the cost impact of the described measures was quantified. Assuming a production volume of 100,000 vehicles per year, the aluminium lightweight measures can be realized for additional part and joining costs of 1,015 €. This value should be compared to the cost reduction due to the battery capacity downsizing potential of 3.3 kWh. Assuming energy-specific battery system costs of 500 €/kWh, the reduction in total battery system costs is 1,650 €. Comparing the additional costs for the lightweight design with the reduction in battery system costs, it can be concluded that the benefit due to lower battery costs more than outweigh the additional costs for the lightweight aluminium vehicle. It shall be noted that to achieve a full aluminium design some parts represent a rather high specific lightweight cost (€/kg lightweighting). This increases the average specific lightweight cost. It is important to understand that even with a lower battery price in the future, the lightweighting of a large number of parts will still be cost efficient. To cover uncertainties concerning several powertrain system cost influencing factors, a cost tool was developed allowing the impact evaluation of a wide variation range of each factor.

Finally, the life cycle analysis of the full-steel and the full-aluminium electric vehicles was performed showing that the aluminium vehicle produces 1.5 tons of greenhouse gas less over the complete lifespan including a mileage of 150,000 km.

Based on the results of this study, it is possible to evaluate the effects of partial material substitution from steel to aluminium for an electric vehicle structure. A lightweight cost ranking can be calculated and the lowest hanging fruits can be identified. Future studies can also focus on the structural impact of additional vehicle properties onto the full-aluminium electric vehicle as well as additional secondary weight reduction potentials.

8 Technical Summary

	Electric reference vehicle	Aluminium target vehicle	Difference	
Vehicle body	375 kg	213 kg	-162 kg	-43.2 %
Battery system	232 kg	207 kg	-25 kg	-10.8 %
Total vehicle weight	**1,328 kg**	**1,140 kg**	**-188 kg**	**-14.2 %**

Tab. 8-1 Weight comparison

	Electric reference vehicle	Aluminium target vehicle	Difference	
Total part costs	520 €	1,270 €	+750 €	+144 %
Total joining costs	315 €	580 €	+265 €	+84.1 %
Total costs	**835 €**	**1,850 €**	**+1,015 €**	**+122 %**

Tab. 8-2 Cost comparison for vehicle body

	Electric reference vehicle	Aluminium target vehicle	Difference	
Energy content	37.6 kWh	34.3 kWh	-3.3 kWh	-8.78 %

Tab. 8-3 Comparison of battery system energy content

	Electric reference vehicle	Aluminium target vehicle	Difference	
Consumption / 200 km	33.3 kWh	30.5 kWh	-2.8 kWh	-8.41 %
Consumption over total mileage (150,000 km)	24,975 kWh	22,875 kWh	-2,100 kWh	-8.41 %

Tab. 8-4 Energy consumption (as extracted from grid)

	Electric reference vehicle	Aluminium target vehicle	Difference	
Life cycle emissions (kg CO_2-Equiv)	14,521 kg	13,026 kg	-1,495 kg	-10.3 %

Tab. 8-5 Comparison of life cycle greenhouse gas emissions

9 Companies and Organisations Responsible for Study

European Aluminium Association AISBL

International Aluminium Institute

Forschungsgesellschaft Kraftfahrwesen mbH Aachen

Alcoa

Aleris

AMAG

Constellium

Hydro

Metra

NOVELIS

SAPA

10 Formula Symbols and Indices

AZT	Allianz Zentrum für Technik Crash Repair Test
BIW	Body-in-White
EAA	European Aluminium Association
EoL	End of Life
Euro NCAP	European New Car Assessment Program
FDS	Flow Drill Screwing
FE	Finite Element
fka	Forschungsgesellschaft Kraftfahrwesen mbH Aachen
FMVSS	Federal Motor Vehicle Safety Standards
GHG	Greenhouse Gas
ICE	Internal Combustion Engine
LCA	Life Cycle Analysis
LME	London Metal Exchange
MIG	Metal Inert Gas
NEDC	New European Driving Cycle
ODB	Offset Deformable Barrier
OEM	Original Equipment Manufacturer
RCAR	Research Council for Automobile Repairs Crash Test
SLC	Super Light Car

a	Cycle-specific mass gradient
A	Vehicle cross section area
b	Cycle-specific absolute consumption
C_d	Air drag coefficient

e_i	Mass factor
e_{Veh}	Specific energy consumption of the vehicle
f_r	Coefficient of friction
F	Force
g	Gravity acceleration
i	Gear ratio
k_{Batt}	Specific battery cost
K_{Batt}	Battery system cost
km/h	Kilometres per hour
m	Mass
mph	Miles per hour
n	Rotation speed
P	Mechanical performance
r	Radius
rpm	Revolutions per minute
$R_{p0.2}$	(Offset) yield strength
s	Driving range
v	Velocity
x	Useable SOC-range
α_{ST}	Angle of road elevation
η	Efficiency factor
ρ	Density

11 Literature

[EAA08] N. N.
Environmental Profile Report for the European Aluminium Industry
European Aluminium Association, Brussels, 2008

[ECE05] N. N.
ECE r101r2e-Europäische Richtlinien zur Bestimmung des Kraftstoffverbrauchs und Emissionen
Economic Comission for Europe, Genf, 2005

[EPA11] N. N.
Federal Regulation
Chapter I – Environmental Protection Agency, Subchapter C – Air Programs
Part 86 – Control of emissions from new and in-use highway vehicles and engines
Environmental Protection Agency, Washington, 2011

[EUR09] N. N.
Frontal Impact – Testing Protocol
Version 5.0
Euro NCAP, Brussels, 2009

[EUR09a] N. N.
Side Impact – Testing Protocol
Version 5.0
Euro NCAP, Brussels, 2009

[EUR09b] N. N.
Pole Side Impact – Testing Protocol
Version 5.0
Euro NCAP, Brussels, 2009

[EUR10] N. N.
Technical Bulletin – Testing of Electric Vehicles
Version 1.0
Euro NCAP, Brussels, 2010

[EUR11] N. N.
Volkswagen Golf Euro NCAP rating of 2004
www.euroncap.com

[FRI98] FRIEDMANN, S.; JONES, C.; MESITI, D.; ANDRE, M; CARMINOT, P
Entwicklung von Bewertungswerkzeugen für Hybridfahrzeuge
VDI-Bericht 1378, Düsseldorf, 1998

[FRI11] FRISCHKNECHT, R.; FLURY, K.
Life cycle assessment of electric mobility: answers and challenges
The International Journal of Life Cycle Assessment, 16/2011, Zürich, 2011

[GOE09] GOEDE, M.; STEHLIN, M.
SuperLIGHT-Car project
An integrated research approach for lightweight car body innovations
Innovative Developments for Lightweight Vehicle Structures, Wolfsburg, 2009

[KAL07] KALHAMMER, F.; KOPF, B. ;SWAN, D. ; ROAN, V. ; WALSH, M.
Status and Prospects for Zero Emissions Vehicle Technology – Report of the ARB Independent Expert Panel 2007
Sacramento, California, 2007

[LUN10] LUNZ, B.; SAUER, D.
Elektromobilität als Herausforderung und Chance für die Fahrzeugsicherheit
Solar Mobility, Februar 2010, Berlin

[MAT05] MATHEYS, J.; van AUTENBOER, W.
EU-Project SUBAT: Final Public Report
Vrije Universiteit Brussel – ETEC, 2005

[NHT04] N. N.
Federal Motor Vehicle Safety Standards and Regulations
Part 571 – Crashworthiness Standard No. 301 Fuel System integrity
National Highway Traffic Safety Administration, Washington, 2004

[PEI11] N. N.
GaBi Software Version 4.4
PE International AG, Leinfelden-Echterdingen, 2011

[SCH11] SCHÖNEBURG, R.; JUSTEN, R.
Elektromobilität als Herausforderung und Chance für die Fahrzeugsicherheit
2. Automobiltechnisches Kolloquium, Garching, 2011

[STE03] STEINRÜCKEN, M.; WELSCH, F.; OEHMKE, B.; HILLMANN, J.
The new VW Golf V – The body in white
Innovative technical concepts
Volkswagen AG, Wolfsburg, 2003

[WAS09] N. N.
World Auto Steel Vehicle life cycle model
Version 2
World Steel Association, Middletown, 2009

12 Appendix

12.1 Description of Analysed Crash Loadcases

12.1.1 Euro NCAP Front Crash

The Euro NCAP based front crash regarded in this study can be characterised as follows [EUR09] (compare Fig. 12-1):

- Impact speed of vehicle onto barrier: 64 km/h (40 mph)
- Vehicle to barrier overlap: 40 %
- Use of standardized offset deformable barrier (ODB)
- Impact angle: 0 degree

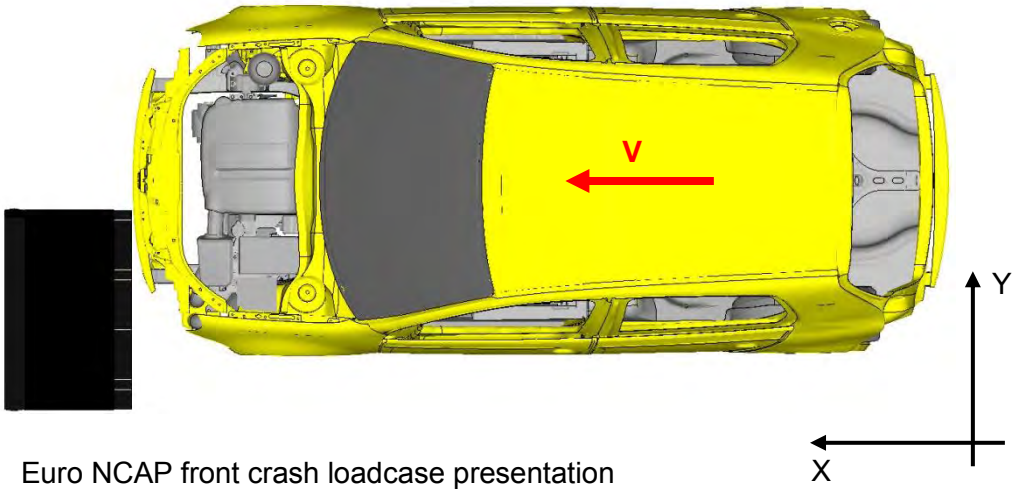

Fig. 12-1 Euro NCAP front crash loadcase presentation

In addition to the vehicle's kerb weight the following weights are applied to the assessed vehicle [EUR09] (compare Fig. 12-2):

- 90 % fuel tank fill (equivalent to 36.7 kg of fuel)
- Two 88 kg Hybrid III dummies on the vehicle's front seats
- 36 kg of extra weight in the luggage compartment
- One 3 year old child dummy (15 kg) and one 1½ year old child dummy (11 kg) on the rear seats

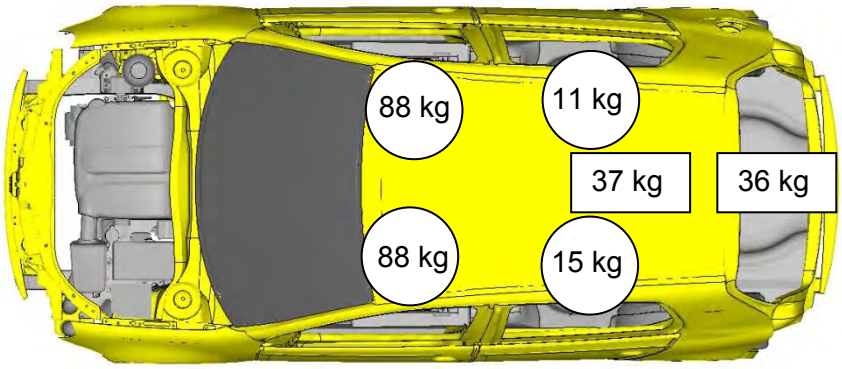

Fig. 12-2 Additional loads for Euro NCAP protocol crash procedure (front crash)

12.1.2 Euro NCAP Side Crash

The Euro NCAP based side crash used for this study can be characterised as follows [EUR09a] (compare Fig. 12-3):

- Impact speed of barrier onto vehicle side: 50 km/h (30 mph)
- Barrier weight: 950 kg
- Use of deformable moving barrier
- Impact angle: 0 degree

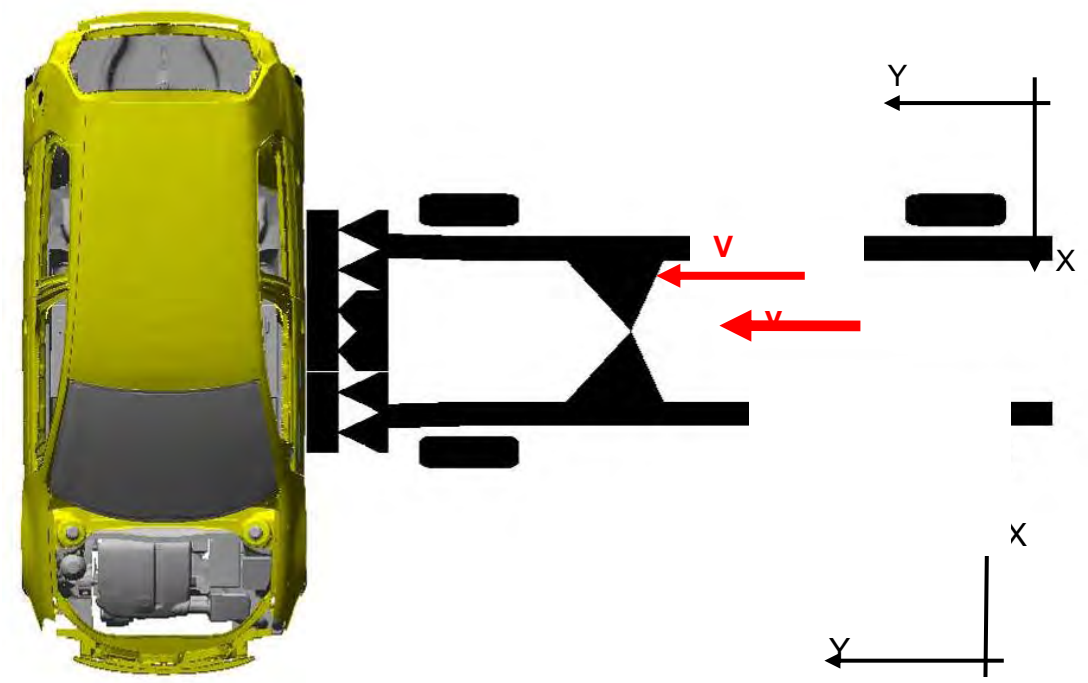

Fig. 12-3 Euro NCAP side crash loadcase presentation

The extra loads applied in addition to the vehicle kerb weight are [EUR09a] (compare Fig. 12-4):

- 20 kg of extra weight in the luggage compartment
- ES-2 dummy (80 kg) on the driver seat
- One 3 year old child dummy (15 kg) and one 1 ½ year old child dummy (11 kg) on the rear seats
- 90 % fuel tank fill (equivalent to 36.7 kg of fuel)

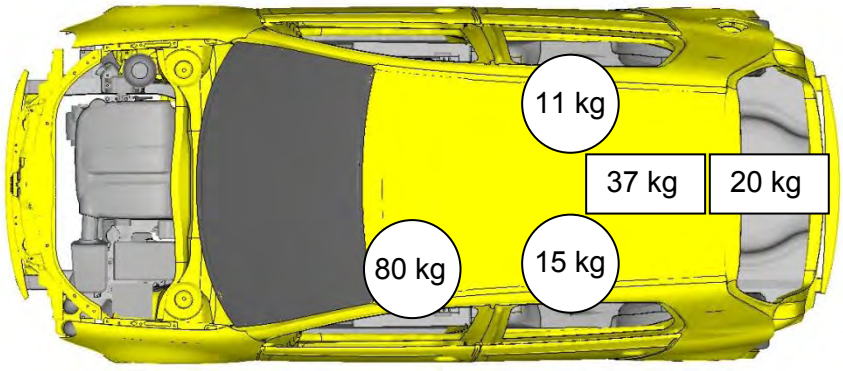

Fig. 12-4 Additional loads for Euro NCAP protocol crash procedure (side crash)

12.1.3 Euro NCAP Pole Side Crash

The Euro NCAP based pole side crash used for this study can be characterised as follows [EUR09b] (compare Fig. 12-5):

- 29 km/h (18 mph) impact speed of vehicle onto pole barrier
- Pole diameter: 254 mm (10 inch)
- Impact direction normal to vehicle side

The extra loads applied in addition to the vehicle kerb weight are the same as for the side impact without child dummies on the rear seats [EUR09b].

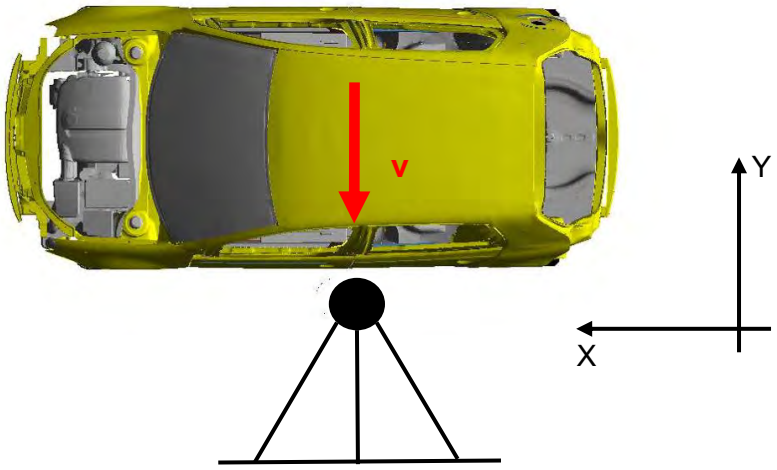

Fig. 12-5 Euro NCAP side pole crash loadcase presentation

12.1.4 FMVSS 301 Rear Crash

The FMVSS 301 based rear crash used for this study can be detailed as follows [NHT04] (compare Fig. 12-6):

- Impact speed of barrier onto vehicle rear end: 48 km/h (30 mph)
- Barrier weight: 1,814 kg
- Vehicle to barrier overlap: 100 %
- Rigid moving barrier

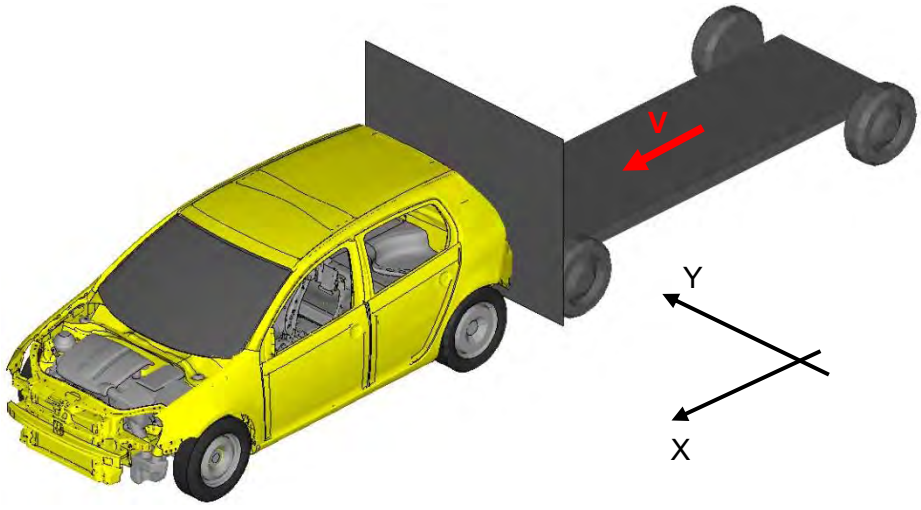

Fig. 12-6 FMVSS 301 rear crash loadcase presentation

Prescribed extra loads normally applied in addition to the vehicle kerb weight are [NHT04] (compare Fig. 12-7):

- Two 75 kg dummies on front seats

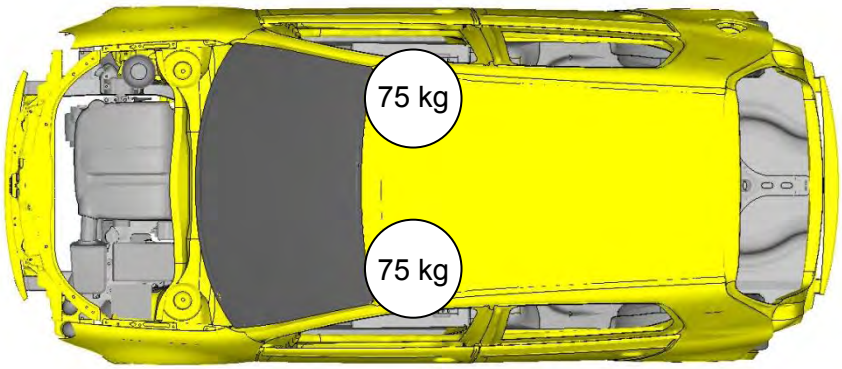

Fig. 12-7 Additional loads for FMVSS 301 protocol crash procedure (rear crash)

The evaluation of this rear impact high speed crash standard focuses on aspects of fuel system integrity [NHT04]. Thus, fuel filling as additional weight is not defined. Instead, a 90 % tank filling is reached with a solvent meant for spillage detection.

12.2 Standard Speed Profiles

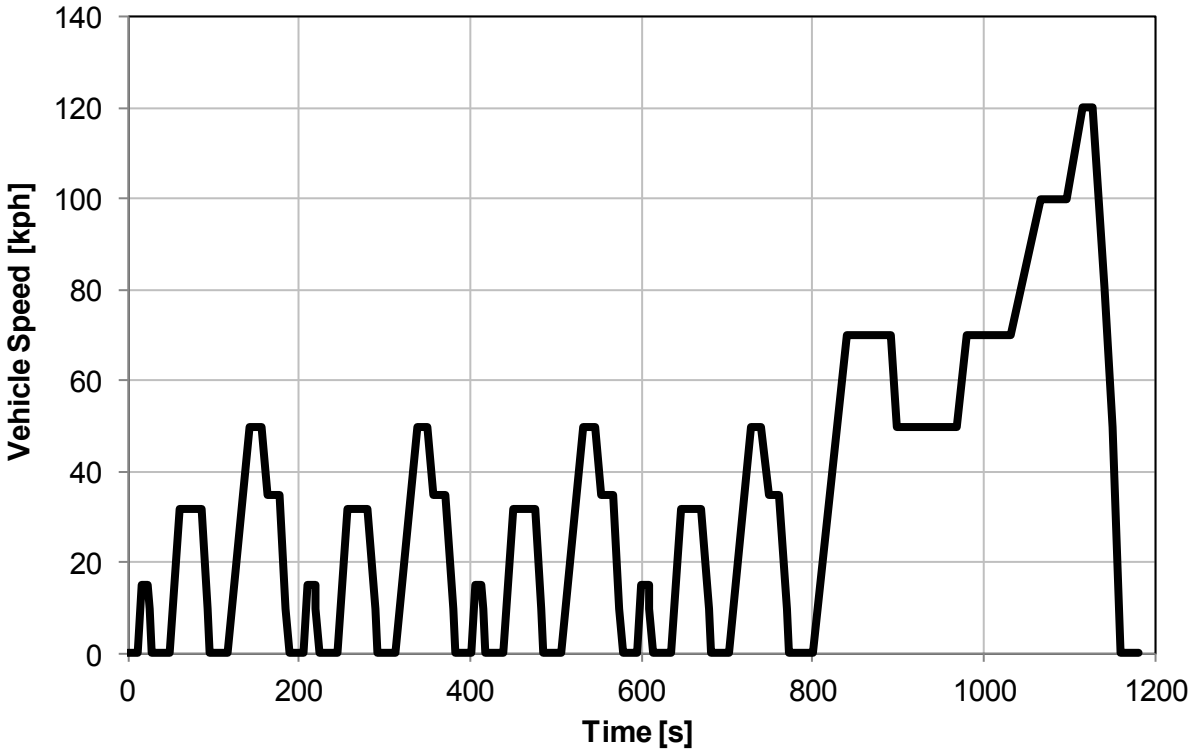

Fig. 12-8 Speed profile New European Driving Cycle (NEDC) [ECE05]

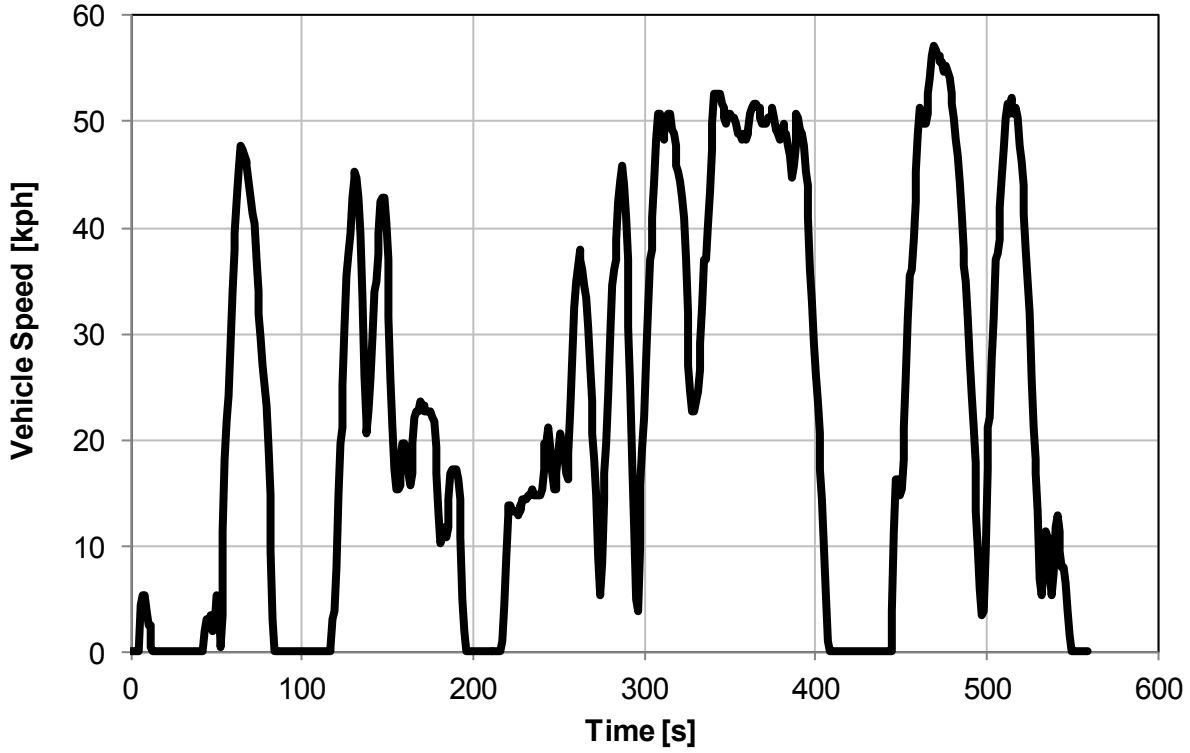

Fig. 12-9: Speed profile Hyzem Urban [FRI98]

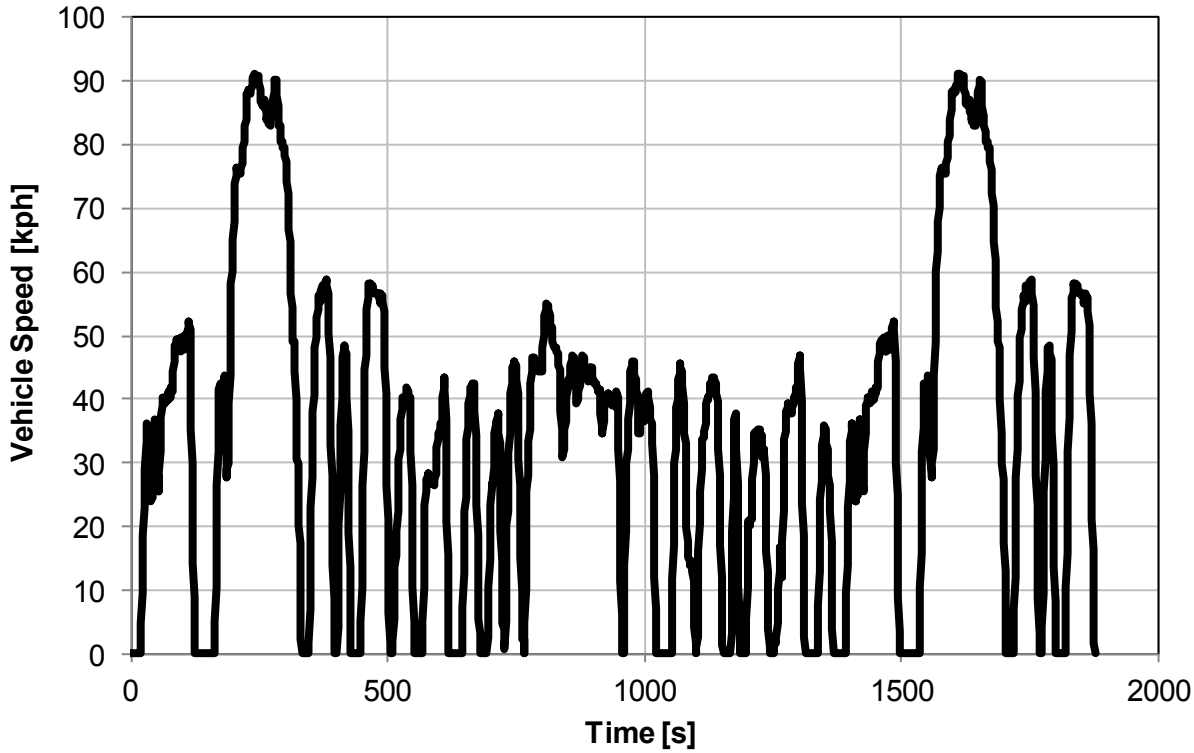

Fig. 12-10 Speed profile EPA City Cycle [EPA11]

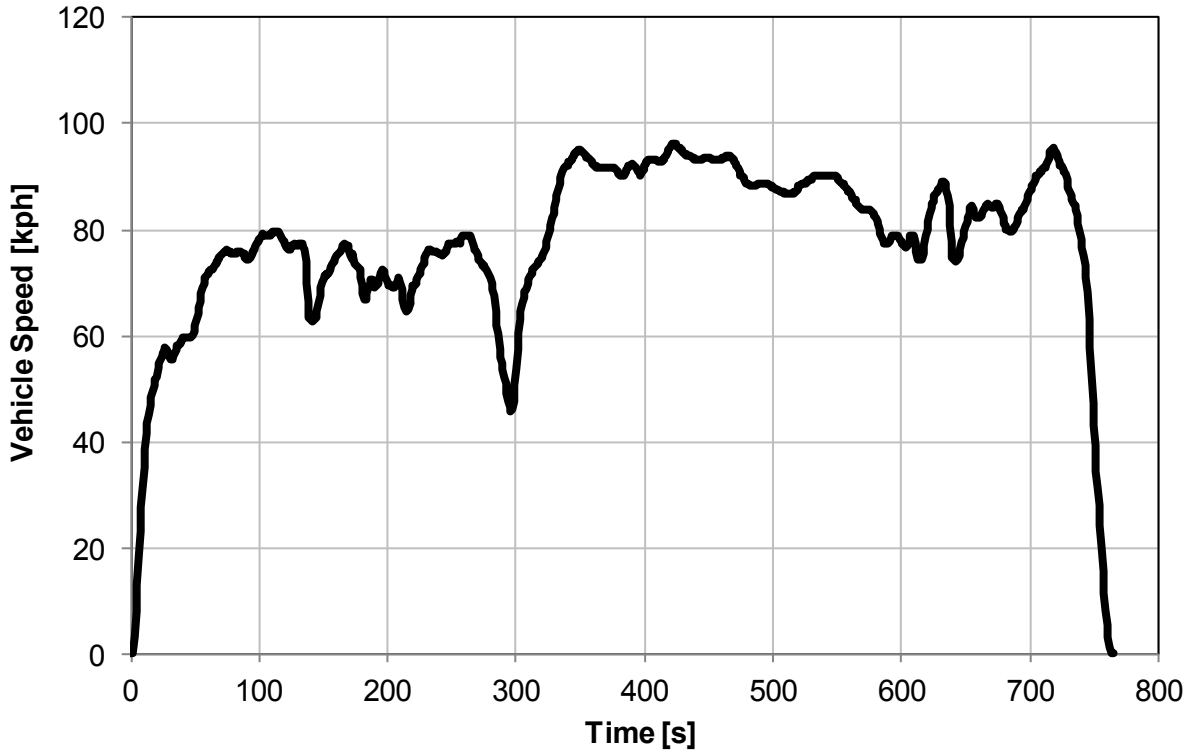

Fig. 12-11 Speed profile EPA Highway Cycle [EPA11]

12.3 Powertrain Dimensioning Characteristics of the Electric Reference Vehicle

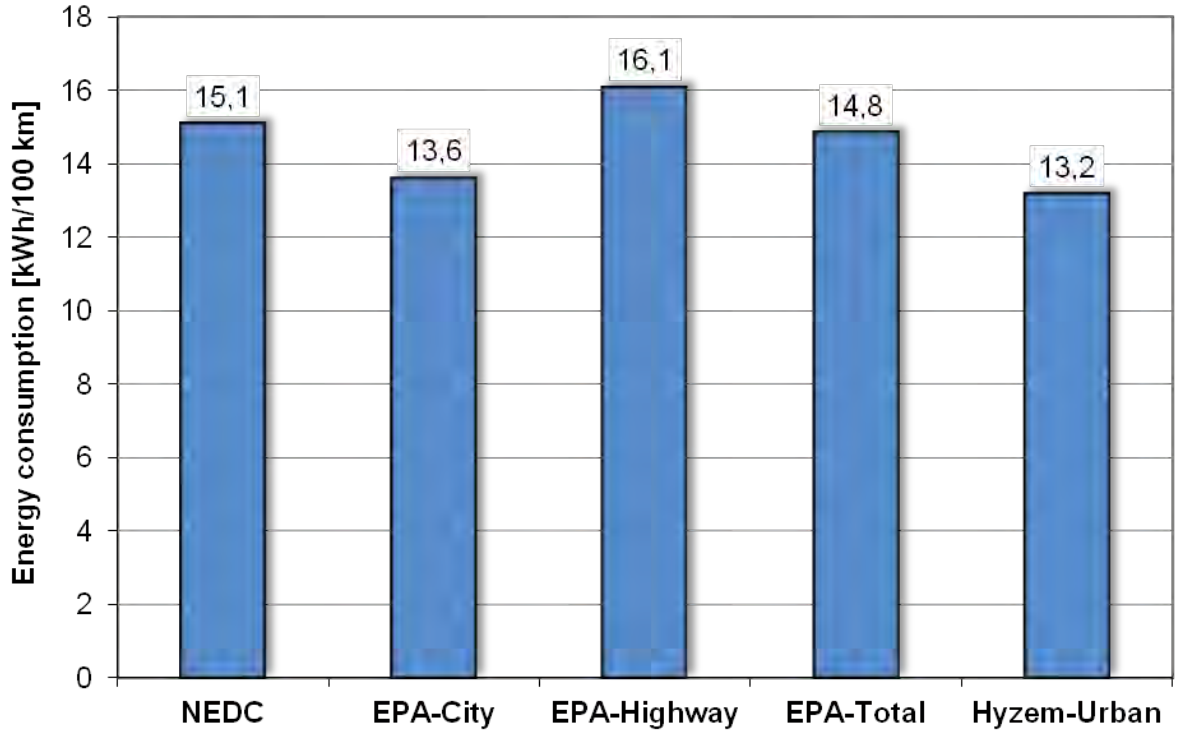

Fig. 12-12 Energy consumption of electric reference vehicle in different driving cycles

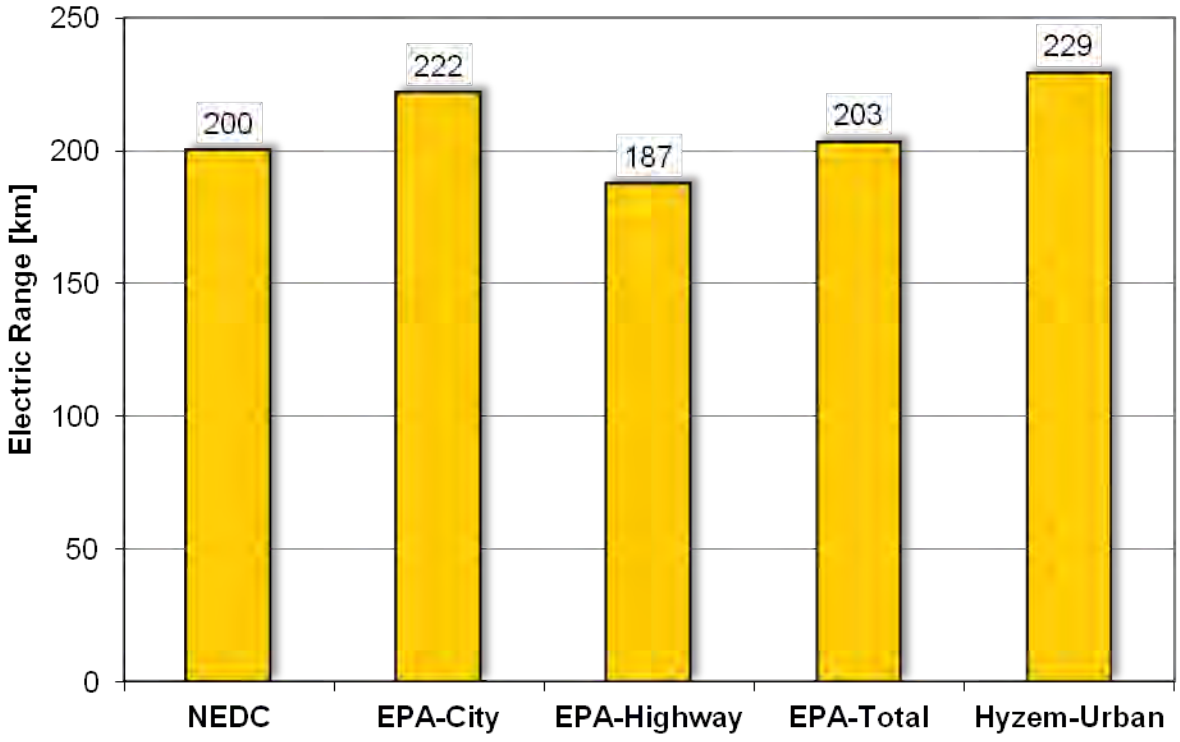

Fig. 12-13 Driving range of electric reference vehicle in different driving cycles